Information theoretic limits of MIMO wireless networks with bounded input and imperfect CSIT

by

Borzoo Rassouli

A thesis submitted in fulfilment of requirements for the degree of
Doctor of Philosophy of Imperial College London

Communications and Signal Processing Research Group
Department of Electrical and Electronic Engineering
Imperial College London

July 2016

Abstract

In this thesis, we investigate some information theoretic limits of two specific types of MIMO wireless networks. In the first one, the effect of channel uncertainty at the transmitter (due to estimation error, feedback latency, and so on) in MIMO broadcast channels is investigated. In this setting, we capture this imperfectness in the bounds for the DoF region of the channel. The second one is the point to point deterministic MIMO channel with input amplitude constraint. For certain settings, the capacity of this channel is derived, while for the general problem, upper and lower bounds for the capacity are obtained.

Acknowledgements

First and foremost, I would like to thank my parents for their love and support throughout my life. Massoumeh Balani and Mohammadreza Rassouli, I am always grateful to you. I also thank my brother, Babak, who always supported me, although I was always the first person whom he performed his new Judo techniques on!

I would like to sincerely thank my supervisor, Dr. Clerckx, for his guidance and support throughout this study, and especially for his confidence in me. I would also like to thank my M.Sc. supervisor Dr. Olfat from whom I learned a lot.

I would like to thank Dr. Tchamkerten and my friend Mohammad Ali Sedaghat for the fruitful discussions relating to chapter 3 of this thesis.

I would like to thank Dr. Peter Barker and Mrs. Margaret Vallance whom I was very lucky to live with.

To all my friends, thank you for your understanding and encouragement in my moments of crisis.

©

Copyright

The copyright of this thesis rests with the author and is made available under a Creative Commons Attribution Non-Commercial No Derivatives licence. Researchers are free to copy, distribute or transmit the thesis on the condition that they attribute it, that they do not use it for commercial purposes and that they do not alter, transform or build upon it. For any reuse or redistribution, researchers must make clear to others the licence terms of this work.

Declaration of Originality

I, Borzoo Rassouli, declare that this thesis titled, 'Information Theoretic Limits of MIMO Wireless Networks With Bounded Input and Imperfect CSIT' and the work presented in it are my own. I confirm that:

- This work was done wholly or mainly while in candidature for a research degree at Imperial College London.
- Where I have consulted the published work of others, this is always clearly attributed.
- Where I have quoted from the work of others, the source is always given. With the exception of such quotations, this thesis is entirely my own work.
- I have acknowledged all main sources of help.
- Where the thesis is based on work done by myself jointly with others, I have made clear exactly what was done by others and what I have contributed myself.

Signed: _____

Date: _____

Contents

List of Figures

Abbreviations

DoF	Degrees of Freedom
MIMO	Multiple Input Multiple Output
MISO	Multiple Input Single Output
BC	Broadcast Channel
IC	Interference Channel
CSI	Channel State Information
CSIT	Channel State Information at Transmitter
CSIR	Channel State Information at Receiver
ZFBF	Zero Forcing Beamforming
i.i.d.	independent and identically distributed
pmf	probability mass function
pdf	probability density function
cdf	cumulative distribution function

Symbols

$\mathbb{R}$	the set of real numbers
$\mathbb{R}_{\geq 0}$	the set of non-negative real numbers
$\mathbb{C}$	the set of complex numbers
$E[\cdot]$	statistical expectation
$(\cdot)^T$	transpose
$(\cdot)^H$	conjugate transpose
$f \sim o(\log P)$	is equivalent to $\lim_{P\to\infty} \frac{f}{\log P} = 0$
$[m : q]$	for a pair of integers $m \leq q$, the discrete interval
	is defined as $[m : q] = \{m, m+1, \ldots, q\}$.
$Y_{[i:j]}$	$= \{Y_i, Y_{i+1}, \ldots, Y_j\}$
Y^n	$= Y([1 : n])$
$CN(\mathbf{0}, \mathbf{\Sigma})$	the circularly symmetric complex Gaussian distribution
	with covariance matrix $\mathbf{\Sigma}$

Chapter 1

Introduction

MIMO wireless networks are of significant interest due to their several beneficial features including the increased multiplexing gain. It is known that in a point to point MIMO channel, knowledge of the channel state at the transmitter does not affect the multiplexing gain, while in MIMO networks such as MIMO broadcast channels, it is crucial to know the channel for interference cancellation. From a more practical point of view, the assumption of perfect CSIT may not always be true due to channel estimation error and feedback latency. Hence, it is interesting to consider the idea of communication under some sort of imperfection in CSIT and see how it degrades the performance. Chapter 2 of this thesis is devoted to this problem.

The remaining part of this thesis deals with communication with peak power constraint. Although the literature on the capacity with average power constraint is extensive, less attention has been paid to the scenario with peak power constraint. Our motivation for investigating this problem is the recent concept of MIMO transmission with a single RF chain.

The more detailed content of this thesis is as follows. In Chapter 2, a MIMO BC is considered in which the effect of imperfect channel state information at the transmitter is investigated. The performance metric is the DoF region which could be interpreted as the region constructed by the number of interference-free private data streams that users receive simultaneously per channel use. A probabilistic model for CSIT is adopted, i.e., the CSI of a user could be perfect, delayed or unknown with corresponding marginal probabilities. Given the marginal probabilities of CSIT, an outer bound is derived for

the DoF region. This outer bound is shown to be tight in certain scenarios. A set of inequalities is derived based on the joint CSIT distribution which shows that in general, the DoF region of the K-user MISO BC (when $K \geq 3$) cannot be characterized completely by the marginal probabilities in contrast to the two-user case. Finally, an outer bound on the DoF region of a two user MIMO BC, in which the CSIT of a user is either perfect or unknown, is provided, and it is shown to be tight in some scenarios.

In Chapter 3, the capacity of a point to point static MIMO channel under peak and average power constraints is investigated. For the identity channel matrix, the capacity-achieving distribution is obtained. It is shown that for a fixed peak power constraint, when the number of antennas is large enough, constant amplitude signaling is optimal. Finally, several upper and lower bounds are obtained on the capacity of the general non-identity channel matrix.

In Chapter 4, the scalar AWGN channel with peak power constraint is considered whose capacity has no closed form expression. The aim of this chapter is to further refine the analytical upper bounds for the capacity of this channel.

In Chapter 5, a 2-by-2 static MIMO channel is considered in which the input is forced to have a fixed amplitude. It is shown that the optimal input has a finite number of mass point on a circle whose radius is the square root of the peak power constraint.

Finally, Chapter 6 is devoted to conclusions and future works.

Chapter 2

DoF Analysis of the MIMO Broadcast Channel with Alternating/Hybrid CSIT

2.1 Overview

In this chapter, we first consider a K-user multiple-input single-output (MISO) broadcast channel (BC) where the channel state information (CSI) of user $i(i = 1, 2, \ldots, K)$ may be instantaneously perfect (P), delayed (D) or not known (N) at the transmitter with probabilities λ_P^i, λ_D^i and λ_N^i, respectively, while perfect CSI is assumed at the receivers. In this setting, according to the three possible CSIT for each user, knowledge of the joint CSIT of the K users could have at most 3^K states. Given the marginal probabilities of CSIT (i.e., λ_P^i, λ_D^i and λ_N^i), we derive an outer bound for the DoF region of the K-user MISO BC. Subsequently, we tighten this outer bound by taking into account a set of inequalities that capture some of the 3^K states of the joint CSIT. One of the consequences of this set of inequalities is that for $K \geq 3$, the DoF region is not completely characterized by the marginal probabilities in contrast to the two-user case. Afterwards, the tightness of these bounds is investigated through the discussion on the achievability. After the discussion on MISO BC, a two user MIMO BC having CSIT among P and N is considered in which an outer bound on the DoF region is provided and it is shown to be tight in some scenarios. Finally, an alternative proof for the DoF region of the

K-user MIMO BC with no CSIT and perfect CSIR is provided. Based on this proof, the capacity region of a certain class of MIMO BC with channel distribution information at the transmitter (CDIT) and perfect CSIR is derived.

2.2 Introduction

In contrast to point to point MIMO communication where the CSIT does not affect the spatial multiplexing gain[1], in a multiple-input single-output (MISO) broadcast channel (BC), knowledge of CSIT is crucial for interference mitigation and beamforming purposes [1]. However, the assumption of perfect CSIT may not always be true in practice due to channel estimation error and feedback latency. Therefore, the idea of communication under some sort of imperfection in CSIT has gained more attention recently. The so called MAT algorithm[2] was presented in [2] where it was shown that in terms of the degrees of freedom[3], even an outdated CSIT can result in significant performance improvement in comparison to the case with no CSIT. Assuming correlation between the feedback information and current channel state (e.g., when the feedback latency is smaller than the coherence time of the channel), the authors in [3] and [4] consider the degrees of freedom in a time correlated MISO BC which is shown to be achievable by a combination of zero forcing beamforming (ZFBF) and MAT algorithm. Following these works, the general case of mixed CSIT and the K-user MISO BC with time correlated delayed CSIT are discussed in [5] and [6], respectively. While all these works consider the concept of delayed CSIT in time domain, [7] and [8] deal with the DoF region and its achievable schemes in a frequency correlated MISO BC where there is no delayed CSIT but imperfect CSIT across subbands, which is more inline with practical systems as Long Term Evolution (LTE) [1]. In [9], the synergistic benefits of alternating CSIT over fixed CSIT was presented in a two user MISO BC with two transmit antennas. In [10] and [11], the MISO BC with hybrid CSIT (Perfect or Delayed) was considered. The recent work of [12] investigates the DoF region of the K-user MISO BC with hybrid CSIT and linear encoding at the transmitter. [13] and [14] show that the optimal sum DoF (in the case of perfect CSIT) is achievable if the CSIT is not too delayed in broadcast channels and interference networks, respectively.

[1] The spatial multiplexing gain is the gain achieved when a system is transmitting different streams of data from the same radio resource in separate spatial dimensions.

[2] The term "MAT" comes from the name of the authors in [2].

[3] defined in section 2.3.

The complete characterization of the MISO BC with perfect, delayed or unknown CSIT is an open problem. The main aim of this chapter is to investigate this problem and provide some answers toward this goal. To this end, our contributions are as follows.

- Given the marginal probabilities of CSIT in a K-user MISO BC, we derive an outer bound for the DoF region.
- A set of inequalities is proposed as an outer bound that captures not only the marginals, but also the joint CSIT distribution. This shows that for the K-user case ($K \geq 3$), marginal probabilities are not sufficient for characterizing the DoF region.
- The tightness of the outer bound is investigated in certain cases.
- A two-user MIMO BC is considered in which the CSI of a user is either perfect or unknown. An outer bound for the DoF region is provided and it is shown to be tight when the joint CSIT probabilities satisfy a certain relationship.
- An alternative proof for the DoF region of the K-user MIMO BC with no CSIT and perfect CSIR is provided. Based on this proof, the capacity region of a certain class of MIMO BC with channel distribution information at the transmitter (CDIT) and perfect CSIR is derived.

This chapter is organized as follows. In section 2.3 the system model and preliminaries are presented. An outer bound is provided in section 2.4 based on the marginal probabilities and the proof is given in section 2.5. Section 2.6 provides an outer bound that depends on the joint CSIT probabilities. The tightness of the outerbounds will be discussed in section 2.7. Section 2.8 investigates a two user MIMO BC with CSIT either perfect or unknown, and section 2.9 discusses the K-user MIMO BC with no CSIT.

2.3 System Model

We consider a MISO BC, in which a base station with M antennas sends independent messages $W_1, \ldots, W_K$ to K single-antenna users ($M \geq K$). In a flat fading scenario, the discrete-time baseband received signal of user k at channel use (henceforth, time

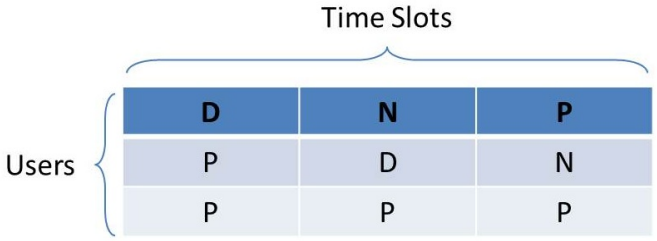

FIGURE 2.1: A CSIT pattern with $\lambda_{DPP} = \lambda_{NDP} = \lambda_{PNP} = \frac{1}{3}$.

instant) t can be written as

$$Y_k(t) = \mathbf{H}_k^H(t)\mathbf{X}(t) + Z_k(t) \ , \ k \in [1:K] \ , \ t \in [1:n] \tag{2.1}$$

where $\mathbf{X}(t) \in C^{(M\times 1)}$ is the transmitted signal at time instant t satisfying the (per codeword) power constraint $\sum_{t=1}^{n} \|\mathbf{x}(t)\|^2 \leq nP$. $Z_k(t)$ and $\mathbf{H}_k(t)$ are the additive white Gaussian noise with unit variance and channel vector of user k, respectively, and are also assumed i.i.d. over the time instants and the users. We assume global perfect Channel State Information at Receivers (CSIR).

The rate tuple $(R_1, R_2, \ldots, R_K)$, in which $R_i = \frac{\log(|W_i|)}{n}$, is achievable if there exists a coding scheme such that the probability of error in decoding W_i at user $i (i \in [1:K])$ can be made arbitrarily small with sufficiently large coding block length. The DoF region is defined as $\{(d_1, \ldots, d_K) | \exists (R_1, R_2, \ldots, R_K) \in C(P)$ such that $d_i = \lim_{P\to\infty} \frac{R_i}{\log P}, \ \forall i\}$ where $C(P)$ is the capacity region (i.e., the closure of the set of achievable rate tuples).

The probabilistic model used in this chapter for CSIT availability allows the transmitter to have a Perfect (P) instantaneous knowledge of the CSI of a particular user at some time instants, whereas at some other time instants it receives the CSI with Delay (D), and finally, for the remaining time instants the CSI of the user is Not known (N) at the transmitter. The CSIT model can be fixed (i.e., as in the hybrid model), alternating, or both (i.e., fixed for a subset of the users and alternating for the remaining subset.) When there is delayed CSIT, we assume that the feedback delay is much larger than the coherence time of the channel making the feedback information completely independent of the current channel state. In this configuration, the joint CSIT of all the K users has at most 3^K states. For example, in a 3 user MISO BC, they will be $PPP, PPD, PPN, PDP, \ldots$ with corresponding probabilities $\lambda_{PPP}, \lambda_{PPD}, \lambda_{PPN}, \lambda_{PDP}, \ldots$ and, as an example, the marginal probability of perfect CSIT for user 1 is $\lambda_P^1 = \sum_{Q,Q' \in \{P,D,N\}} \lambda_{PQQ'}$.

P	D	D
D	P	D
D	D	P

FIGURE 2.2: A symmetric CSIT pattern for the 3-user MISO BC with the marginals $\lambda_P = \frac{1}{3}, \lambda_D = \frac{2}{3}$.

By CSIT pattern we refer to the knowledge of CSIT represented in a space-time matrix where the rows and columns represent users and time slots, respectively. The channel remains fixed within each time slot, while it changes independently from one slot to another. For simplicity, we assume that the delayed CSI arrives at the transmitter after one time slot. Figure 2.1 shows an example of a CSIT pattern, in which the transmitter knows the channels of users 2 and 3 perfectly at time slot 1 and has no information about the channel of user 1. The CSI of user 1 will be known in the next time slot due to feedback delay and is completely independent of the channel in time slot 2.

Finally, a symmetric CSIT pattern means that the marginal probabilities of perfect, delayed and unknown CSIT are the same across the users, i.e. $\lambda_Q^i = \lambda_Q, \ \forall i \in [1 : K], Q \in \{P, D, N\}$. As an example, Figure 2.2 shows a symmetric CSIT pattern for the 3-user MISO BC in which $\lambda_P = \frac{1}{3}, \lambda_D = \frac{2}{3}$.

2.4 An outer bound given the marginals

Theorem 2.1. *Let $\pi^j(.)$ be an arbitrary permutation of size j over the indices $(1, 2, \ldots, K)$, and $\alpha_{\pi^j}(.)$ be an ordering of π^j satisfying*[4]

$$(\lambda_P^{\alpha_{\pi^j}(i)} + \lambda_D^{\alpha_{\pi^j}(i)}) \leq (\lambda_P^{\alpha_{\pi^j}(i+1)} + \lambda_D^{\alpha_{\pi^j}(i+1)}) \quad , \quad i \in [1 : j-1]. \tag{2.2}$$

Given the marginal probabilities of CSIT for user i, an outer bound for the DoF region of the K-user MISO BC with M transmit antennas at the transmitter ($M \geq K$) is defined

[4]The reason for arranging the users according to the sum of the perfect and delayed CSIT probabilities becomes clear in (2.28).

by the following sets of inequalities

$$\sum_{i=1}^{j}\frac{d_{\pi^j(i)}}{i}\leq 1+\sum_{i=2}^{j}\frac{\sum_{r=1}^{i-1}\lambda_P^{\pi^j(r)}}{i(i-1)} \tag{2.3}$$

$$\sum_{i=1}^{j}d_{\pi^j(i)}\leq 1+\sum_{i=1}^{j-1}(\lambda_P^{\alpha_{\pi^j(i)}}+\lambda_D^{\alpha_{\pi^j(i)}}) \quad , \quad \forall\pi^j,\ j\in[1:K]. \tag{2.4}$$

For the symmetric scenario, the sets of inequalities are simplified as

$$\sum_{i=1}^{j}\frac{d_{\pi^j(i)}}{i}\leq 1+\lambda_P\sum_{i=2}^{j}\frac{1}{i} \tag{2.5}$$

$$\sum_{i=1}^{j}d_{\pi^j(i)}\leq 1+(j-1)(\lambda_P+\lambda_D) \quad , \quad \forall\pi^j,\ j\in[1:K]. \tag{2.6}$$

For $K=2$, the outer bound boils down to the optimal DoF region in [9].

2.5 Proof of Theorem 2.1

For simplicity, we assume $j=K$, since it is obvious that each subset of users with cardinality j ($j<K$) can be regarded as a j-user BC. Also, we assume the identity permutation (i.e., $\pi^K(i)=i$) while the results could be easily applied to any other arbitrary permutation.

2.5.1 Proof of (2.3)

First, we improve the channel by giving the message and observation of user i to users $[i+1:K]$ ($i\in[1:K-1]$). Hence, from Fano's inequality,

$$nR_i\leq I(W_i;Y_{[1:i]}^n|W_{[1:i-1]},\Omega^n)+n\epsilon_n \tag{2.7}$$

where Ω^n denotes the global CSIR up to time instant n, $W_0=\emptyset$ and ϵ_n goes to zero as n goes to infinity. By this improvement, channel input and outputs (i.e., the enhanced observations of users) form a Markov chain which results in a physically degraded broadcast channel [15]. Therefore, according to [16], since feedback does not increase the capacity of physically degraded broadcast channels, we can ignore the delayed CSIT (D) and

replace them with No CSIT (N). Therefore, it is equivalent to having the channel of user i perfectly known with probability λ_P^i and not known otherwise. From now on, we ignore the term $n\epsilon_n$ for simplicity (since later it will be divided by n and $n \to \infty$) and write

$$\sum_{i=1}^{K} \frac{nR_i}{i} \leq \sum_{i=1}^{K} \frac{I(W_i; Y_{[1:i]}^n | W_{[1:i-1]}, \Omega^n)}{i} \tag{2.8}$$

$$\leq h(Y_1^n|\Omega^n) + \sum_{i=2}^{K} \left[\frac{h(Y_{[1:i]}^n | W_{[1:i-1]}, \Omega^n)}{i} - \frac{h(Y_{[1:i-1]}^n | W_{[1:i-1]}, \Omega^n)}{i-1} \right] + no(\log P) \tag{2.9}$$

where $Y_0 = \emptyset$ and we have used the fact that $\frac{h(Y_{[1:K]}^n | W_{[1:K]}, \Omega^n)}{nK} \sim o(\log P)$, since with the knowledge of $W_{[1:K]}$ and Ω^n, the observations $Y_{[1:K]}^n$ can be reconstructed within the noise distortion. Before going further, the following lemma is needed.

Lemma 1. Let $\Gamma_N = \{Y_1, Y_2, \ldots, Y_N\}$ be a set of $N(\geq 2)$ arbitrary random variables and $\Psi_i^j(\Gamma_N)$ be a sliding window of size j over Γ_N $(1 \leq i, j \leq N)$ starting from Y_i i.e.,

$$\Psi_i^j(\Gamma_N) = Y_{(i-1)_N+1}, Y_{(i)_N+1}, \ldots, Y_{(i+j-2)_N+1}$$

where $(.)_N$ defines the modulo N operation. Then,

$$(N-m)h(Y_{[1:N]}|A) \leq \sum_{i=1}^{N} h(\Psi_i^{N-m}(\Gamma_N)|A) \quad , \quad 1 \leq m \leq N-1 \tag{2.10}$$

where A is an arbitrary condition.

Before proving the lemma, the following example clarifies the usage of this lemma. Consider $N = 4$ and $m = 1$. We have

$$\Gamma_4 = \{Y_1, Y_2, Y_3, Y_4\}$$
$$\Psi_1^3(\Gamma_4) = Y_1, Y_2, Y_3$$
$$\Psi_2^3(\Gamma_4) = Y_2, Y_3, Y_4$$
$$\Psi_3^3(\Gamma_4) = Y_3, Y_4, Y_1$$
$$\Psi_4^3(\Gamma_4) = Y_4, Y_1, Y_2.$$

Therefore, (2.10) is equivalent to

$$3h(Y_1, Y_2, Y_3, Y_4) \leq h(Y_1, Y_2, Y_3) + h(Y_2, Y_3, Y_4) + h(Y_3, Y_4, Y_1) + h(Y_4, Y_1, Y_2).$$

Note that the number of entropies on the left hand side is the same as the number of arguments of the entopies on the right hand side and vice versa.

Proof. We prove the lemma by showing that for every fixed $m(\geq 1)$, (2.10) holds for all $N(\geq m+1)$ using induction. It is obvious that for every $m(\geq 1)$, (2.10) holds for $N = m+1$. In other words, $h(Y_{[1:N]}|A) \leq \sum_{i=1}^{N} h(Y_i|A)$. Now, considering that (2.10) is valid for $N(\geq m+1)$, we show that it also holds for $N+1$. Replacing N with $N+1$, we have

$$\begin{aligned}
&(N+1-m)h(Y_{[1:N+1]}|A) \\
&= h(Y_{[1:N+1]}|A) + (N-m)h(Y_{[1:N-1]}, \overbrace{Y_N, Y_{N+1}}^{Z}|A) \\
&\leq h(Y_{[1:N+1]}|A) + \sum_{i=1}^{N} h(\Psi_i^{N-m}(\Phi_N)|A) && (2.11) \\
&= h(Y_{[1:N+1]}|A) + \sum_{i=1}^{m} h(\Psi_i^{N-m}(\Phi_N)|A) + \sum_{i=m+1}^{N} h(\Psi_i^{N+1-m}(\Gamma_{N+1})|A) && (2.12) \\
&= h(Y_{[N-m+1:N]}|Y_{N+1}, Y_{[1:N-m]}, A) + \sum_{i=1}^{m} h(\Psi_i^{N-m}(\Phi_N)|A) + h(Y_{N+1}, Y_{[1:N-m]}|A) \\
&\quad + \sum_{i=m+1}^{N} h(\Psi_i^{N+1-m}(\Gamma_{N+1})|A) && (2.13) \\
&= h(Y_{[N-m+1:N]}|Y_{N+1}, Y_{[1:N-m]}, A) + \sum_{i=1}^{m} h(\Psi_i^{N-m}(\Phi_N)|A) + \sum_{i=m+1}^{N+1} h(\Psi_i^{N+1-m}(\Gamma_{N+1})|A) \\
&= \sum_{i=1}^{m} h(Y_{N-m+i}|Y_{N+1}, Y_{[1:N-m+i-1]}, A) + \sum_{i=1}^{m} h(Y_{[i:N-m+i-1]}|A) \\
&\quad + \sum_{i=m+1}^{N+1} h(\Psi_i^{N+1-m}(\Gamma_{N+1})|A) && (2.14)
\end{aligned}$$

$$\leq \sum_{i=1}^{m} h(Y_{N-m+i}|Y_{[i:N-m+i-1]}, A) + \sum_{i=1}^{m} h(Y_{[i:N-m+i-1]}|A) + \sum_{i=m+1}^{N+1} h(\Psi_i^{N+1-m}(\Gamma_{N+1})|A) \tag{2.15}$$

$$= \sum_{i=1}^{m} h(\Psi_i^{N+1-m}(\Gamma_{N+1})|A) + \sum_{i=m+1}^{N+1} h(\Psi_i^{N+1-m}(\Gamma_{N+1})|A)$$

$$= \sum_{i=1}^{N+1} h(\Psi_i^{N+1-m}(\Gamma_{N+1})|A) \tag{2.16}$$

where in (2.11), $\Phi_N = \{Y_{[1:N-1]}, Z\}$ and we have used the validity of (2.10) for N. In (2.12), we have used the fact that $\Psi_i^{N+1-m}(\Gamma_{N+1}) = \Psi_i^{N-m}(\Phi_N)$ for $i \in [m+1:N]$. In (2.13), the chain rule of entropies is used and in (2.14), the sliding window is written in terms of its elements. Finally, in (2.15), the fact that conditioning reduces the differential entropy is used. Therefore, since $m(\geq 1)$ was chosen arbitrarily and (2.10) is valid for $N = m+1$ and from its validity for $N(\geq m+1)$ we could show it also holds for $N+1$, we conclude that (2.10) holds for all values of m and N satisfying $1 \leq m \leq N-1$. □

Each term in the summation of (2.9) can be rewritten as

$$\frac{(i-1)h(Y_{[1:i]}^n|W_{[1:i-1]}, \Omega^n) - ih(Y_{[1:i-1]}^n|W_{[1:i-1]}, \Omega^n)}{i(i-1)}$$

$$= \frac{(i-1)h(\Gamma_i|T_{i,n}) - ih(Y_{[1:i-1]}^n|T_{i,n})}{i(i-1)}$$

$$\leq \frac{\sum_{r=1}^{i} \left[h(\Psi_r^{i-1}(\Gamma_i)|T_{i,n}) - h(Y_{[1:i-1]}^n|T_{i,n})\right]}{i(i-1)} \tag{2.17}$$

$$= \frac{\sum_{r=1}^{i-1} \left[h(Y_i^n|E_{r,i}, T_{i,n}) - h(Y_r^n|E_{r,i}, T_{i,n})\right]}{i(i-1)} \tag{2.18}$$

where $\Gamma_i = \{Y_{[1:i]}^n\}$, $T_{i,n} = \{W_{[1:i-1]}, \Omega^n\}$ and $E_{r,i} = \{Y_{[1:i-1]}^n\} - \{Y_r^n\}$. (2.17) is from the application of Lemma 1 ($m = 1$) and (2.18) is from the chain rule of entropies. Before going further, the following lemma is needed. This lemma, which is based on [17], is the key part in the proof.

Lemma 2. In the K-user MISO BC defined in (2.1), for the users $m, q \in [1:K]$ $(m \neq q)$, we have

$$\lim_{n,P\to\infty} \frac{h(Y_m^n|A) - h(Y_q^n|A)}{n \log P} \leq \begin{cases} 1 & \text{CSIT of } q \text{ is } P \\ 0 & \text{CSIT of } q \text{ is } N \end{cases} \tag{2.19}$$

where A is a condition such as the condition of entropies in (2.18) or later in (2.25). Interestingly, (2.19) is only a function of the CSIT of the second user.

Proof. Based on the four possible states for the joint CSIT of m and q, we have

1. CSIT of m is N or P and CSIT of q is P

$$h(Y_m^n|A) - h(Y_q^n|A) \leq \underbrace{h(Y_m^n|A)}_{\leq n\log(P)} - \underbrace{h(Y_q^n|A, W_{[1:K]})}_{no(\log P)} \tag{2.20}$$

   A Gaussian input with the conditional covariance matrix of $\Sigma_{X|A} = P\mathbf{u}_q^{\perp}\mathbf{u}_q^{\perp H}$ achieves the upper bound, where $\mathbf{u}_q^{\perp}$ is a unit vector in the direction orthogonal to $\mathbf{H}_q$ (since $\mathbf{H}_q$ is known).

2. CSIT of m is N and CSIT of q is N

   In this case both Y_m^n and Y_q^n are statistically equivalent (i.e., having the same probability density functions, and subsequently, the same entropies.) Therefore,

$$h(Y_m^n|A) - h(Y_q^n|A) = 0 \tag{2.21}$$

3. CSIT of m is P and CSIT of q is N

   This is the second result of Theorem 1 in [17],i.e., "Settling the PN conjecture".[5].

□

From (2.9) and (2.18), we have

$$\begin{aligned}\sum_{i=1}^{K}\frac{nR_i}{i} \leq & \sum_{i=2}^{K}\sum_{r=1}^{i-1}\frac{h(Y_i^n|A_{r,i}) - h(Y_r^n|A_{r,i})}{i(i-1)} \\ & + n\log P + no(\log P) \\ \leq & \, n\log P + \sum_{i=2}^{K}\sum_{r=1}^{i-1}\frac{n\lambda_P^r}{i(i-1)}\log P + no(\log P)\end{aligned} \tag{2.22}$$

[5]The differential entropy terms in the left hand side of (2.19) can be written in terms of the expectation of the difference of entropies conditioned on the realizations of A. Since the conditional probability density functions exist and have a bounded peak, the same steps of [17] as discretization, considering the cannonical form and bounding the cardinality of aligned image set can be applied.

where $A_{r,i}$ is the condition of the entropies in (2.18) and (2.22) is from the application of lemma 2 and the fact that n is sufficiently large. Therefore,

$$\sum_{i=1}^{K} \frac{d_i}{i} \leq 1 + \sum_{i=2}^{K} \frac{\sum_{r=1}^{i-1} \lambda_P^r}{i(i-1)}. \tag{2.23}$$

It is obvious that the same approach can be applied to any other permutations on $(1, 2, \ldots, K)$ which results in (2.3).

2.5.2 Proof of (2.4)

We enhance the channel in two ways:

1. Like the approach in [9], whenever there is delayed CSIT (D), we assume that it is perfect instantaneous CSIT (P), but we keep the probability of delayed CSIT. In other words, the CSIT of user i is perfect with probability $\lambda_P^i + \lambda_D^i$ and unknown otherwise.

2. We give the message of user i to users $[i+1 : K]$.

Therefore,

$$nR_i \leq I(W_i; Y_i^n | W_{[1:i-1]}, \Omega^n) + n\epsilon_n \ , \ \forall i \in [1 : K]. \tag{2.24}$$

By summing (2.24) over users and writing the mutual information in terms of differential entropies,

$$\sum_{i=1}^{K} nR_i \leq \overbrace{h(Y_1^n | \Omega^n)}^{\leq n \log P} + \sum_{i=2}^{K} \left[h(Y_i^n | W_{[1:i-1]}, \Omega^n) - h(Y_{i-1}^n | W_{[1:i-1]}, \Omega^n) \right] + no(\log P). \tag{2.25}$$

By applying the results of Lemma 2 to (2.25), we have

$$\sum_{i=1}^{K} d_i \leq 1 + \sum_{i=2}^{K} (\lambda_P^{i-1} + \lambda_D^{i-1}) = 1 + \sum_{i=1}^{K-1} (\lambda_P^i + \lambda_D^i). \tag{2.26}$$

P	N	N
N	P	N
N	N	P

FIGURE 2.3: A symmetric CSIT pattern for the 3-user MISO BC.

Let $\pi^K(.)$ be an arbitrary permutation of size K on $(1,\ldots,K)$. Applying the same reasoning, we have

$$\sum_{i=1}^{K} d_i \leq 1 + \sum_{i=1}^{K-1} (\lambda_P^{\pi^K(i)} + \lambda_D^{\pi^K(i)}) \quad , \quad \forall \pi^K(.). \tag{2.27}$$

(2.27) results in K inequalities all having the same left hand side. Therefore,

$$\sum_{i=1}^{K} d_i \leq 1 + \min_{\pi^K(.)} \sum_{i=1}^{K-1} (\lambda_P^{\pi^K(i)} + \lambda_D^{\pi^K(i)}) \tag{2.28}$$

This is due to the possible orders of channel enhancements and it is obvious that $\alpha_{\pi^K}(.)$ will minimize (2.28) if it satisfies (2.2) (for $j = K$.)

2.6 An outer bound capturing the joint CSIT probabilities

In the previous section, an outer bound was provided in terms of the marginal probabilities. In this section, we tighten the outer bound by introducing a set of inequalities that captures the joint CSIT probabilities. We start with simple motivating examples. Consider the pattern shown in Figure 2.3 with $\lambda_{PNN} = \lambda_{NPN} = \lambda_{NNP} = \frac{1}{3}$. By Fano's inequality, we write,

$$nR_1 \leq I(W_1; Y_1^n | \Omega^n) \tag{2.29}$$

$$nR_1 \leq I(W_1; Y_1^n | \Omega^n, W_2). \tag{2.30}$$

Adding (2.29) and (2.30) results in

$$2nR_1 \leq I(W_1; Y_1^n | \Omega^n) + I(W_1; Y_1^n | \Omega^n, W_2). \tag{2.31}$$

By doing the same for R_2, we have

$$2nR_2 \leq I(W_2; Y_2^n|\Omega^n) + I(W_2; Y_2^n|\Omega^n, W_1). \tag{2.32}$$

Finally, the rate of user 3 is written as

$$nR_3 \leq I(W_3; Y_3^n|\Omega^n, W_1, W_2). \tag{2.33}$$

Therefore,

$$\begin{aligned}
2nR_1 + 2nR_2 + nR_3 \leq & \underbrace{h(Y_2^n|\Omega^n, W_1) - h(Y_1^n|\Omega^n, W_1)}_{\leq \frac{n}{3}\log P} + h(Y_3^n|\Omega^n, W_1, W_2) \\
& \underbrace{+h(Y_1^n|\Omega^n, W_2) - h(Y_2^n|\Omega^n, W_2)}_{\leq \frac{n}{3}\log P} + \underbrace{h(Y_1^n|\Omega^n)}_{\leq n\log P} + \underbrace{h(Y_2^n|\Omega^n)}_{\leq n\log P} \\
& \underbrace{-h(Y_1^n|\Omega^n, W_1, W_2) - h(Y_2^n|\Omega^n, W_1, W_2)}_{\leq -h(Y_1^n, Y_2^n|\Omega^n, W_1, W_2)} \qquad (2.34) \\
\leq & \frac{8n}{3}\log P + h(Y_3^n|\Omega^n, W_1, W_2) - h(Y_1^n, Y_2^n|\Omega^n, W_1, W_2) \qquad (2.35) \\
= & \underbrace{h(Y_3^n|\Omega^n, W_1, W_2) - h(Y_{2,PNN}^n, Y_{1,NPN}^n, Y_{1,NNP}^n|\Omega^n, W_1, W_2)}_{o(\log P)} \\
& + \frac{8n}{3}\log P \\
& \underbrace{-h(Y_{1,PNN}^n, Y_{2,NPN}^n, Y_{2,NNP}^n|\Omega^n, W_1, W_2, Y_{2,PNN}^n, Y_{1,NPN}^n, Y_{1,NNP}^n)}_{\leq -h(Y_{1,PNN}^n, Y_{2,NPN}^n, Y_{2,NNP}^n|\Omega^n, W_1, W_2, Y_{2,PNN}^n, Y_{1,NPN}^n, Y_{1,NNP}^n, W_3) \sim o(\log P)} \\
& \qquad (2.36) \\
\leq & \frac{8n}{3}\log P \qquad (2.37)
\end{aligned}$$

where in (2.34), lemma 2 is applied to the differences resulting in the values written under the braces. We have split the observations of users 1 and 2 in terms of the joint CSIT, i.e., $Y_1^n = (Y_{1,PNN}^n, Y_{1,NPN}^n, Y_{1,NNP}^n)$ and $Y_2^n = (Y_{2,PNN}^n, Y_{2,NPN}^n, Y_{2,NNP}^n)$ such that, for example, $Y_{2,PNN}^n$ denotes the received signal of user 2 when the joint CSIT is PNN. (2.36) is due to the facts that there is at least one unknown CSIT (N) in the joint states of user 1 and user 2 (i.e., PN, NP and NN. see rows 1 and 2 of the CSIT pattern shown in figure 2.3). Therefore, we have the following inequalities for the pattern shown

in figure 2.3

$$\begin{aligned} 2d_1 + 2d_2 + d_3 &\leq \frac{8}{3} \\ 2d_1 + d_2 + 2d_3 &\leq \frac{8}{3} \\ d_1 + 2d_2 + 2d_3 &\leq \frac{8}{3}. \end{aligned} \tag{2.38}$$

From (2.38), the sum DoF of the pattern in figure 2.3 has the upper bound of $\frac{8}{5}$, while it can be easily verified that for the pattern with PPP in the first slot and NNN in the next two slots, which has the same marginals as in figure 2.3, the sum DoF is $\frac{5}{3}(\geq \frac{8}{5})$. This simple example confirms that for the K-user MISO BC ($K \geq 3$), the marginal probabilities are not sufficient in characterizing the DoF region[6]. Motivated by this simple example, we can have the following set of inequalities for the 3-user MISO BC with P and N

$$\begin{aligned} 2d_1 + 2d_2 + d_3 &\leq 2 + 2\lambda_P + \lambda_{PP-} \\ 2d_1 + d_2 + 2d_3 &\leq 2 + 2\lambda_P + \lambda_{P-P} \\ d_1 + 2d_2 + 2d_3 &\leq 2 + 2\lambda_P + \lambda_{-PP} \end{aligned} \tag{2.39}$$

where a dashed line in the above means that the CSIT of the corresponding user is not important (for example, $\lambda_{PP-} = \lambda_{PPP} + \lambda_{PPN}$ which is a summation over all the possible states for the CSIT of user 3). By looking at the difference of entropies in (2.35), it is observed that this difference is of order $o(\log P)$ when there is at least one N in the joint CSIT of users 1 and 2 (i.e., PNN, PNP, NPN, NPP, NNP and NNN) and, therefore, is upperbounded by $n(\lambda_{PPP}+\lambda_{PPN})\log P$. This results in the first inequality of (2.39) and the same reasoning applies to the remaining two inequalities. (2.39) is a set of inequalities that captures the joint CSIT probabilities and is not only a function of the marginals.

Now consider the pattern shown in figure 2.4 for the 4-user MISO BC. From (2.31),

[6]It is important to emphasize on the difference between the following two statements
a) Two CSIT patterns with **different marginals** can have the **same** DoF regions.
b) Two CSIT patterns with **the same marginals** can have **different** DoF regions.
The first statement is already known in literature. For example, by comparing the original 2-user MAT (i.e., $\lambda_D = 1$) and the scheme DN,ND,NN in [9], it is concluded that both of them have the sum DoF of 4/3, while having different marginal prbabilities (for the latter, $\lambda_D = \frac{1}{3}$). However, the set of inequalities proposed in this section addresses the second statement which is a new problem and cannot result from the first statement.

P	N	N	N
N	P	N	N
N	N	P	N
N	N	N	P

FIGURE 2.4: A symmetric CSIT pattern for the 4-user MISO BC.

(2.32) and (2.33), we can write

$$\begin{aligned}
2n(R_1+R_2+R_3) \leq & \underbrace{h(Y_2^n|\Omega^n,W_1)-h(Y_1^n|\Omega^n,W_1)}_{\leq \frac{n}{4}\log P} \\
& \underbrace{+h(Y_1^n|\Omega^n,W_2)-h(Y_2^n|\Omega^n,W_2)}_{\leq \frac{n}{4}\log P}+\underbrace{h(Y_1^n|\Omega^n)}_{\leq n\log P}+\underbrace{h(Y_2^n|\Omega^n)}_{\leq n\log P} \\
& \underbrace{+h(Y_3^n|\Omega^n,W_1,W_2)-h(Y_1^n|\Omega^n,W_1,W_2)}_{\leq \frac{n}{4}\log P} \\
& \underbrace{+h(Y_3^n|\Omega^n,W_1,W_2)-h(Y_2^n|\Omega^n,W_1,W_2)}_{\leq \frac{n}{4}\log P} \\
& -2h(Y_3^n|\Omega^n,W_1,W_2,W_3) \\
\leq & \, 3n\log P-2h(Y_3^n|\Omega^n,W_1,W_2,W_3) \qquad (2.40)
\end{aligned}$$

Alternatively, we can change the role of users 1 and 3 and write

$$\begin{aligned}
2nR_1 &\leq I(W_1;Y_1^n|\Omega^n,W_2,W_3)+I(W_1;Y_1^n|\Omega^n,W_2,W_3) \\
2nR_2 &\leq I(W_2;Y_2^n|\Omega^n)+I(W_2;Y_2^n|\Omega^n,W_3) \\
2nR_3 &\leq I(W_3;Y_3^n|\Omega^n)+I(W_3;Y_3^n|\Omega^n,W_2).
\end{aligned}$$

Following the same reasoning in (2.40), we have

$$2n(R_1+R_2+R_3) \leq 3n\log P-2h(Y_1^n|\Omega^n,W_1,W_2,W_3). \qquad (2.41)$$

Adding (2.40) and (2.41), we have

$$\begin{aligned}
4n(R_1+R_2+R_3) &\leq 6n\log P-2\left(h(Y_1^n|\Omega^n,W_1,W_2,W_3)+h(Y_3^n|\Omega^n,W_1,W_2,W_3)\right) \\
&\leq 6n\log P-2h(Y_1^n,Y_3^n|\Omega^n,W_1,W_2,W_3). \qquad (2.42)
\end{aligned}$$

For the rate of user 4, we can write

$$\begin{aligned} 2nR_4 &\leq 2I(W_4; Y_4^n|\Omega^n, W_1, W_2, W_3) \\ &= 2h(Y_4^n|\Omega^n, W_1, W_2, W_3) \underbrace{-2h(Y_4^n|\Omega^n, W_1, W_2, W_3, W_4)}_{o(\log P)}. \end{aligned} \tag{2.43}$$

Adding (2.42) and (2.43), we get

$$\begin{aligned} &4n(R_1 + R_2 + R_3) + 2nR_4 \\ &\leq 6n \log P + 2\left(h(Y_4^n|\Omega^n, W_1, W_2, W_3) - h(Y_1^n, Y_3^n|\Omega^n, W_1, W_2, W_3)\right) \qquad (2.44) \\ &\leq 6n \log P + \\ &\underbrace{2\left(h(Y_4^n|\Omega^n, W_1, W_2, W_3) - h(Y_{3,PNNN}^n, Y_{1,NPNN}^n, Y_{1,NNPN}^n, Y_{1,NNNP}^n|\Omega^n, W_1, W_2, W_3)\right)}_{o(\log P)} \\ &- 2h(T_n|Y_{3,PNNN}^n, Y_{1,NPNN}^n, Y_{1,NNPN}^n, Y_{1,NNNP}^n, \Omega^n, W_1, W_2, W_3) \qquad (2.45) \\ &\leq 6n \log P \underbrace{-2h(T_n|Y_{3,PNNN}^n, Y_{1,NPNN}^n, Y_{1,NNPN}^n, Y_{1,NNNP}^n, \Omega^n, W_1, W_2, W_3, W_4)}_{o(\log P)}. \end{aligned}$$

$$\tag{2.46}$$

where $T_n = \{Y_1^n, Y_3^n\} - \{Y_{3,PNNN}^n, Y_{1,NPNN}^n, Y_{1,NNPN}^n, Y_{1,NNNP}^n\}$. Therefore, we have

$$2d_1 + 2d_2 + 2d_3 + d_4 \leq 3 \tag{2.47}$$

In the left hand side of (2.47), user 4 has the coefficient of 1 and the remaining 3 users have the coefficient of 2. Also, instead of changing the roles of user 1 and 3, roles of user 2 and 3 or roles of user 1 and 2 could have been changed. Although this $\binom{3}{2}$ changes would not result in a new inequality due to the structure of the pattern shown in figure 2.4, these changes of the roles of the remaining 3 users (with coefficient 2) are necessary in general. Therefore, motivated by this simple example, we can have a set of inequalities for the 4-user MISO BC with P and N.

$$\begin{aligned} 2d_1 + 2d_2 + 2d_3 + d_4 &\leq 2 + 4\lambda_P + \min\{\lambda_{PP--}, \lambda_{P-P-}, \lambda_{-PP-}\} \\ d_1 + 2d_2 + 2d_3 + 2d_4 &\leq 2 + 4\lambda_P + \min\{\lambda_{-PP-}, \lambda_{-P-P}, \lambda_{--PP}\} \\ 2d_1 + d_2 + 2d_3 + 2d_4 &\leq 2 + 4\lambda_P + \min\{\lambda_{P-P-}, \lambda_{P--P}, \lambda_{--PP}\} \\ 2d_1 + 2d_2 + d_3 + 2d_4 &\leq 2 + 4\lambda_P + \min\{\lambda_{P--P}, \lambda_{PP--}, \lambda_{-P-P}\} \end{aligned} \tag{2.48}$$

where each inequality in (2.48) is obtained from $\binom{3}{2}$ inequalities each of which with the same left hand side. The general K-user MISO BC can be addressed by using the following definition

$$\lambda(a,b) = \text{ The probability that the CSIT of users } a \text{ and } b \text{ is perfect.}$$
$$a,b \in [1:K]\ ,\ a \neq b. \tag{2.49}$$

Theorem 2.2. *Let $\pi^j(.)$ be an arbitrary permutation of size j over $[1:K]$. For the K-user symmetric MISO BC with no delayed CSIT, we have*[7]

$$2\sum_{i=1}^{j-1} d_{\pi^j(i)} + d_{\pi^j(j)} \leq 2 + 2(j-2)\lambda_P + \min_{a,b\in[1:j-1]:a<b}\{\lambda(\pi^j(a),\pi^j(b))\} \quad \forall \pi^j, j \in [3:K]. \tag{2.50}$$

Proof. The proof is a straightforward generalization of the previous examples. □

2.7 On the achievability

In this section, we consider the bounds in (2.6) for the symmetric scenario. [8] For $K \geq 3$, we show that given the marginal probabilities of CSIT, there exists at least one CSIT pattern that achieves the outer bound in the following two scenarios.

2.7.1 $\lambda_D = 0$

In this case, $2^K - 1$ inequalities in (2.5) are active and the remaining inequalities become inactive. The reason can be easily verified from the inequalities, however, a simpler intuitive way is to consider that when there is no delayed CSIT, those inequalities derived from the degraded broadcast channel are inactive. In this case, the region is defined by $2^K - 1$ hyperplanes in R_+^K and has the following K corner points

$$(1,\lambda_P,\ldots,\lambda_P),(\lambda_P,1,\lambda_P,\ldots,\lambda_P),\ldots,(\lambda_P,\ldots,\lambda_P,1) \tag{2.51}$$

[7] The assumptions of symmetric scenario and no delayed CSIT are only used for the readability of formulations. It is important to note that the approach in this section can be applied to the general asymmetric scenario including the delayed CSIT (in this case, the delay is enhanced to perfect instantaneous as in subsection 2.5.2).

[8] The main goal of this section is to show that these bounds can become tight and are not always loose.

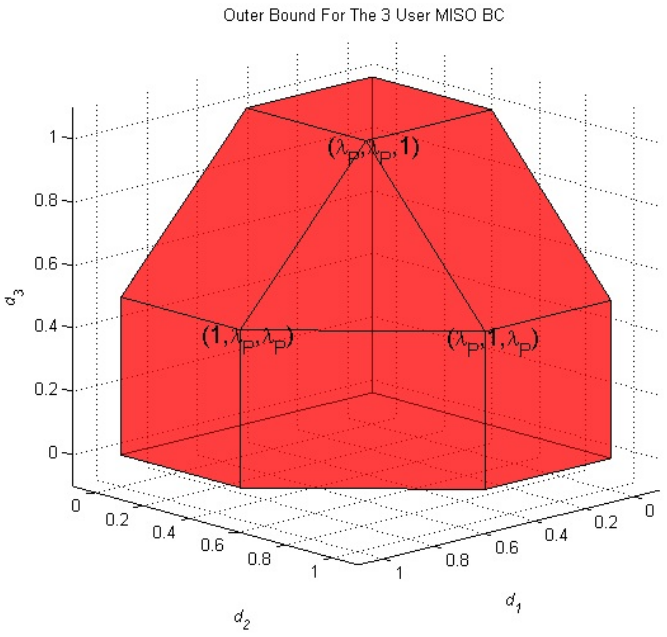

FIGURE 2.5: Region in case A for 3 user BC

The corner points have the unique characteristic that the whole region can be constructed by time sharing between them. Therefore, the achievability of these points is equivalent to the achievability of the whole region. Figure 2.5 shows the region for the 3 user broadcast channel. The corner points are simply achieved by a scheme that has N time slots and consists of two parts: in the first $\lambda_P N$ time slots, zero forcing beamforming (ZFBF) is carried out where each user receives one interference-free symbol. In the remaining $\lambda_N N$ time slots, only one particular user (depending on the corner point of interest) is scheduled.

2.7.2 $\lambda_N \leq \frac{\lambda_D}{\sum_{j=2}^{K} \frac{1}{j}}$

Before going further, we need the following simple lemma.

Lemma 3. The minimum probability of delayed CSIT for sending order-j symbols in the K-user MAT is

$$\lambda_D^{min}(K,j) = 1 - \frac{K-j+1}{K\sum_{i=j}^{K}\frac{1}{i}}. \tag{2.52}$$

Proof. From [2], the MAT algorithm is based on a concatenation of K phases. Phase j takes $(K-j+1)\binom{K}{j}$ order-j messages as its input, takes $\binom{K}{j}$ time slots and produces $j\binom{K}{j+1}$ order-$j+1$ messages as its output. In each time slot of phase j, the transmitter

sends a random linear combination of the $(K-j+1)$ symbols to a subset S of receivers , $|S| = j$. Sending the overheard interferences from the remaining $(K-j)$ receivers to receivers in subset S enables them to successfully decode their $(K-j+1)$ symbols by constructing a set of $(K-j+1)$ linearly independent equations. Therefore, the transmitter needs to know the channel of only $(K-j)$ receivers. In other words, at each time slot of phase j, the feedback of $(K-j)$ CSI is enough. In the MAT algorithm the number of output symbols that phase j produces should match the number of input symbols of phase $j+1$. The ratio between the input of phase $j+1$ and output of phase j is:

$$\frac{(K-j)\binom{K}{j+1}}{j\binom{K}{j+1}} = \frac{(K-j)}{j}.$$

This means that $(K-j)$ repetition of phase j will produce the inputs needed by j repetition of phase $j+1$. In general, in order to have an integer number for repetitions, we multiply phase 1 by $K!$ (i.e., repeat it $K!$ times), phase 2 by $\frac{K!}{(K-1)}$, and so on. Therefore, phase j will be repeated $((j-1)!(K-j)!)K$ times which takes $((j-1)!(K-j)!)K\binom{K}{j}$ time slots. Since $(K-j)$ feedbacks from each time slot is sufficient, the number of feedbacks will be $((j-1)!(K-j)!)K\binom{K}{j}(K-j)$. For a successive decoding or order-j symbols, all the higher order symbols must be decoded successfully. Therefore, instead of having delayed CSIT at all time instants from all users, the minimum probability of delayed CSIT is the number of feedbacks from phase j to K divided by the whole number of time slots multiplied by the number of users,

$$\begin{aligned}\lambda_D^{min}(K,j) &= \frac{\sum_{i=j}^{K}(i-1)!(K-i)!K\binom{K}{i}(K-i)}{\sum_{i=j}^{K}(i-1)!(K-i)!K\binom{K}{j+1}K} \\ &= 1 - \frac{K-j+1}{K\sum_{i=j}^{K}\frac{1}{i}}.\end{aligned}$$

□

In this case (i.e., $\lambda_N \leq \frac{\lambda_D}{\sum_{j=2}^{K}\frac{1}{j}}$), the $2^K - K - 1$ inequalities having $\sum_i d_i$ (summation with equal weights) in the left-hand side become inactive and the remaining $\sum_{j=1}^{K} j!\binom{K}{j}$ inequalities are active which construct $\sum_{j=1}^{K} j!\binom{K}{j}$ hyperplanes in R_+^K. The region has $2^K - 1$ corner points. In other words, if the coordinates of a point are shown as $(p_1, p_2, \ldots, p_K)$, there are $\binom{K}{j}$ $(j \in [1:K])$ points where j of its K coordinates are $\frac{1+\lambda_P\sum_{i=2}^{j}\frac{1}{i}}{\sum_{i=1}^{j}\frac{1}{i}}$ and the remaining $K-j$ coordinates are λ_P. The region for the 3 user

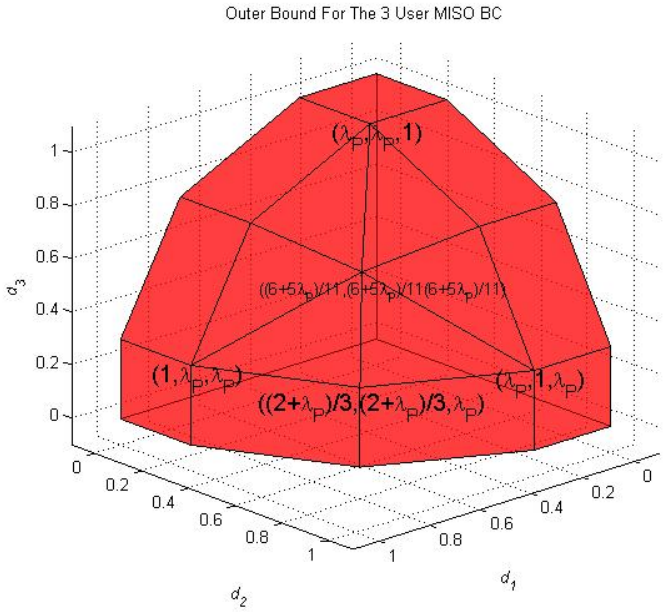

FIGURE 2.6: Region in case B for 3 user BC

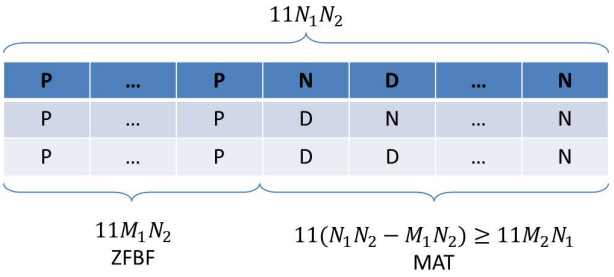

FIGURE 2.7: Achievable scheme in case B for 3 user BC

broadcast channel and the achievable scheme are shown in figure 2.6 and figure 2.7, respectively. The achievable scheme is based on a concatenation of ZFBF and MAT as follows. For the $\binom{K}{j}$ corner points, we write

$$\lambda_P = \frac{M_1}{N_1}, \lambda_D = \frac{M_2}{N_2}, \lambda_D^{min}(j,1) = \frac{m}{n} \tag{2.53}$$

where m, n, M_i and N_i $(i = 1, 2)$ are integers. Making a common denominator between λ_P and λ_D we have

$$\lambda_P = \frac{nM_1N_2}{nN_1N_2}, \lambda_D = \frac{nN_1M_2}{nN_1N_2}. \tag{2.54}$$

We construct nN_1N_2 time slots where the CSIT of each user can be Perfect (P) or Delayed (D) in nM_1N_2 or nN_1M_2 time slots, respectively. In the first nM_1N_2 time slots, ZFBF is carried out. In the remaining $n(N_1N_2 - M_1N_2)$ time slots, j-user MAT

P	N
P	N
N	P

FIGURE 2.8: An example.

algorithm is done. At each time slot of the ZFBF part, 1 interference-free symbol is received by each user and in the MAT part, $\frac{n(N_1N_2-M_1N_2)}{1+\frac{1}{2}+\cdots+\frac{1}{j}}$ symbols are sent to each of the users in subset S (with $|S|=j$) where S depends on the corner point of interest. In order to do the MAT algorithm in the second part, the minimum probability of delayed CSIT should be met

$$nN_1M_2 \geq \lambda_D^{min}(j)n(N_1N_2 - M_1N_2) \tag{2.55}$$

Dividing both sides by nN_1N_2,

$$\lambda_D \geq \lambda_D^{min}(j,1)(1-\lambda_P) = \lambda_D^{min}(j,1)(\lambda_D+\lambda_N) \tag{2.56}$$

which results in

$$\lambda_N \leq \frac{\lambda_D}{\sum_{i=2}^{j}\frac{1}{i}}. \tag{2.57}$$

Since it should be valid for all j, we have

$$\lambda_N \leq \frac{\lambda_D}{\sum_{i=2}^{K}\frac{1}{i}}. \tag{2.58}$$

which is the condition assumed in this case.

Finally, through an example, we show that the bounds in Theorem 2.2 can be tight. Consider the pattern shown in figure 2.8. According to sections 2.4 and 2.6, the DoF region has the following outer bound

$$0 \leq d_1, d_2, d_3 \leq 1 \quad , \quad d_1+d_2 \leq \frac{3}{2} \tag{2.59}$$

$$2d_1+d_2+2d_3 \leq 3 \tag{2.60}$$

$$d_1+2d_2+2d_3 \leq 3. \tag{2.61}$$

The achievable point $(d_1,d_2,d_3)=(\frac{1}{2},\frac{1}{2},\frac{3}{4})$ makes the inequalities in (2.60) and (2.61) tight therefore, it is on the boundary of DoF region. This point is achievable as shown in figure 2.9 where the receivers are called A,B and C. Symbols are shown in red where

u_C	$L_2(u_C, u_A)$	v_A	...
v_C	...	v_B	$L_3(v_C, u_B)$
$L_1(u_C, v_C, w_C)$	u_C	...	v_C

FIGURE 2.9: The achievable scheme for the boundary point $(\frac{1}{2}, \frac{1}{2}, \frac{3}{4})$.

the transmitter has perfect CSIT and those received signals that are not important in the achievability scheme are shown as "...".

2.8 Two user MIMO

In previous sections, the K-user MISO BC was considered. The general MIMO BC is more challenging due to the mismatch between the number of receive antennas[9]. In this section, we consider a two user MIMO BC where each user is equipped with N_k ($k \in [1:2]$) antennas and a base station with $M(\geq N_1 + N_2)$ antennas wishes to send two independent messages W_1 and W_2 to their corresponding receivers. The received signal of user k is given by

$$\mathbf{Y}_k(t) = \mathbf{H}_k^H(t)\mathbf{X}(t) + \mathbf{W}_k(t) \ , \ k \in [1:2] \ , \ t \in [1:n] \tag{2.62}$$

where the channel matrices are assumed to be full rank almost surely. We assume that the CSI of a particular user is either instantaneously Perfect (P) or Not known (N) resulting in the four possible states PP, PN, NP and NN with corresponding probabilities $\lambda_{PP}, \lambda_{PN}, \lambda_{NP}$ and λ_{NN}. Let $Y_{i,j}$ denote the received signal at the j^{th} antenna of user i ($i \in [1:2], j \in [1:N_i]$). Without loss of generality, we assume $N_1 \geq N_2$. An outer bound on the DoF region is provided in Theorem 3 and its achievability is discussed afterwards.

Theorem 2.3. *An outer bound for the DoF region of the channel in (2.62) is given by*

$$\frac{d_1}{N_1} + \frac{d_2}{N_2} \leq 1 + \lambda_{PP} + \lambda_{NP} = 1 + \lambda_P^2 \tag{2.63}$$

$$d_1 + d_2 \leq N_1 + N_2(\lambda_{PP} + \lambda_{PN}) = N_1 + N_2\lambda_P^1 \tag{2.64}$$

[9]It is important to note that with different number of antennas, as stated in [18], the dimensions of useful signals and interference signals are not the same in contrast to the symmetric case. Furthermore, the users have different capabilities of decoding which must be taken into account in the achievability schemes.

Proof. By enhancing user 1 with the message of user 2, Fano's inequality (ignoring $n\epsilon_n$) results in

$$nR_1 \leq I(W_1; \mathbf{Y}_1^n|\Omega^n, W_2) = h(\mathbf{Y}_1^n|\Omega^n, W_2) - \underbrace{h(\mathbf{Y}_1^n|\Omega^n, W_1, W_2)}_{no(\log P)} \tag{2.65}$$

$$nR_2 \leq I(W_2; \mathbf{Y}_2^n|\Omega^n) = \underbrace{h(\mathbf{Y}_2^n|\Omega^n)}_{\leq nN_2 \log P} - h(\mathbf{Y}_2^n|\Omega^n, W_2). \tag{2.66}$$

Ignoring $o(\log P)$, we have

$$n(N_2R_1 + N_1R_2) \leq nN_1N_2 \log P + N_2 h(\mathbf{Y}_1^n|\Omega^n, W_2) - N_1 h(\mathbf{Y}_2^n|\Omega^n, W_2) \tag{2.67}$$

$$\leq nN_1N_2 \log P + \sum_{i=1}^{N_1} h(\Psi_i^{N_2}(\Gamma_{N_1})|\Omega^n, W_2) - N_1 h(\mathbf{Y}_2^n|\Omega^n, W_2) \tag{2.68}$$

$$= nN_1N_2 \log P + \sum_{i=1}^{N_1} \left[h(\Psi_i^{N_2}(\Gamma_{N_1})|\Omega^n, W_2) - h(\mathbf{Y}_2^n|\Omega^n, W_2)\right] \tag{2.69}$$

$$\leq nN_1N_2 \log P + nN_1N_2(\lambda_{PP} + \lambda_{NP}) \log P \tag{2.70}$$

where in (2.68), Lemma 1 has been applied with Γ_{N_1} denoting the N_1 elements of $\mathbf{Y}_1^n$ (i.e., $\mathbf{Y}_{1,[1:N_1]}^n$) and $m = N_1 - N_2$. Applying the same procedure of section 2.4 and lemma 2 to each term of the summation in (2.69) results in (2.70). By dividing both sides of (2.70) by $n \log P$ and taking the limit $n, P \to \infty$, (2.63) is obtained.

For the inequality in (2.64), we have

$$\begin{aligned}
nR_1 &\leq I(W_1; \mathbf{Y}_1^n|\Omega^n) \\
&= I(W_1; Y_{1,[1:N_2]}^n|\Omega^n) + I(W_1; Y_{1,[N_2+1:N_1]}^n|\Omega^n, Y_{1,[1:N_2]}^n) \\
&= h(Y_{1,[1:N_2]}^n|\Omega^n) - h(Y_{1,[1:N_2]}^n|\Omega^n, W_1) + h(Y_{1,[N_2+1:N_1]}^n|\Omega^n, Y_{1,[1:N_2]}^n) \\
&\quad - h(Y_{1,[N_2+1:N_1]}^n|\Omega^n, Y_{1,[1:N_2]}^n, W_1) \\
&\leq \underbrace{h(Y_{1,[1:N_2]}^n)}_{\leq nN_2 \log P} - h(Y_{1,[1:N_2]}^n|\Omega^n, W_1) + \underbrace{h(Y_{1,[N_2+1:N_1]}^n)}_{\leq n(N_1-N_2) \log P} - \underbrace{h(Y_{1,[N_2+1:N_1]}^n|\Omega^n, Y_{1,[1:N_2]}^n, W_1, W_2)}_{no(\log P)}
\end{aligned} \tag{2.71}$$

$$\leq nN_1 \log P - h(Y_{1,[1:N_2]}^n|\Omega^n, W_1) - no(\log P) \tag{2.72}$$

where in (2.71), we used the fact that conditioning reduces the entropy. We enhance user 2 with the message of user 1. Therefore,

$$nR_2 \leq I(W_2; \mathbf{Y}_2^n|\Omega^n, W_1) = h(\mathbf{Y}_2^n|\Omega^n, W_1) - \underbrace{h(\mathbf{Y}_2^n|\Omega^n, W_1, W_2)}_{no(\log P)}. \tag{2.73}$$

By adding (2.72) and (2.73), we get

$$nR_1 + nR_2 \leq nN_1 \log P + \underbrace{h(\mathbf{Y}_2^n|\Omega^n, W_1) - h(Y_{1,[1:N_2]}^n|\Omega^n, W_1)}_{\leq nN_2(\lambda_{PP}+\lambda_{PN})\log P} - 2no(\log P) \tag{2.74}$$

where the same procedure of section 2.4 has been applied to the difference in (2.74). Therefore,

$$d_1 + d_2 \leq N_1 + N_2(\lambda_{PP} + \lambda_{PN}) = N_1 + N_2\lambda_P^1. \tag{2.75}$$

□

In the sequel, we show that when $\lambda_{PN} \leq \frac{N_2}{N_1}\lambda_{NP}$, the outer bound, which is defined by (2.63) and (2.64), is tight. Specifically, we show the achievability of the inner bound defined by the following inequalities

$$\frac{d_1}{N_1} + \frac{d_2}{N_2} \leq 1 + \lambda_P^2 \tag{2.76}$$

$$d_1 + d_2 \leq N_1 + N_2(\lambda_{PP} + \min(\lambda_{PN}, \frac{N_2}{N_1}\lambda_{NP})). \tag{2.77}$$

It is obvious that when $\lambda_{PN} \leq \frac{N_2}{N_1}\lambda_{NP}$, the inner bound coincides with the outer bound. We consider a block of n (sufficiently large) time instants. In this block, there are $n\lambda_{PN}$ time instants in the PN state (i.e., where the CSI of user 1 is perfectly known and CSI of user 2 is unknown), $n\lambda_{NP}$ time instants in the NP state, $n\lambda_{PP}$ time instants in the PP state and $n\lambda_{NN}$ time instants in the NN state. Without loss of generality, we assume n is chosen in such a way that all these numbers are integers. From now on, whenever it is said that N symbols are sent orthogonal to the matrix $\mathbf{H}$, it is meant that these N symbols are precoded by a matrix whose columns are chosen from the null space of $\mathbf{H}^H$.

The following achievable schemes are based on a simple interference cancellation scheme. In other words, if at each of the m time instants in the PN state, N_1 private symbols are sent to user 1 and N_2 private symbols are sent (orthogonal to the channel of user 1) to user 2, user 2 needs to get rid of nN_1 interfering symbols from user 1 to decode

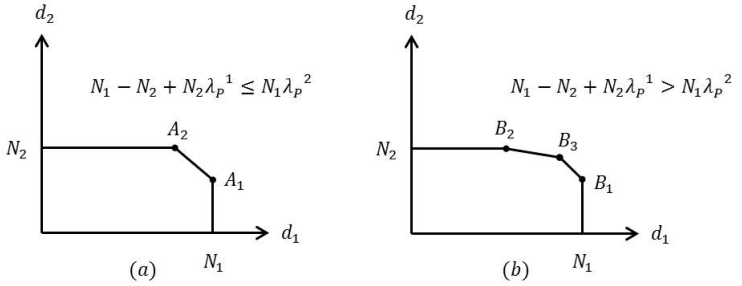

FIGURE 2.10: The DoF region when $N_1\lambda_{PN} \leq N_2\lambda_{NP}$.

its own symbols. If we pick $m\frac{N_1}{N_2}$ time instants in the NP state, at each of these time instants, N_2 interfering symbols can be sent to user 2 and since these interfering symbols are already known at user 1, N_1 new private symbols can be sent (orthogonal to the channel of user 2) to user 1. This could be viewed as a generalization of the $S_3^{\frac{3}{2}}$ [9] to the MIMO case where the mismatch between the number of receiving antennas across the users is taken into account. The achievability is divided into two scenarios.

2.8.1 $N_1\lambda_{PN} \leq N_2\lambda_{NP}$

In this case, the region is shown in figure 2.10.

2.8.1.1 $N_1 - N_2 + N_2\lambda_P^1 \leq N_1\lambda_P^2$

The region (figure 2.10 (a)) has the corner points $A_1(N_1, N_2\lambda_P^1)$ and $A_2(N_1 - N_2 + N_2\lambda_P^1, N_2)$.

The achievability of A_1 is as follows.

Phase 1: At each of the $n\lambda_{PN}$ time instants, N_1 and N_2 private symbols are sent to user 1 and user 2, respectively. These N_2 private symbols are sent orthogonal to $\mathbf{H}_1(t)$. Therefore, user 1 receives its intended $nN_1\lambda_{PN}$ symbols and user 2 receives $n(N_1 + N_2)\lambda_{PN}$ symbols. User 1 can decode its symbols immediately, while user 2 has to get rid of $nN_1\lambda_{PN}$ interfering symbols.

Phase 2: Among the $n\lambda_{NP}$ time instants in the NP state, $\frac{N_1}{N_2}n\lambda_{PN}(\leq n\lambda_{NP})$ time instants are selected. At each of these selected time instants, N_2 interfering symbols of phase 1 are sent to user 2 and N_1 new private symbols are sent to user 1. These N_1 private symbols are sent orthogonal to $\mathbf{H}_2(t)$. User 2 receives the $nN_1\lambda_{PN}$ interfering

symbols which enables it to decode its private symbols in phase 1. The interfering symbols of user 2 are already known at user 1, therefore, user 1 can successfully decode its private symbols in this phase.

Phase 3: In the remaining time instants in the NP state (i.e., $n\lambda_{NP} - \frac{N_1}{N_2}n\lambda_{PN}$) and all the $n\lambda_{NN}$ time instants, N_1 private symbols are sent to user 1.

Phase 4: In all the $n\lambda_{PP}$ time instants, N_1 and N_2 private messages orthogonal to $\mathbf{H}_2(t)$ and $\mathbf{H}_1(t)$, respectively are sent to user 1 and user 2.

Therefore, user 1 and user 2 can, respectively, decode nN_1 and $nN_2(\lambda_{PP}+\lambda_{PN})$ private symbols in the block of n time instants which achieves the first corner point $(N_1, N_2\lambda_P^1)$.

The achievability of A_2 is as follows.

Phase 1: Among the $n\lambda_{NP}$ time instants in the NP state, $n\frac{N_1}{N_2}\lambda_{PN}$ time instants are selected. At each of these selected time instants, N_2 and N_1 private symbols are sent to user 2 and user 1, respectively. These N_1 private symbols are sent orthogonal to $\mathbf{H}_2(t)$. Therefore, user 2 can decode $nN_1\lambda_{PN}$ private symbols and user 1 receives $n(N_1+N_2)\frac{N_1}{N_2}\lambda_{PN}$ symbols of which $nN_1\lambda_{PN}$ symbols are interferers.

Phase 2: At each of the $n\lambda_{PN}$ time instants, N_1 interfering symbols in phase 1 are sent to user 1 and N_2 private symbols to user 2. These N_2 private symbols are sent orthogonal to $\mathbf{H}_1(t)$. Therefore, user 1 is able to decode its private symbols in phase 1.

Phase 3: There are $n\lambda_{NP}-\frac{N_1}{N_2}n\lambda_{PN}$ remaining time instants in the NP state. $n\lambda_{NN}\frac{(N_1-N_2)}{N_2}$ of them are selected (note that $n\lambda_{NN}\frac{(N_1-N_2)}{N_2} \leq n\lambda_{NP}-\frac{N_1}{N_2}n\lambda_{PN}$ due to the condition in the figure 2.10(a)). At each of these selected time instants, N_2 and N_1 private symbols are sent to user 2 and user 1, respectively. These N_1 private symbols are sent orthogonal to $\mathbf{H}_2(t)$. Therefore, user 1 has to get rid of $n\lambda_{NN}(N_1-N_2)$ interfering symbols.

Phase 4: At each of the $n\lambda_{NN}$ time instants, N_2 private symbols are sent to user 2 and N_1-N_2 interfering symbol from phase 3 are sent to user 1. The interfering symbols are already known at user 2, therefore user 2 successfully decodes its symbols. User 1, having N_1 antennas, is capable of decoding all the sent symbols in this phase.

Phase 5: In the remaining time instants in the NP states, N_2 and N_1-N_2 private symbols are sent to user 2 and user 1, respectively. These N_1-N_2 private symbols are sent orthogonal to $\mathbf{H}_2(t)$.

Phase 6: The same as phase 4 for the achievability of A_1

Therefore, user 1 and user 2 can, respectively, decode $n(N_1 - N_2 + N_2\lambda_P^1)$ and nN_2 private symbols in the block of n time instants which achieves the second corner point.

2.8.1.2 $N_1 - N_2 + N_2\lambda_P^1 > N_1\lambda_P^2$

The region (figure 2.10 (b)) has the corner points $B_1(N_1, N_2\lambda_P^1)$, $B_2(N_1\lambda_P^2, N_2)$ and $B_3(N_1 - \frac{N_1N_2(\lambda_P^2-\lambda_P^1)}{N_1-N_2}, \frac{N_1N_2\lambda_P^2-N_2^2\lambda_P^1}{N_1-N_2})$.

The achievability of B_1 is the same as that of A_1 and the achievability of B_2 is as follows.

Phase 1 and 2: Similar to the phase 1 and phase 2 in the achievability of A_2.

Phase 3: There are $n\lambda_{NP} - \frac{N_1}{N_2}n\lambda_{PN}$ remaining time instants in the NP state. At each of these remaining time instants, N_2 and N_1 private symbols are sent to user 2 and user 1, respectively. These N_1 private symbols are sent orthogonal to $\mathbf{H}_2(t)$. Therefore, user 1 has to get rid of $nN_2\lambda_{NP} - nN_1\lambda_{PN}$ interfering symbols.

Phase 4: There are $n\lambda_{NN}$ time instant in the NN state. $\frac{nN_2\lambda_{NP}-nN_1\lambda_{PN}}{N_1-N_2}$ of them are selected (note that $n\lambda_{NN} > \frac{nN_2\lambda_{NP}-nN_1\lambda_{PN}}{N_1-N_2}$ due to the condition in the figure 2.10(b)) At each of these selected time instants, N_2 private symbols are sent to user 2 and N_1-N_2 interfering symbols from phase 3 are sent to user 1. Therefore, with N_1 antennas, user 1 can decode its private symbols in phase 3. Since these interfering symbols are already known at user 2, it can successfully decode its N_2 private symbols in this phase.

Phase 5: In the remaining time instants in the NN states, N_2 private symbols are sent to user 2.

Phase 6: The same as phase 4 in the achievability A_1.

Therefore, user 1 and user 2 can, respectively, decode $nN_1\lambda_P^2$ and nN_2 private symbols in the block of n time instants which achieves the second corner point.

The achievability of B_3 follows the same lines as the achievability of B_2 except that in phase 5, in the remaining NN time instants, instead of sending N_2 private symbols to user 2, N_1 private symbols are sent to user 1.

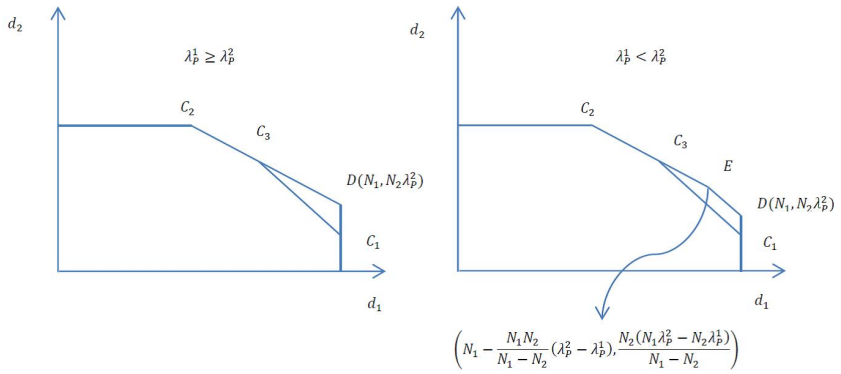

FIGURE 2.11: The achievable DoF region (i.e., the inner bound) and the outer bound when $N_1\lambda_{PN} > N_2\lambda_{NP}$.

In conclusion, the outer bound in Theorem 2.3 is the optimal DoF region in this case (i.e., $N_1\lambda_{PN} \leq N_2\lambda_{NP}$).

2.8.2 $N_1\lambda_{PN} > N_2\lambda_{NP}$

In this case, the achievable region has three corner points $C_1(N_1, N_2\lambda_{PP} + \frac{N_2^2}{N_1}\lambda_{NP})$, $C_2(N_1\lambda_P^2, N_2)$ and $C_3(N_1 - N_2\lambda_{NP}, N_2\lambda_P^2 + \frac{N_2^2}{N_1}\lambda_{NP})$. This is shown in figure 2.11 along with the outer bound where the outer bound has two corner points (C_2 and D) when $\lambda_P^1 \geq \lambda_P^2$ and three corner points otherwise (i.e., C_2, E and D).

The achievability of C_1 is as follows.

Phase 1: There are $n\lambda_{PN}$ time instants in the PN state and $n\frac{N_2}{N_1}\lambda_{NP} (\leq n\lambda_{PN})$ of them are selected. At each of these selected time instants, N_1 and N_2 private symbols are sent to user 1 and user 2, respectively. These N_2 symbols are sent orthogonal to $\mathbf{H}_1(t)$. Therefore, user 1 receives its intended $nN_2\lambda_{NP}$ symbols and user 2 receives $n(N_1 + N_2)\frac{N_2}{N_1}\lambda_{NP}$ symbols. User 1 can decode its symbols immediately, while user 2 has to get rid of $nN_2\lambda_{NP}$ interfering symbols.

Phase 2: At each of the $n\lambda_{NP}$ time instants in the NP state, N_2 interfering symbols of phase 1 are sent to user 2 and N_1 private symbols are sent to user 1. These N_1 symbols are sent orthogonal to $\mathbf{H}_2(t)$. User 2 receives the $nN_2\lambda_{NP}$ interfering symbols which enables it to decode its private symbols in phase 1. Since these interfering symbols are already known at user 1, it can successfully decode its N_1 private symbols in this phase.

Phase 3: In the remaining time instants in the PN state (i.e., $n\lambda_{PN} - \frac{N_2}{N_1}n\lambda_{NP}$) and all the $n\lambda_{NN}$ time instants, N_1 private symbols are sent to user 1.

Phase 4: The same as phase 4 in the achievability of A_1.

Therefore, user 1 and user 2 can, respectively, decode nN_1 and $n(N_2\lambda_{PP} + \frac{N_2^2}{N_1}\lambda_{NP})$ private symbols in the block of n time instants which achieves the first corner point.

The achievability of C_2 is as follows.

Phase 1: At each of $n\lambda_{NP}$ time instants, N_2 and N_1 private symbols are sent to user 2 and user 1, respectively. These N_1 symbols are sent orthogonal to $\mathbf{H}_2(t)$. Therefore, user 2 can decode its intended $nN_2\lambda_{NP}$ symbols and user 1 receives $n(N_1 + N_2)\lambda_{NP}$ symbols of which $nN_2\lambda_{NP}$ are interferes.

Phase 2: Among the $n\lambda_{PN}$ time instants in the PN state, $n\frac{N_2}{N_1}\lambda_{NP}(\leq n\lambda_{PN})$ time instants are selected. At each of these selected time instants, N_1 interfering symbols of phase 1 are sent to user 2 and N_2 private symbols are sent to user 2. These N_2 symbols are sent orthogonal to $\mathbf{H}_1(t)$. Therefore, user 1 can decode its private symbols in phase 1.

Phase 3: In the remaining time instants in the PN state (i.e., $n\lambda_{PN} - \frac{N_2}{N_1}n\lambda_{NP}$) and all the $n\lambda_{NN}$ time instants, N_2 private symbols are sent to user 2.

Phase 4: The same as phase 4 in the achievability of A_1.

Therefore, user 1 and user 2 can, respectively, decode $nN_1\lambda_P^2$ and nN_2 private symbols in the block of n time instants which achieves the second corner point.

The achievability of C_3 follows the same lines as the achievability of C_2 with the difference that in phase 3, in the remaining time instants in the PN state and all the $n\lambda_{NN}$ time instants, instead of sending N_2 private symbols to user 2, N_1 private symbols are sent to user 1.

As an example, figure 2.12 shows the achievability of the corner point B_3 in figure 2.10(b). In this example, $\lambda_{PN} = \lambda_{PP} = \frac{1}{6}, \lambda_{NP} = \lambda_{NN} = \frac{1}{3}$. u and v are private symbols from (independently) Gaussian encoded codewords for user 1 and user 2, respectively and $n = 12$. When the CSI of a user is known at the transmitter, it is shown in red.

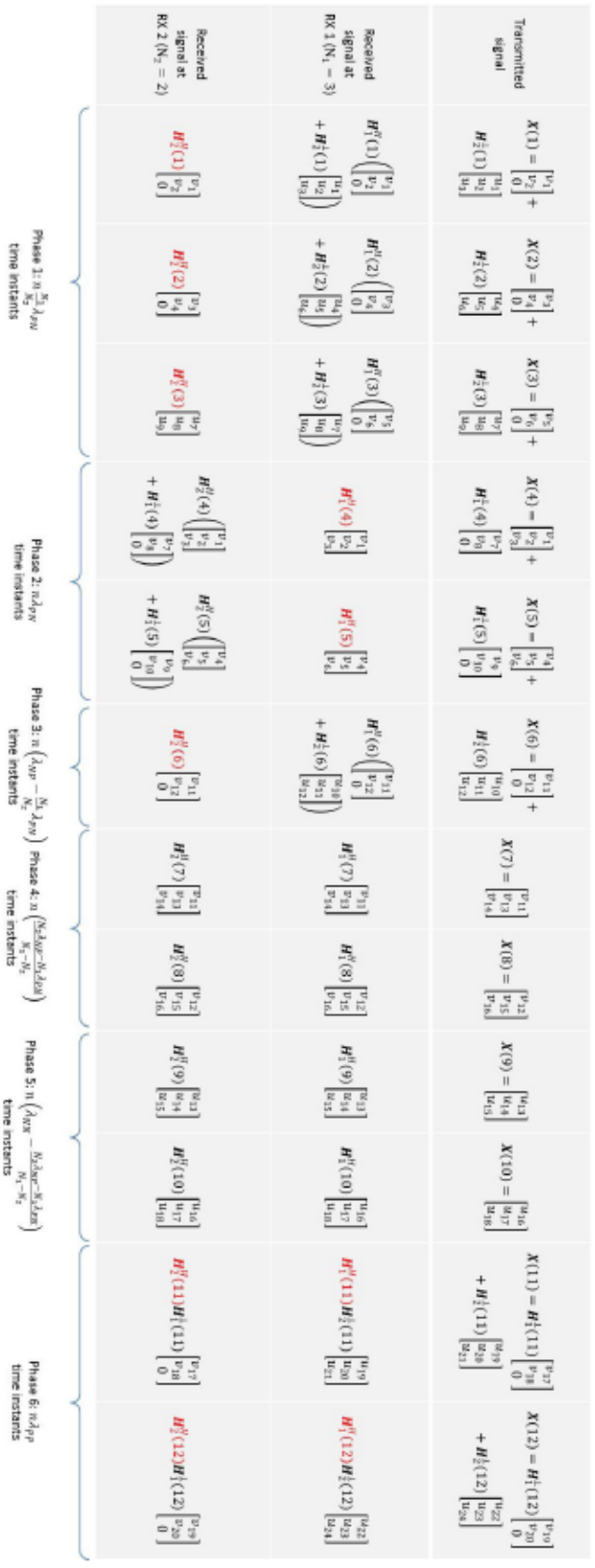

FIGURE 2.12: An example for achieving the corner point $B_3(N_1 - \frac{N_1N_2(\lambda_P^2 \quad \lambda_P^1)}{N_1 \quad N_2}, \frac{N_1N_2\lambda_P^2 \quad N_2^2\lambda_P^1}{N_1 \quad N_2}) = (2, \frac{5}{3})$. In this example $\lambda_{PN} = \lambda_{PP} = \frac{1}{6}, \lambda_{NP} = \lambda_{NN} = \frac{1}{3}$.

2.9 MIMO BC with no CSIT

The DoF region of the MIMO BC with no CSIT was first shown in [19], [20] for the two user case and later in [21] for the general K-user BC.

In this section, we provide an alternative proof for the results obtained in the mentioned papers based on Lemma 1 of section 2.5.1, where its advantage over [21] is in extending the results of [20] for the capacity region of special two-user broadcast channels to special K-user BCs.

We consider a MIMO BC, in which a transmitter with M antennas sends independent messages $W_1, \ldots, W_K$ to K users (receivers), where each receiver is equipped with N_i receive antennas ($i \in [1:K]$). The discrete-time baseband received signal of user i at channel use t can be written as

$$\tilde{\mathbf{Y}}_i(t) = \mathbf{H}_i^H(t)\mathbf{X}(t) + \mathbf{Z}_i(t) \ , \ i \in [1:K] \ , \ t \in [1:n] \tag{2.78}$$

where $\mathbf{X}(t) \in \mathbb{C}^{M\times 1}$ is the transmitted signal satisfying the (per codeword) power constraint $\sum_{t=1}^{n} \|\mathbf{x}(t)\|^2 \leq nP$. $\mathbf{H}_i(t) \in \mathbb{C}^{M\times N_i}$ and $\mathbf{Z}_i(t) \in \mathbb{C}^{N_i\times 1}$ are, respectively, the channel matrix and the additive noise vector of receiver i. The elements of $\mathbf{H}_i(t)$ are i.i.d. across time and users. The noise vectors and the elements of the channel matrices are drawn from continuous probability density functions (independent of $\mathbf{X}(t)$) and the channel matrices are assumed to be full rank almost surely. We assume no CSIT and perfect local channel state information at the receiver (CSIR) i.e., at time slot t, user i has perfect knowledge of $\mathbf{H}_i([1:t])$.

Theorem 2.4. *[21]: The DoF region of the K-user MIMO BC with no CSIT and perfect CSIR is given by*

$$D = \{(d_1, d_2, \ldots, d_K) \in \mathbb{R}_{\geq 0}^K | \sum_{i=1}^{K} \frac{d_i}{r_i} \leq 1\} \tag{2.79}$$

where $r_i = \min\{M, N_i\}$.

2.9.1 An alternative proof for 2.79

Unlike [19] and [20], the proof is not based on the degradedness of the MIMO BC under no CSIT. Without loss of generality, we assume $N_1 \geq N_2 \geq \ldots \geq N_K$ and we enhance

the channel by giving the messages of users $[i+1:K]$ to user i. We also assume that each user not only knows its own channel, but also has perfect knowledge of the other users' channels. In other words, perfect global CSIR is assumed. It is obvious that this assumption does not reduce the outer bound which means that the bound with local CSIR is inside the bound with global CSIR; however, the achievability is based on only local CSIR. The region is further enhanced by giving all the noise vectors to each user. According to the Fano's inequality

$$nR_i \leq I(W_i; \tilde{\mathbf{Y}}_i^n | \Omega^n, \Lambda^n, W_{[i+1:K]}) + n\epsilon_n \quad , \; i \in [1:K] \tag{2.80}$$

where $W_{K+1} = \emptyset$ and ϵ_n goes to zero as n goes to infinity. Ω^n is the global channel state information up to time slot n and Λ^n denotes the set of all the noise vectors across the users (extended over n time slots). Let S_i denote the index set of the $r_i (= \min\{M, N_i\})$ linearly independent elements of the N_i-dimensional vector $\mathbf{H}_i^H \mathbf{X}$ (note that S_i is not necessarily unique). We decompose the N_i-dimensional received signal of user i as $\tilde{\mathbf{Y}}_i = (\mathbf{Y}_i, \hat{\mathbf{Y}}_i)$ where $\mathbf{Y}_i$ corresponds to the set of r_i linearly independent elements having their index in S_i , i.e. $\mathbf{Y}_i = \tilde{\mathbf{Y}}_{i,S_i}$, and $\hat{\mathbf{Y}}_i$ can be reconstructed by linear combination of the elements in $\mathbf{Y}_i$ within noise level (for example, when $M < N_i$, we have $r_i = M$. Therefore, given M linearly independent observations is sufficient reconstruct the M transmitted symbols within the noise level.). From the chain rule of mutual information,

$$nR_i \leq I(W_i; \mathbf{Y}_i^n | \Omega^n, \Lambda^n, W_{[i+1:K]}) + \underbrace{I(W_i; \hat{\mathbf{Y}}_i^n | \Omega^n, \Lambda^n, W_{[i+1:K]}, \mathbf{Y}_i^n)}_{o(\log P)} + n\epsilon_n. \tag{2.81}$$

For simplicity, we ignore $n\epsilon_n$ (since later it will be divided by n and $n \to \infty$) and the term with $o(\log P)$ and write

$$\begin{aligned}
\sum_{i=1}^{K} \frac{nR_i}{r_i} &\leq \sum_{i=1}^{K} \frac{I(W_i; \mathbf{Y}_i^n | \Omega^n, \Lambda^n, W_{[i+1:K]})}{r_i} \\
&\leq \underbrace{\frac{h(\mathbf{Y}_K^n | \Omega^n, \Lambda^n)}{r_K}}_{\leq n \log P} + \sum_{i=1}^{K-1} \left[\frac{h(\mathbf{Y}_i^n | \Omega^n, \Lambda^n, W_{[i+1:K]})}{r_i} - \frac{h(\mathbf{Y}_{i+1}^n | \Omega^n, \Lambda^n, W_{[i+1:K]})}{r_{i+1}} \right]
\end{aligned} \tag{2.82}$$

where we have used the fact that $\frac{h(\mathbf{Y}_1^n|\Omega^n,\Lambda^n,W_{[1:K]})}{r_1} \sim o(\log P)$, since with the knowledge of $\Omega^n, \Lambda^n, W_{[1:K]}$, the observation $\mathbf{Y}_1^n$ can be reconstructed.

Each term in the summation of (2.82) can be written as

$$\frac{r_{i+1}h(\mathbf{Y}_i^n|S_{i,n}) - r_i h(\mathbf{Y}_{i+1}^n|S_{i,n})}{r_i r_{i+1}} \tag{2.83}$$

$$= \frac{r_{i+1}h(\mathbf{Y}_{i,1}^n, \mathbf{Y}_{i,2}^n, \ldots, \mathbf{Y}_{i,r_i}^n|S_{i,n})}{r_i r_{i+1}} - \frac{r_i h(\mathbf{Y}_{i+1}^n|S_{i,n})}{r_i r_{i+1}} \tag{2.84}$$

$$\leq \frac{\sum_{p=1}^{r_i} h(\Psi_p^{r_{i+1}}(\Gamma_{r_i})|S_{i,n})}{r_i r_{i+1}} - \frac{r_i h(\mathbf{Y}_{i+1}^n|S_{i,n})}{r_i r_{i+1}} \tag{2.85}$$

$$= \sum_{p=1}^{r_i} \left[\frac{h(\Psi_p^{r_{i+1}}(\Gamma_{r_i})|S_{i,n})}{r_i r_{i+1}} - \frac{h(\mathbf{Y}_{i+1}^n|S_{i,n})}{r_i r_{i+1}} \right] \tag{2.86}$$

$$= \sum_{p=1}^{r_i} \left[\frac{h(\mathbf{A}_{p,i,n}\mathbf{X}^n + \mathbf{B}_{p,i,n}|S_{i,n})}{r_i r_{i+1}} - \frac{h(\mathbf{C}_{i,n}\mathbf{X}^n + \mathbf{D}_{i,n}|S_{i,n})}{r_i r_{i+1}} \right] \tag{2.87}$$

$$= 0 \tag{2.88}$$

where $S_{i,n} = \{\Omega^n, \Lambda^n, W_{[i+1:K]}\}$ and in (2.85), since $r_{i+1} \leq r_i$, the result of Lemma 1 is applied (with $N - m = r_{i+1}$ and $N = r_i$) in which $\Gamma_{r_i} = \{\mathbf{Y}_{i,1}^n, \mathbf{Y}_{i,2}^n, \ldots, \mathbf{Y}_{i,r_i}^n\}$ is the set of r_i linearly independent elements in $\mathbf{Y}_i^n$. In (2.87), we write $\Psi_p^{r_{i+1}}(\Gamma_{r_i})$ and $\mathbf{Y}_{i+1}^n$ as large nr_{i+1} dimensional vectors as follows. $\Psi_p^{r_{i+1}}(\Gamma_{r_i}) = \mathbf{A}_{p,i,n}\mathbf{X}^n + \mathbf{B}_{p,i,n}$ and $\mathbf{Y}_{i+1}^n = \mathbf{C}_{i,n}\mathbf{X}^n + \mathbf{D}_{i,n}$ where $\mathbf{A}_{p,i,n}$ and $\mathbf{C}_{i,n}$ ($\in C^{nr_{i+1}\times nM}$) capture the channel coefficients over the n time slots, $\mathbf{X}^n$ is the nM dimensional input vector and $\mathbf{B}_{p,i,n}$ and $\mathbf{D}_{i,n}$ capture the noise vectors over the n time slots. Since $\mathbf{A}_{p,i,n}$ and $\mathbf{C}_{i,n}$ are identically distributed channel coefficients and the noise terms are provided at each user, the arguments of the differential entropies in (2.87) are statistically equivalent (i.e., have the same probability density function) which results in (2.88). Therefore, (2.82) is simplified to

$$\sum_{i=1}^{K} \frac{nR_i}{r_i} \leq n \log P. \tag{2.89}$$

After dividing both sides by $n \log P$ and taking the limit $n, P \to \infty$, we get

$$\sum_{i=1}^{K} \frac{d_i}{r_i} \leq 1. \tag{2.90}$$

The above DoF region is achieved by a simple time sharing across the users where only local CSIR assumption is necessary.

Finally, it can be observed that the assumption of independent channels across the users was not used in the proof and since it does not change the achievability, it is not a necessary condition and can be relaxed.

2.9.2 Capacity region analysis

In this section we consider i.i.d. Gaussian channels and noise vectors. We also assume $M \geq N_1 \geq N_2 \geq \ldots \geq N_K$ which results in $N_i = N_i (i \in [1:K])$ and therefore, $\tilde{\mathbf{Y}}_i^n = \mathbf{Y}_i^n$. From Fano's inequality,

$$\begin{aligned}\sum_{i=1}^{K} \frac{nR_i}{N_i} &\leq \sum_{i=1}^{K} \frac{I(W_i; \mathbf{Y}_i^n | \Omega^n, W_{[i+1:K]})}{N_i} \\ &\leq \frac{h(\mathbf{Y}_K^n|\Omega^n)}{r_K} - \underbrace{\frac{h(\mathbf{Y}_1^n|\Omega^n, W_{[1:K]})}{r_1}}_{n\log(2\pi e)} \qquad (2.91) \\ &\quad + \underbrace{\sum_{i=1}^{K-1} \left[\frac{h(\mathbf{Y}_i^n|\Omega^n, W_{[i+1:K]})}{N_i} - \frac{h(\mathbf{Y}_{i+1}^n|\Omega^n, W_{[i+1:K]})}{r_{i+1}} \right]}_{\leq 0} \qquad (2.92)\end{aligned}$$

where the last non-positive term is a result of lemma 1. From the above results, we get an outer bound for the achievable rate region as

$$\sum_{i=1}^{K} \frac{R_i}{N_i} \leq \frac{h(\mathbf{Y}_K^n|\Omega^n)}{nr_K} - \log(2\pi e). \qquad (2.93)$$

Therefore, an outer bound for the ergodic capacity region is

$$\sum_{i=1}^{K} \frac{R_i}{N_i} \leq \frac{\max_{\mathbf{\Sigma}_X : \mathrm{tr}(\mathbf{\Sigma}_X) \leq P} E\left[\log\det(\mathbf{I}_{r_K} + \mathbf{H}_K^H \mathbf{\Sigma}_X \mathbf{H}_K)\right]}{r_K} \qquad (2.94)$$

and since the channels have i.i.d. Gaussian elements, the optimal input covariance matrix is $\frac{P}{M}\mathbf{I}_M$ [22]. Hence,

$$\begin{aligned}C^o(P) = \{(R_1, R_2, \ldots, R_K) \in \mathbb{R}_{\geq 0}^K | \\ R_i \leq E\left[\log\det(\mathbf{I}_{N_i} + \frac{P}{M}\mathbf{H}_i^H \mathbf{H}_i)\right] \ \forall i \\ \sum_{i=1}^{K} \frac{R_i}{N_i} \leq \frac{E\left[\log\det(\mathbf{I}_{r_K} + \frac{P}{M}\mathbf{H}_K^H \mathbf{H}_K)\right]}{r_K}\} \qquad (2.95)\end{aligned}$$

It is obvious that the outer bound is more affected by the capacity of the point-to-point link from the transmitter to the user with the lowest number of receive antennas.

Definition. We define a class of channels (a set of matrices) $\Theta(p, q, m)$ where each channel (matrix) in this class has its elements drawn from the distribution p in such a way that the optimal input covariance matrix for achieving the capacity of the point-to-point link from the transmitter to the virtual user defined by this channel is diagonal with equal entries. The details for this condition are given in [23, Exercise 8.6]. We also assume that for each channel in this class, all the singular values have the distribution q. In other words,

$$\begin{aligned}\Theta(p,q,m) = \big\{ & H \in C^{m\times n}\ \forall n \le m | \text{ Elements of } H \sim p, \\ & \arg \max_{\mathbf{\Sigma}_X : \mathrm{tr}(\mathbf{\Sigma}_X) \le P} E\left[\log\det(\mathbf{I}_n + H^H \mathbf{\Sigma}_X H)\right] = \frac{P}{m}\mathbf{I}_m, \\ & \text{and } \lambda_i(H^H H) \sim q, \forall i = 1, \ldots, \mathrm{rank}(H) \big\}. \end{aligned} \tag{2.96}$$

Theorem 2.5. *In a K-user Gaussian MIMO BC with $M \ge N_1 \ge N_2 \ge \ldots \ge N_K$ and all the channels from the class of $\Theta(p, q, M)$, the capacity region with CDIT is given by*

$$C(P) = \left\{ (R_{[1:K]}) \in \mathbb{R}^K_{\ge 0} | \sum_{i=1}^{K} \frac{R_i}{N_i} \le E_q\left[\log(1 + \frac{P}{M}\lambda)\right] \right\} \tag{2.97}$$

where $E_q\left[\log(1 + \frac{P}{M}\lambda)\right] = \int \log(1 + \frac{P}{M}x) q(x) dx$.

Proof. According to (2.94) and the properties of $\Theta(p, q, M)$, we have

$$\sum_{i=1}^{K} \frac{R_i}{N_i} \le \frac{\sum_{i=1}^{r_K} E\left[\log(1 + \frac{P}{M}\lambda_i(\mathbf{H}_K^H \mathbf{H}_K))\right]}{r_K}. \tag{2.98}$$

If the singular values of $\mathbf{H}_K$ have the same distribution, we can write

$$\sum_{i=1}^{K} \frac{R_i}{N_i} \le E\left[\log(1 + \frac{P}{M}\lambda_1(\mathbf{H}_K^H \mathbf{H}_K))\right]. \tag{2.99}$$

Also, if the singular values have the same distribution across the users, the outer bound is easily achieved by orthogonal transmission strategies, and therefore it is the optimal capacity region. □

A special case of theorem 2.5 was shown for the two user Gaussian MIMO BC in [20], in which all the eigenvalues of $\mathbf{H}_k^H \mathbf{H}_k (k = 1, 2)$ are unity.

Chapter 3

On the Capacity of Vector Gaussian Channels With Bounded Inputs

3.1 Overview

The capacity of a static multiple-input multiple-output (MIMO) channel under the peak and average power constraints is investigated. For the identity channel matrix, the approach of [24] is generalized to the higher dimension settings to derive the necessary and sufficient conditions for the optimal input probability density function. This approach avoids the usage of the identity theorem of the holomorphic functions of several complex variables which seems to fail in the multi-dimensional scenarios. It is proved that the support of the capacity-achieving distribution is a finite set of hyper-spheres with mutually independent phases and amplitude in the spherical domain. Subsequently, it is shown that when the average power constraint is relaxed, if the number of antennas is large enough, the capacity has a closed form solution and constant amplitude signaling at the peak power achieves it. Moreover, it will be observed that in a discrete-time memoryless Gaussian channel, the average power constrained capacity, which results from a Gaussian input distribution, can be closely obtained by an input distribution whose support set of its magnitude is discrete and finite. Finally, we investigate some upper

and lower bounds for the capacity of the non-identity channel matrix and evaluate their performance as a function of the condition number of the channel.

3.2 Introduction

The capacity of a point-to-point communication system subject to peak and average power constraints was investigated in [25] for the scalar Gaussian channel where it was shown that the capacity-achieving distribution is unique and has a probability mass function with a finite number of mass points. In [24], Shamai and Bar-David gave a full account on the capacity of a quadrature Gaussian channel under the aforementioned constraints and proved that the optimal input distribution has a discrete amplitude and a uniform independent phase. This discreteness in the optimal input distribution was surprisingly shown in [26] to be true even without a peak power constraint for the Rayleigh-fading channel when no channel state information (CSI) is assumed either at the receiver or the transmitter. Following this work, the authors in [27] and [28] investigated the capacity of noncoherent AWGN and Rician-fading channels, respectively. In [29], a point to point real scalar channel is considered in which sufficient conditions for the additive noise are provided such that the support of the optimal bounded input has a finite number of mass points. These sufficient conditions are also useful in multi-user settings as shown in [30] for the MAC channel under bounded inputs.

The analysis of the MIMO channel under the peak power constraints per antenna is a straightforward problem after changing the vector channel into parallel AWGN channels and applying the results of [25] or [24]. Recently, the vector Gaussian channel under the peak and average power constraints, where the peak power constraint is on the norm of the input vector, has become more practical by the new scheme proposed in [31]. More specifically, this scheme enables multiple antenna transmission using only one RF chain and the peak power constraint (i.e., a peak constraint on the norm of the input vector rather than on each antenna separately) is the very result of this single RF chain. The capacity of the vector Gaussian channel under the peak and average power constraints has been explored in [32] and [33]. However, according to [34], it seems that the results of the aforementioned papers in the higher dimension settings are not rigorous due to the usage of the Identity Theorem for holomorphic functions of several complex variables without fulfilling its conditions. As shown by an example in Section

IV of [34], a holomorphic function of several complex variables can be zero on $\mathbb{R}^n$, but not necessarily zero on $\mathbb{C}^n$. Since $\mathbb{R}^n$ is not an open subset of $\mathbb{C}^n$, the identity theorem cannot be applied. Therefore, the problem of finding the capacity of a MIMO channel under the peak and average power constraints has remained open. To this end, the contributions of this chapter are as follows.

- For the identity channel matrix, the approach of [24] is generalized to the vector Gaussian channel in which the complex extension will be done only on a single variable which is the amplitude of the input in the spherical coordinates. The necessary and sufficient conditions for the optimality of the input distribution are derived and it is proved that the magnitude of the capacity-achieving distribution has a probability mass function over a finite number of mass points which determines a finite number of hyper spheres in the spherical coordinates. Further, the magnitude and the phases of the capacity-achieving distribution are mutually independent and the phases are distributed in a way that the points are uniformly distributed on each of the hyper spheres.

- It is shown that if the average power constraint is relaxed, when the ratio of peak power to the number of dimensions remains below a certain threshold (≈ 3.4), the constant amplitude signaling at the peak power achieves the capacity.

- It is also shown that for a fixed SNR, the gap between the Shannon capacity and the constant amplitude signaling decreases as $O(\frac{1}{n})$ for large values of n, where n denotes the number of dimensions.

- Finally, the case of the non-identity channel matrix is considered where we start from the MISO channel and show that the support of the optimal input does not necessarily have discrete amplitude. Afterwards, several upper bounds and lower bounds are provided for the general n by m MIMO channel capacity. The performance of these bounds are evaluated numerically as a function of the condition number of the channel.

The chapter is organized as follows. The system model and some preliminaries are provided in Section 3.3, respectively. The main result of this chapter is given in Section 3.4 for the identity channel. The general case of the non-identity channel matrix is briefly investigated in Section 3.5. Numerical results are given in Section 3.6.

3.3 System Model and preliminaries

In a discrete-time memoryless vector Gaussian channel, the input-output relationship for the identity channel is given by

$$\mathbf{Y}(t) = \mathbf{X}(t) + \mathbf{W}(t), \tag{3.1}$$

where $\mathbf{X}(t)$, $\mathbf{Y}(t)$ $(\in \mathbb{R}^n)$ denote the input and output of the channel, respectively. $t \in \mathcal{Z}^+$ denotes the channel use index and $\{\mathbf{W(t)}\}$ is an i.i.d. vector noise process with $\mathbf{W}(t) \sim N(\mathbf{0}, \mathbf{I}_n)$ (and independent of $\mathbf{X}(t)$) for every transmission t. [1]

The capacity of the channel in (3.1) under the peak and the average power constraints is

$$C(u_p, u_a) = \sup_{F_{\mathbf{X}}(\mathbf{x}):\|\mathbf{X}\|^2 \le u_p,\ E[\|\mathbf{X}\|^2] \le u_a} I(\mathbf{X};\mathbf{Y}) \tag{3.2}$$

where $F_{\mathbf{X}}(\mathbf{x})$ denotes the cumulative distribution function (CDF) of the input vector, and u_p, u_a are the upper bounds for the peak and the average power, respectively. Throughout this report, any operator that involves a random variable reads with the term *almost-surely* (e.g. $\|\mathbf{X}\|^2 \le u_p$)[2].

It is obvious that

$$\sup_{F_{\mathbf{X}}(\mathbf{x}):\|\mathbf{X}\|^2 \le u_p,\ E[\|\mathbf{X}\|^2] \le u_a} I(\mathbf{X};\mathbf{Y}) \le \sup_{F_{\mathbf{X}}(\mathbf{x}):E[\|\mathbf{X}\|^2] \le \min(u_p,u_a)} I(\mathbf{X};\mathbf{Y}). \tag{3.3}$$

Therefore, a trivial upper bound for the capacity is given by

$$C(u_p, u_a) \le C_G = \frac{n}{2} \ln\left(1 + \frac{\min(u_p, u_a)}{n}\right) \tag{3.4}$$

where C_G is achieved by a Gaussian input vector distributed as $N\left(\mathbf{0}, \frac{\min(u_p,u_a)}{n}\mathbf{I}_n\right)$.

We formulate the optimization problem in (3.2) in the spherical domain. The rational behind this change of coordinates is due to the spherical symmetry of the white Gaussian noise and the constraints which, as it will be clear, enables us to perform the optimization problem only on the magnitude of the input. By writing the mutual information in terms

[1] It is obvious that the m-dimensional complex AWGN channel can be mapped to the channel in (3.1) with $n = 2m$.

[2] More precisely, let Ω be the sample space of the probability model over which the random vector $\mathbf{X}$ is defined. $\|\mathbf{X}\|^2 \overset{a.s.}{\le} u_p$ is equivalent to $\Pr\{\omega \in \Omega |\ \|\mathbf{X}(\omega)\|^2 \le u_p\} = 1$.

of differential entropies, we have

$$I(\mathbf{X};\mathbf{Y}) = h(\mathbf{Y}) - h(\mathbf{Y}|\mathbf{X}) = h(\mathbf{Y}) - \frac{n}{2}\ln 2\pi e \tag{3.5}$$

where the entropies are in nats. Motivated by the spherical symmetry of the white Gaussian noise and the constraints, $\mathbf{Y}$ and $\mathbf{X}$ can be written in spherical coordinates as

$$\mathbf{Y} = R\mathbf{a}(\mathbf{\Psi}) \quad , \quad \mathbf{X} = P\mathbf{a}(\mathbf{\Theta}) \tag{3.6}$$

where R and P denote the magnitude of the output and the input, respectively. $\mathbf{\Psi} = [\Psi_1, \Psi_2, \ldots, \Psi_{n-1}]^T$ and $\mathbf{\Theta} = [\Theta_1, \Theta_2, \ldots, \Theta_{n-1}]^T$ are, respectively, the phase vectors of the output and the input, in which Ψ_i, $\Theta_i \in [0, \pi] (i \in [1 : n-2])$ and Ψ_{n-1},$\Theta_{n-1} \in [0, 2\pi)$. $\mathbf{a}(\phi) = [a_1(\phi), \ldots, a_n(\phi)]^T$ is a unit vector in which

$$a_k(\phi) = \begin{cases} \cos\phi_k \prod_{i=1}^{k-1} \sin\phi_i & k \in [1 : n-1] \\ \prod_{i=1}^{k-1} \sin\phi_i & k = n \end{cases} . \tag{3.7}$$

As it will become clear later, this change of coordinates avoids the usage of the identity theorem for holomorphic functions of several complex variables. The optimization problem in (3.2) is equivalent to

$$C(u_p, u_a) = \sup_{F_{P,\mathbf{\Theta}}(\rho,\theta): P^2 \le u_p,\ E(P^2) \le u_a} h(\mathbf{Y}) - \frac{n}{2}\ln 2\pi e. \tag{3.8}$$

The differential entropy of the output is given by

$$h(\mathbf{Y}) = -\int_{\mathbb{R}^n} f_{\mathbf{Y}}(\mathbf{y}) \ln f_{\mathbf{Y}}(\mathbf{y}) d\mathbf{y} \tag{3.9}$$

$$= -\int_0^\infty \underbrace{\int_0^\pi \cdots \int_0^\pi}_{n-2 \text{ times}} \int_0^{2\pi} f_{\mathbf{Y}}(\mathbf{y}(r,\psi)) \ln f_{\mathbf{Y}}(\mathbf{y}(r,\psi)) |\frac{\partial \mathbf{y}}{\partial(r,\psi)}| d\psi dr \tag{3.10}$$

$$= -\int_0^\infty \underbrace{\int_0^\pi \cdots \int_0^\pi}_{n-2 \text{ times}} \int_0^{2\pi} f_{R,\mathbf{\Psi}}(r,\psi) \ln \frac{f_{R,\mathbf{\Psi}}(r,\psi)}{|\frac{\partial \mathbf{y}}{\partial(r,\psi)}|} d\psi dr \tag{3.11}$$

$$= h(R,\mathbf{\Psi}) + \int_0^\infty f_R(r) \ln r^{n-1} dr + \sum_{i=1}^{n-2} \int_0^\pi f_{\Psi_i}(\psi_i) \ln \sin^{n-i-1}\psi_i d\psi_i \tag{3.12}$$

where $|\frac{\partial \mathbf{y}}{\partial(r,\psi)}| (= r^{n-1} \prod_{i=1}^{n-2} \sin^{n-i-1}\psi_i)$ is the Jacobian of the transform and $h(R,\mathbf{\Psi})$ denotes the joint entropy of the output variables. The conditional pdf of $R, \mathbf{\Psi}$ conditioned

on $P, \boldsymbol{\Theta}$ is given by

$$f_{R,\boldsymbol{\Psi}|P,\boldsymbol{\Theta}}(r,\psi|\rho,\theta) = \frac{1}{(\sqrt{2\pi})^n} e^{-\frac{r^2+\rho^2-2r\rho\mathbf{a}^T(\theta)\mathbf{a}(\psi)}{2}} r^{n-1} \prod_{i=1}^{n-2} \sin^{n-i-1}\psi_i. \tag{3.13}$$

From (3.13), the joint pdf of the magnitude and phases of the output is

$$f_{R,\boldsymbol{\Psi}}(r,\psi) = \int_0^{\infty} \underbrace{\int_0^{\pi} \dots \int_0^{\pi}}_{n-2 \text{ times}} \int_0^{2\pi} f_{R,\boldsymbol{\Psi}|P,\boldsymbol{\Theta}}(r,\psi|\rho,\theta) d^n F_{P,\boldsymbol{\Theta}}(\rho,\theta) \tag{3.14}$$

in which $F_{P,\boldsymbol{\Theta}}(\rho,\theta)$ denotes the joint CDF of $(P,\boldsymbol{\Theta})$. By integrating (3.14) over the phase vector ψ, we have

$$f_R(r) = \int_0^{\infty} L(r,\rho) f_P(\rho) d\rho \tag{3.15}$$

where [3]

$$L(r,\rho) = \underbrace{\int_0^{\pi} \dots \int_0^{\pi}}_{n-2 \text{ times}} \int_0^{2\pi} f_{R,\boldsymbol{\Psi}|P,\boldsymbol{\Theta}}(r,\psi|\rho,\theta) d\psi_{n-1} \dots d\psi_1. \tag{3.16}$$

It is obvious that

$$h(R,\boldsymbol{\Psi}) \le h(R) + \sum_{i=1}^{n-1} h(\Psi_i) \le h(R) + \sum_{i=1}^{n-2} h(\Psi_i) + \ln 2\pi \tag{3.17}$$

where the first inequality is tight iff the elements of $\{R, \Psi_1, \dots, \Psi_{n-1}\}$ are mutually independent, and the second inequality becomes tight iff Ψ_{n-1} is uniformly distributed over $[0, 2\pi)$. From (3.12) and (3.17)

$$h(\mathbf{Y}) \le h(R) + \sum_{i=1}^{n-2} h(\Psi_i) + \int_0^{\infty} f_R(r) \ln r^{n-1} dr + \sum_{i=1}^{n-2} \int_0^{\pi} f_{\Psi_i}(\psi_i) \ln \sin^{n-i-1}\psi_i d\psi_i + \ln 2\pi. \tag{3.18}$$

For the sake of readability, the following change of variables is helpful

$$V = \frac{R^n}{n} \ , \ U_i = \int_0^{\Psi_i} \sin^{n-i-1}\delta d\delta \ , \ i \in [1 : n-2]. \tag{3.19}$$

[3] The reason that $L(r,\rho)$ is not a function of the phase vector θ is due to the spherically symmetric distribution of the white Gaussian noise. In other words, $L(r,\rho)$ is the integral of the Gaussian pdf $N(\mathbf{x},\mathbf{I})$ over the surface of an n-sphere with radius r which is invariant to the position of $\mathbf{x}$ as long as $\|\mathbf{x}\| = \rho$, i.e.

$$L(r,\|\mathbf{x}\|) = \int_{\|\mathbf{y}\|=r} \frac{e^{-\frac{\|\mathbf{y}-\mathbf{x}\|^2}{2}}}{(\sqrt{2\pi})^n} d\mathbf{y} = \frac{e^{-\frac{r^2+\|\mathbf{x}\|^2}{2}}}{(\sqrt{2\pi})^n} \int_{\|\mathbf{y}\|=r} e^{\mathbf{x}^t\mathbf{y}} d\mathbf{y}$$

which is constant on $\|\mathbf{x}\| = \rho$. (3.15) implies that in the AWGN channel in (3.1), $f_R(r)$ is induced only by $f_P(\rho)$ and not $f_{\boldsymbol{\Theta}}(\theta)$.

Since $R \geq 0$ and $\Psi_i \in [0, \pi](i \in [1 : n-2])$, it is easy to show that the two mappings $R \to V$ and $\Psi_i \to U_i$ (defined in (3.19)) are invertible. Also, the support set of U_i is $S_{U_i} = [0, \alpha_i]$ where $\alpha_i = \frac{\sqrt{\pi}\Gamma(\frac{n-i}{2})}{\Gamma(\frac{n-i+1}{2})}$ (the Gamma function is defined as $\Gamma(t) = \int_0^\infty x^{t-1}e^{-x}dx$.) From (3.15), the pdf of V is [4]

$$f_V(v) = f_V(v; F_P) = \int_0^\infty K_n(v, \rho) dF_P(\rho) \tag{3.20}$$

where the notation $; F_P$ in $f_V(v; F_P)$ is to emphasize that V has been induced by F_P. Note that the integral transform in (3.20) is invertible as shown in Appendix D. The kernel $K_n(v, \rho)$ is given by

$$\begin{aligned} K_n(v,\rho) &= \frac{L(\sqrt[n]{nv}, \rho)}{(\sqrt[n]{nv})^{n-1}} \\ &= \underbrace{\int_0^\pi \cdots \int_0^\pi}_{n-2 \text{ times}} \int_0^{2\pi} \frac{1}{(\sqrt{2\pi})^n} e^{-\frac{(\sqrt[n]{nv})^2 + \rho^2 - 2\sqrt[n]{nv}\rho \mathbf{a}^T(\theta)\mathbf{a}(\psi)}{2}} \prod_{i=1}^{n-2} \sin^{n-i-1}\psi_i d\psi_{n-1} \ldots d\psi_1 \end{aligned} \tag{3.21}$$

$$= e^{-\frac{(\sqrt[n]{nv})^2+\rho^2}{2}} \begin{cases} \frac{I_{\frac{n}{2}-1}(\rho\sqrt[n]{nv})}{(\rho\sqrt[n]{nv})^{\frac{n}{2}-1}} & \rho v \neq 0 \\ \frac{1}{\Gamma(\frac{n}{2})2^{\frac{n}{2}-1}} & \rho v = 0 \end{cases} \quad \forall n \geq 2 \tag{3.22}$$

where $I_\alpha(.)$ is the modified bessel function of the first kind and order α. The calculations are provided in Appendix A. Note that $K_n(v, \rho)$ is continuous on its domain. The differential entropy of V is

$$\begin{aligned} h(V) &= h(V; F_P) \\ &= -\int_0^\infty f_V(v; F_P) \ln f_V(v; F_P) dv \\ &= -\int_0^\infty f_R(r) \ln \frac{f_R(r)}{r^{n-1}} dr. \end{aligned} \tag{3.23}$$

The differential entropy of U_i is given by

$$\begin{aligned} h(U_i) &= -\int_{S_{U_i}} f_{U_i}(u) \ln f_{U_i}(u) du \\ &= -\int_0^\pi f_{\Psi_i}(\psi_i) \ln \frac{f_{\Psi_i}(\psi_i)}{\sin^{n-i-1}\psi_i} d\psi_i \quad , \quad i \in [1 : n-2]. \end{aligned} \tag{3.24}$$

[4] The existence of $f_V(v)$ is guaranteed by the Gaussian distribution of the additive noise.

Rewriting (3.8), we have

$$\begin{aligned} C(u_p, u_a) &= \sup_{F_{P,\boldsymbol{\Theta}}(\rho,\theta):P^2\le u_p, E[P^2]\le u_a} h(\mathbf{Y}) - \frac{n}{2}\ln 2\pi e \\ &\le \sup_{F_{P,\boldsymbol{\Theta}}(\rho,\theta):P^2\le u_p, E[P^2]\le u_a} \left\{ h(V;F_P) + \sum_{i=1}^{n-2} h(U_i) + (1-\frac{n}{2})\ln 2\pi - \frac{n}{2} \right\} \qquad (3.25) \\ &\le \sup_{F_P(\rho):P^2\le u_p, E[P^2]\le u_a} h(V;F_P) + \sum_{i=1}^{n-2}\ln\alpha_i + (1-\frac{n}{2})\ln 2\pi - \frac{n}{2} \qquad (3.26) \end{aligned}$$

where (3.25) results from (3.18), (3.23) and (3.24). (3.26) is due to the fact that since S_{U_i} (the support of U_i) is bounded, $h(U_i)$ is maximized when U_i is uniformly distributed. It is easy to verify that if the magnitude and phases of the input are mutually independent with the phases having the distributions

$$\Theta_{n-1} \sim U[0, 2\pi) \ , \ f_{\Theta_i}(\theta_i) = \alpha_i^{-1}\sin^{n-i-1}\theta_i \quad , \quad i \in [1 : n-2], \qquad (3.27)$$

the magnitude and phases of the output become mutually independent with the phases having the distributions

$$\Psi_{n-1} \sim U[0, 2\pi) \ , \ f_{\Psi_i}(\psi_i) = \alpha_i^{-1}\sin^{n-i-1}\psi_i \quad , \quad i \in [1 : n-2] \qquad (3.28)$$

where $\alpha_i = \frac{\sqrt{\pi}\Gamma(\frac{n-i}{2})}{\Gamma(\frac{n-i+1}{2})}$. In other words, having the input distribution

$$F_{P,\boldsymbol{\Theta}}(\rho,\theta) = \frac{\theta_{n-1}}{2\pi} F_P(\rho) \prod_{i=1}^{n-2} \int_0^{\theta_i} \alpha_i^{-1}\sin^{n-i-1}\theta d\theta \qquad (3.29)$$

results in

$$F_{R,\boldsymbol{\Psi}}(r,\psi) = \frac{\psi_{n-1}}{2\pi} F_R(r) \prod_{i=1}^{n-2} \int_0^{\psi_i} \alpha_i^{-1}\sin^{n-i-1}\psi d\psi. \qquad (3.30)$$

The above result can be easily checked either by solving for $f_{R,\boldsymbol{\Psi}}(r,\psi)$ in (3.14) or by the fact that the summation of two independent spherically symmetric random vectors is still spherically symmetric.[5] Also, note that having Ψ_i $(i = 1, \ldots, n-2)$ distributed as (3.28) implies uniform U_i on $[0, \alpha_i]$ $(i = 1, \ldots, n-2)$. It can be observed that the input pdf in (3.29) makes the inequalities in (3.25) and (3.26) tight. Since the constraint is only

[5]The magnitude and the unit vector of a spherically symmetric random vector are independent and the unit vector is uniformly distributed on the unit ball. It can be verified that this property is equivalent to the vector having the distribution of (3.30) in spherical coordinates.

on the magnitude of the input and $f_V(v)$ is induced only by $f_P(\rho)$, it is concluded that the optimal input distribution must have mutually independent phases and magnitude with the phases being distributed as (3.27). Therefore,

$$C(u_p, u_a) = \sup_{F_P(\rho): P^2 \le u_p, E[P^2] \le u_a} h(V; F_P) + \sum_{i=1}^{n-2} \ln \alpha_i + (1 - \frac{n}{2}) \ln 2\pi - \frac{n}{2}. \tag{3.31}$$

Before proceeding further, it is interesting to check whether the problem in (3.31) boils down to the classical results when the peak power constraint is relaxed (i.e., $u_p \to \infty$). From the definition of V,

$$E[V^{\frac{2}{n}}] = \frac{1}{\sqrt[n]{n^2}} E[n + P^2]. \tag{3.32}$$

This can be verified by a change of variable (i.e., $V = \frac{R^n}{n}$) and using the derivative of (D.6) with respect to β. Therefore, when $u_p \to \infty$, the problem in (3.31) becomes maximization of the differential entropy over all the distributions having a bounded moment of order $\frac{2}{n}$ which is addressed in Appendix B for an arbitrary moment. Substituting m with $\frac{2}{n}$ and A with $\frac{n+u_a}{\sqrt[n]{n^2}}$ in (B.3), the optimal distribution for V is obatined and from (3.20), the corresponding $f_{P^*}(\rho)$ has the general Rayleigh distribution as

$$f_{P^*}(\rho) = \frac{n^{\frac{n}{2}} \rho^{n-1} e^{-\frac{n\rho^2}{2u_a}}}{2^{\frac{n-2}{2}} u_a^{\frac{n}{2}} \Gamma(\frac{n}{2})} \tag{3.33}$$

which is the only solution, since (3.20) is an invertible transform (see Appendix D). Furthermore, it can be verified that the maximum is

$$C(\infty, u_a) = \frac{n}{2} \ln(1 + \frac{u_a}{n}) \tag{3.34}$$

which coincides with the classical results for the identity channel matrix [22].

Similar to [25] and [24], we define the marginal entropy density of V as

$$\tilde{h}_V(x; F_P) = -\int_0^\infty K_n(v, x) \ln f_V(v; F_P) dv \tag{3.35}$$

which satisfies

$$h(V; F_P) = \int_0^\infty \tilde{h}_V(\rho; F_P) dF_P(\rho). \tag{3.36}$$

(3.35) is shown to be an invertible transform in Appendix D and this property will become useful later on.

3.4 Main results

Let ϵ_P denote the set of points of increase[6] of $F_P(\rho)$ in the interval $[0, \sqrt{u_p}]$. The main result of the chapter is given in the following theorem.

Theorem 3.1. *The supremization in (3.31), which is for the identity channel matrix, has a unique solution and the optimal input achieving the supremum (and therefore the maximum) has the following distribution in the spherical coordinates,*

$$F^*_{P,\mathbf{\Theta}}(\rho,\theta) = \frac{\theta_{n-1}}{2\pi} F^*_P(\rho) \prod_{i=1}^{n-2} \int_0^{\theta_i} \alpha_i^{-1} \sin^{n-i-1}\theta d\theta \tag{3.37}$$

where $F^*_P(\rho)$ has a finite number of points of increase (i.e., ϵ_{P^*} has a finite cardinality). Further, the necessary and sufficient condition for $F^*_P(\rho)$ to be optimal is the existence of a $\lambda(\geq 0)$ for which

$$\tilde{h}_V(\rho; F^*_P) \leq h(V; F^*_P) + \lambda(\rho^2 - u_a) \ , \ \forall \rho \in [0, \sqrt{u_p}] \tag{3.38}$$

$$\tilde{h}_V(\rho; F^*_P) = h(V; F^*_P) + \lambda(\rho^2 - u_a) \ , \ \forall \rho \in \epsilon_{P^*}. \tag{3.39}$$

Note that when the average power constraint is relaxed (i.e., $u_a \geq u_p$), $\lambda = 0$.

Proof. The phases of the optimal input distribution have already been shown to be mutually independent and have the distribution in (3.27) being independent of the magnitude. Therefore, it is sufficient only to show the optimal distribution of the input magnitude. This is proved by reductio ad absurdum. In other words, it is shown that having an infinite number of points of increase results in a contradiction. The detailed proof is given in Appendix C. □

Remark 1. When the average power constraint is relaxed (i.e. $u_a \geq u_p$), the following input distribution is asymptotically ($\frac{u_p}{n} \to 0$) optimal

$$F^{**}_{P,\mathbf{\Theta}}(\rho,\theta) = \frac{\theta_{n-1}}{2\pi} u(\rho - \sqrt{u_p}) \prod_{i=1}^{n-2} \int_0^{\theta_i} \alpha_i^{-1} \sin^{n-i-1}\theta d\theta \tag{3.40}$$

[6] A point Z is said to be a point of increase of a distribution if for any open set Γ containing Z, we have $\Pr\{\Gamma\} > 0$.

where $u(.)$ is the unit step function. Further, the resulting capacity is given by

$$C(u_p, u_p) \approx \frac{u_p}{2} \quad \text{when} \quad \frac{u_p}{n} \ll 1. \tag{3.41}$$

Later, in the numerical results section, we observe that the density in (3.40) remains optimal for the non-vanishing ratio $\frac{u_p}{n}$ when it is below a certain threshold.

Proof. Since the density in (3.40) has spherical symmetry, it is sufficient to show that $F_P^{**}(\rho) = u(\rho - \sqrt{u_p})$ is optimal when $\frac{u_p}{n} \to 0$. From (3.4), we have

$$\lim_{\frac{u_p}{n}\to 0} C(u_p, u_a) \leq \frac{u_p}{2}. \tag{3.42}$$

The CDF $F_P^{**}(\rho) = u(\rho - \sqrt{u_p})$ induces the following output pdf

$$f_V(v; F_P^{**}) = K_n(v, \sqrt{u_p}) = e^{-\frac{(\sqrt[n]{nv})^2 + u_p}{2}} \frac{I_{\frac{n}{2}-1}(\sqrt{u_p}\sqrt[n]{nv})}{(\sqrt{u_p}\sqrt[n]{nv})^{\frac{n}{2}-1}}. \tag{3.43}$$

When $\frac{u_p}{n}$ is small,

$$\lim_{\frac{u_p}{n}\to 0} h(V; F_P^{**}) = \lim_{\frac{u_p}{n}\to 0} -\int_0^\infty f_V(v; F_P^{**}) \ln f_V(v; F_P^{**}) dv \tag{3.44}$$

$$= \lim_{\frac{u_p}{n}\to 0} \int_0^\infty e^{-\frac{(\sqrt[n]{nv})^2 + u_p}{2}} \frac{I_{\frac{n}{2}-1}(\sqrt{u_p}\sqrt[n]{nv})}{(\sqrt{u_p}\sqrt[n]{nv})^{\frac{n}{2}-1}} \left[\frac{(\sqrt[n]{nv})^2 + u_p}{2} - \ln\left(\frac{I_{\frac{n}{2}-1}(\sqrt{u_p}\sqrt[n]{nv})}{(\sqrt{u_p}\sqrt[n]{nv})^{\frac{n}{2}-1}} \right) \right] dv \tag{3.45}$$

$$= \frac{n}{2} + \ln\left(\Gamma(\frac{n}{2}) 2^{\frac{n}{2}-1}\right) + \lim_{\frac{u_p}{n}\to 0} \left\{ u_p - \int_0^\infty e^{-\frac{(\sqrt[n]{nv})^2 + u_p}{2}} \frac{I_{\frac{n}{2}-1}(\sqrt{u_p}\sqrt[n]{nv})}{(\sqrt{u_p}\sqrt[n]{nv})^{\frac{n}{2}-1}} \ln\left(1 + \frac{u_p(\sqrt[n]{nv})^2}{2n}\right) dv \right\} \tag{3.46}$$

$$= \frac{n}{2} + \ln\left(\Gamma(\frac{n}{2}) 2^{\frac{n}{2}-1}\right) + \lim_{\frac{u_p}{n}\to 0} \left\{ u_p - \frac{u_p}{n}(\frac{n+u_p}{2}) \right\} \tag{3.47}$$

$$= \frac{n}{2} + \ln\left(\Gamma(\frac{n}{2}) 2^{\frac{n}{2}-1}\right) + \frac{u_p}{2}. \tag{3.48}$$

where in (3.46), we have approximated the modified bessel function with the first two terms in its power series expansion as follows

$$I_n(x) \approx \frac{x^n}{\Gamma(n+1)2^n}(1 + \frac{x^2}{4(n+1)}) \quad , \quad \frac{x}{n} \to 0. \tag{3.49}$$

In (3.47), we use the approximation $\ln(1+x) \approx x$ $(x \ll 1)$ and in (3.48), the higher order term is neglected. Given the input distribution F_P^{**}, the achievable rate with small ratio $\frac{u_p}{n}$ is given by (see (3.31))

$$\lim_{\frac{u_p}{n}\to 0} h(V; F_P^{**}) + \sum_{i=1}^{n-2} \ln \alpha_i + (1-\frac{n}{2}) \ln 2\pi - \frac{n}{2} = \frac{u_p}{2} \tag{3.50}$$

where we have used the fact that

$$\sum_{i=1}^{n-2} \ln \alpha_i = -\ln \Gamma(\frac{n}{2}) + \frac{n-2}{2} \ln \pi. \tag{3.51}$$

From (3.50) and (3.42), it is concluded that the pdf in (3.40) is asymptotically optimal for $\frac{u_p}{n} \ll 1$ when $u_p \leq u_a$. Note that the distribution in (3.40) is not the only asymptotically optimal distribution. There are many possible alternatives, one of which, for example, is the binary PAM in each dimension with the points $-\sqrt{\frac{u_p}{n}}$ and $\sqrt{\frac{u_p}{n}}$ which can be verified to have an achievable rate of $\frac{u_p}{2}$ when $\frac{u_p}{n} \ll 1$. Specifically, in the low peak power regime $(u_p \ll 1)$, a sufficient condition for the input distribution to be asymptotically optimal is as follows. First, it has a constant magnitude at $\sqrt{u_p}$. Second, its Θ_1 is independent of $(P, \Theta_2, \ldots, \Theta_{n-1})$ and has a zero first Fourier coefficient

$$\int_0^{\pi} e^{j\theta} f_{\Theta_1}(\theta) d\theta = 0. \tag{3.52}$$

The claim is justified by noting that fulfilling the second condition results in the spherical symmetric output distribution of (3.30) as follows. Using the approximation $e^x \approx 1 + x$ $(x \ll 1)$, at small values of u_p, (3.13) can be approximated as

$$f_{R,\mathbf{\Psi}|P,\mathbf{\Theta}}(r, \psi|\rho, \theta) \approx \frac{1}{(\sqrt{2\pi})^n} e^{-\frac{r^2+\rho^2}{2}} (1 + r\rho \mathbf{a}^T(\theta)\mathbf{a}(\psi)) r^{n-1} \prod_{i=1}^{n-2} \sin^{n-i-1} \psi_i. \tag{3.53}$$

If Θ_1 is independent of $(\Theta_2, \ldots, \Theta_{n-1}, P)$, substituting (3.53) in (3.14) results in

$$f_{R,\mathbf{\Psi}}(r, \psi) \approx \int_0^{\infty} \underbrace{\int_0^{\pi} \ldots \int_0^{\pi}}_{n-3 \text{ times}} \int_0^{2\pi} \int_0^{\pi} \frac{1}{(\sqrt{2\pi})^n} e^{-\frac{r^2+\rho^2}{2}} (1 + r\rho \mathbf{a}^T(\theta)\mathbf{a}(\psi)) r^{n-1} \cdot \prod_{i=1}^{n-2} \sin^{n-i-1} \psi_i dF_{\Theta_1}(\theta_1) d^{n-1} F_{P,\mathbf{\Theta}_2^{n-1}}(\rho, \theta_2^{n-1}) \tag{3.54}$$

where $\theta_2^{n-1} = (\theta_2, \theta_3, \ldots, \theta_{n-1})$. If Θ_1 has a zero first Fourier coefficient, due to the structure of $\mathbf{a}(\theta)$ (see (3.7)), we have

$$\int_0^{\pi} \mathbf{a}^T(\theta)\mathbf{a}(\psi) dF_{\Theta_1}(\theta_1) = 0. \tag{3.55}$$

Therefore, (3.54) simplifies as

$$f_{R,\mathbf{\Psi}}(r,\psi) \approx \int_0^{\infty} \frac{1}{(\sqrt{2\pi})^n} e^{-\frac{r^2+\rho^2}{2}} r^{n-1} \prod_{i=1}^{n-2} \sin^{n-i-1}\psi_i dF_P(\rho) \tag{3.56}$$

which implies that when $u_p \to 0$, having Θ_1 independent of all other spherical variables with a zero first Fourier coefficient results in the output distribution in (3.30) which makes the inequalities (3.25) and (3.26) tight. Finally, fulfilling the first condition (i.e., having a constant magnitude at $\sqrt{u_p}$) validates the previous reasoning starting from (3.43).

The asymptotic optimality of the constant-magnitude signaling in (3.40) can alternatively be proved by inspecting the behavior of the marginal entropy density $\tilde{h}_V(\rho; F_P)$ when $\frac{u_p}{n}$ is sufficiently small. From (3.20)

$$f_V(v; F_P) \to \frac{e^{-\frac{(\sqrt[n]{nv})^2}{2}}}{\Gamma(\frac{n}{2})2^{\frac{n}{2}-1}} \underbrace{\int_0^{\infty} e^{-\frac{\rho^2}{2}} dF_P(\rho)}_{\text{constant} = C} \text{ when } \frac{u_p}{n} \to 0. \tag{3.57}$$

Therefore,

$$\begin{aligned}
\tilde{h}_V(\rho; F_P) &= -\int_0^{\infty} e^{-\frac{(\sqrt[n]{nv})^2+\rho^2}{2}} \frac{I_{\frac{n}{2}-1}(\rho\sqrt[n]{nv})}{(\rho\sqrt[n]{nv})^{\frac{n}{2}-1}} \ln f_V(v; F_P) dv \\
&\to \int_0^{\infty} e^{-\frac{(\sqrt[n]{nv})^2+\rho^2}{2}} \frac{I_{\frac{n}{2}-1}(\rho\sqrt[n]{nv})}{(\rho\sqrt[n]{nv})^{\frac{n}{2}-1}} \left[\frac{(\sqrt[n]{nv})^2}{2} + \ln\left(\frac{\Gamma(\frac{n}{2})2^{\frac{n}{2}-1}}{C}\right)\right] dv \qquad (3.58) \\
&= \frac{\rho^2+n}{2} + \ln\left(\frac{\Gamma(\frac{n}{2})2^{\frac{n}{2}-1}}{C}\right) \qquad (3.59)
\end{aligned}$$

It is obvious that (3.59) is a (strictly) convex (strictly) increasing function. Hence, the necessary and sufficient conditions in (3.38) and (3.39) are satisfied if and only if the input has only one point of increase at $\sqrt{u_p}$ which proves the asymptotic optimality of (3.40) for $\frac{u_p}{n} \ll 1$ and $u_a \geq u_p$. □

Remark 2. For a fixed SNR, the gap between the Shannon capacity and the constant amplitude signaling decreases as $O(\frac{1}{n})$ for large values of n.

Proof. By writing the first two terms of the Taylor series expansion of the logarithm (i.e., $\ln(1+x) \approx x - \frac{x^2}{2}, x \ll 1$), we have

$$\text{when } n \to \infty \quad , \quad \frac{n}{2}\ln(1+\frac{u_p}{n}) \approx \frac{u_p}{2} - \frac{u_p^2}{4n}. \tag{3.60}$$

From (3.47), the achievable rate obtained by the constant envelope signaling is

$$\text{when } n \to \infty \quad , \quad I(\mathbf{X};\mathbf{Y}) \approx \frac{u_p}{2} - \frac{u_p^2}{2n}. \tag{3.61}$$

This shows that the gap between achievable rate and the Shannon capacity decreases as $\frac{u_p^2}{4n}(= O(\frac{1}{n}))$, when n goes to infinity. □

While remark 2 shows an asymptotic behavior of the gap, the following remark provides an analytical lower bound for any values of n.

Remark 3. The following lower bound holds for the capacity of constant amplitude signaling.

$$\sup_{F_{\mathbf{X}}(\mathbf{x}):\|\mathbf{X}\|^2=u_p} I(\mathbf{X};\mathbf{Y}) \geq \frac{n-1}{2}\log\left(1 + \frac{2^{\frac{2}{n-1}-1}u_p}{e\left[(n-1)\Gamma(\frac{n-1}{2})\right]^{\frac{2}{n-1}}}\right). \tag{3.62}$$

Proof. Let $\mathbf{X}'$ and $\mathbf{X}'$ be defined as

$$\mathbf{X}' = [X_1, X_2, \ldots, X_{N-1}, 0]^T \quad , \quad \mathbf{Y}' = [Y_1, Y_2, \ldots, Y_{N-1}, 0]^T. \tag{3.63}$$

Due to the Markov chain $\mathbf{X}' \leftrightarrow \mathbf{X} \leftrightarrow \mathbf{Y} \leftrightarrow \mathbf{Y}'$ and the fact that $\|\mathbf{X}\|^2 = u_p$ implies $\|\mathbf{X}'\|^2 \leq u_p$, we can write

$$\sup_{F_{\mathbf{X}}(\mathbf{x}):\|\mathbf{X}\|^2=u_p} I(\mathbf{X};\mathbf{Y}) \geq \sup_{F_{\mathbf{X}'}(\mathbf{x}'):\|\mathbf{X}'\|^2\leq u_p} I(\mathbf{X}';\mathbf{Y}') \tag{3.64}$$

$$= \sup_{F_{\mathbf{X}'}(\mathbf{x}'):\|\mathbf{X}'\|^2\leq u_p} h(\mathbf{Y}';F_{\mathbf{X}'}) - \frac{n-1}{2}\log 2\pi e \tag{3.65}$$

$$\geq \sup_{F_{\mathbf{X}'}(\mathbf{x}'):\|\mathbf{X}'\|^2\leq u_p} \frac{n-1}{2}\log\left(2^{\frac{2}{n-1}h(\mathbf{X}')} + 2\pi e\right) - \frac{n-1}{2}\log 2\pi e \tag{3.66}$$

$$= \frac{n-1}{2}\log\left(1 + \frac{2^{\frac{2}{n-1}-1}u_p}{e\left[(n-1)\Gamma(\frac{n-1}{2})\right]^{\frac{2}{n-1}}}\right) \tag{3.67}$$

where in (3.66), the $(n-1)$-dimensional EPI has been used[7] and (3.67) is due to the fact that for the $(n-1)$-dimensional vector $\mathbf{X}'$, we can write

$$\sup_{F_{\mathbf{X}'}(\mathbf{x}'):\|\mathbf{X}'\|^2\leq u_p} h(\mathbf{X}') = \log\left(\frac{2(\pi u_p)^{\frac{n-1}{2}}}{(n-1)\Gamma(\frac{n-1}{2})}\right) \quad , \quad n \geq 2 \tag{3.68}$$

whose proof follows the same steps from (3.110) to (3.117) with $\lambda = 0$ and $a = \frac{n}{(\sqrt{u_p})^n}$. □

The asymptotic decrease of the gap in remark 2 can be alternatively proved by using the lower bound in (3.67) which is provided in Appendix E.

Remark 4. When $u_a < u_p$, the following input distribution is asymptotically ($u_a \to 0$) optimal

$$F^{**}_{P,\mathbf{\Theta}}(\rho,\theta) = \left[(1-\frac{u_a}{u_p})u(\rho) + \frac{u_a}{u_p}u(\rho-\sqrt{u_p})\right]\frac{\theta_{n-1}}{2\pi}\prod_{i=1}^{n-2}\int_0^{\theta_i}\alpha_i^{-1}\sin^{n-i-1}\theta d\theta \tag{3.69}$$

[7]The Entropy Power Inequality (EPI) states that if $\mathbf{X}$ and $\mathbf{Y}$ are two independent n-dimensional vectors which have pdfs, and $\mathbf{Z} = \mathbf{X} + \mathbf{Y}$, then

$$2^{\frac{2h(\mathbf{Z})}{n}} \geq 2^{\frac{2h(\mathbf{X})}{n}} + 2^{\frac{2h(\mathbf{Y})}{n}}.$$

Note that the reduction of dimensions from n to $n-1$ in (3.63) is necessary. The reason is that the usage of the n-dimensional EPI is NOT permissible for the constant amplitude vector, since an n-dimensional vector with a fixed norm has at most $(n-1)$ degrees of freedom (or equivalently at most $(n-1)$-dimensional support).

and the resulting capacity is given by

$$C(u_p, u_p) \approx \frac{u_a}{2} \quad \text{when} \quad u_a \ll 1. \tag{3.70}$$

Proof. The proof is given in Appendix F. □

Remarks 1 and 4 are essential for the initial stage of the simulation results when either u_a or u_p are assumed to be very small at first and afterwards they are increased gradually by a step size.

Remark 5. The fact that the magnitude of the optimal input distribution has a finite number of mass points remains unchanged if the average constraint in (3.2) is generalized as

$$E(g(P)) \leq u_a \tag{3.71}$$

in which $g(z)$ is holomorphic on an open subset $\mathbb{D}(\subseteq \mathbb{C})$ which includes the non-negative real line (i.e., $\mathbb{R}_{\geq 0} \subset \mathbb{D}$).

Proof. The proof is given in Appendix G. □

Remark 6. The peak power constraint in (3.2) can be generalized to

$$\|P\|^2 \overset{a.s.}{\in} \mathbb{D}_{u_p} \subseteq [0, u_p]. \tag{3.72}$$

Proof. Since all the conditions (compactness, continuity, etc.) remain unchanged, the support of the optimal input distribution will be some concentric shells having the mass points of the magnitude in $\mathbb{D}_{u_p}$. □

3.5 The MIMO case with deterministic channel

First, we consider the multiple-input single-output (MISO) channel in which (3.1) changes to

$$Y(t) = \mathbf{h}^T \mathbf{X}(t) + W(t) \tag{3.73}$$

where $\mathbf{h}(\in \mathbb{R}^{n\times 1})$ is the deterministic channel vector and $W \sim N(0,1)$. Let $X_{new} = \mathbf{h}^T\mathbf{X}$. The capacity of this channel under the peak and average power constraints is given by

$$\begin{aligned}
C(u_p,u_a) &= \sup_{F_{\mathbf{X}}(\mathbf{x}):\|\mathbf{X}\|^2\le u_p,\ E[\|\mathbf{X}\|^2]\le u_a} I(\mathbf{X};Y) \\
&= \sup_{F_{\mathbf{X}}(\mathbf{x}):\|\mathbf{X}\|^2\le u_p,\ E[\|\mathbf{X}\|^2]\le u_a} I(\mathbf{X},X_{new};Y) && (3.74)\\
&= \sup_{F_{\mathbf{X}}(\mathbf{x}):\|\mathbf{X}\|^2\le u_p,\ E[\|\mathbf{X}\|^2]\le u_a} I(X_{new};Y) + \underbrace{I(\mathbf{X};Y|X_{new})}_{=0} && (3.75)\\
&= \sup_{F_{\mathbf{X}}(\mathbf{x}):\|\mathbf{X}\|^2\le u_p,\ E[\|\mathbf{X}\|^2]\le u_a} I(X_{new};Y) \\
&\le \sup_{F_{X_{new}}(x):|X_{new}|\le\sqrt{u_p}\|\mathbf{h}\|,\ E[|X_{new}|^2]\le u_a\|\mathbf{h}\|^2} I(X_{new};Y) && (3.76)
\end{aligned}$$

where (3.74) is due to the fact that X_{new} is a function of $\mathbf{X}$ and (3.75) is a result of the following Markov chain $\mathbf{X} \longrightarrow X_{new} \longrightarrow Y$. (3.76) is due to the fact that any input cdf having the support $\|\mathbf{X}\|^2 \le u_p$ and satisfying $E[\|\mathbf{X}\|^2] \le u_a$ induces a cdf for X_{new} with the support in $[-\sqrt{u_p}\|\mathbf{h}\|, \sqrt{u_p}\|\mathbf{h}\|]$ and satisfying $E[|X_{new}|^2] \le u_a\|\mathbf{h}\|^2$. This could be readily verified by the following convex optimization problem

$$\begin{aligned}
&\max_{\mathbf{x}} \mathbf{h}^T\mathbf{x} \\
&\text{S.t. } \|\mathbf{x}\|^2 \le u_p
\end{aligned} \qquad (3.77)$$

where the maximum is $\sqrt{u_p}\|\mathbf{h}\|$ and it is achieved when $\mathbf{x}$ is matched to the channel (i.e., $\mathbf{x} = \sqrt{u_p}\frac{\mathbf{h}}{\|\mathbf{h}\|}$). Further, from Cauchy-Schwartz inequality, we have

$$E[|X_{new}|^2] = E[|\mathbf{h}^t\mathbf{X}|^2] \le E[\|\mathbf{h}\|^2]E[\|\mathbf{X}\|^2] \le u_a\|\mathbf{h}\|^2 \qquad (3.78)$$

where the inequalities change to equality iff $\mathbf{X}$ is in the direction of $\mathbf{h}$ and $E[\|\mathbf{X}\|^2] = u_a$.

The supremization in (3.76) is the same problem of finding the capacity of a scalar Gaussian channel which has been addressed in [25] where it was shown that the optimal input distribution is a pmf over a finite set of points in the interval defined by the peak power constraint and also it satisfies the average power inequality with equality. It is obvious that having $\mathbf{X}$ located on the hyperplane $\mathbf{h}^T\mathbf{X} = e_i$ (confined in the ball $\|\mathbf{X}\|^2 \le u_p$) with probability p_i results in having X_{new} equal to the mass point $e_i \in [-\sqrt{u_p}\|\mathbf{h}\|, \sqrt{u_p}\|\mathbf{h}\|]$ with probability p_i. If the average power constraint is relaxed

(i.e., $u_a \geq u_p$), the support of the capacity-achieving distribution of the MISO channel with the input bounded in a ball becomes a finite number of hyper planes confined in that ball (all of these hyperplane have the normal vector $\mathbf{h}$). Note that the discrete amplitude property is no longer a necessity for the optimal input distribution in contrast to the MIMO with identity channel. In other words, the necessary and sufficient condition for the optimality is that $\mathbf{X}$ is located in each of these hyperplanes with the corresponding probabilities. There is a common characteristic of the optimal input distribution in both the MIMO (with identity channel) and MISO scenarios which is the fact that the support of the optimal input distribution does not include any open set in $\mathbb{R}^n$. Finally, if the average power constraint is active (i.e., $u_a < u_p$), the support of the optimal input becomes a finite number of mass points in the direction of $\mathbf{h}$ (from (3.78) and the fact that $E[|X_{new}|^2] = u_a\|\mathbf{h}\|^2$) and confined in the ball $\|\mathbf{X}\|^2 \leq u_p$.

For the general deterministic MIMO channel, we have

$$\mathbf{Y}'(t) = \mathbf{H}\mathbf{X}'(t) + \mathbf{W}'(t) \tag{3.79}$$

where $\mathbf{H} \in \mathbb{R}^{n_r \times n_t}$ denotes the deterministic channel. By an SVD (i.e., $\mathbf{H} = \mathbf{D}\mathbf{\Lambda}\mathbf{N}^T$ where $\mathbf{D} \in \mathbb{R}^{n_r \times n_r}$, $\mathbf{\Lambda} \in \mathbb{R}^{n_r \times n_t}$, $\mathbf{N} \in \mathbb{R}^{n_t \times n_t}$), we get

$$\tilde{\mathbf{Y}}'(t) = \mathbf{D}^T\mathbf{Y}'(t) = \mathbf{\Lambda}\underbrace{\mathbf{N}^T\mathbf{X}'(t)}_{\tilde{\mathbf{X}}'(t)} + \underbrace{\mathbf{D}^T\mathbf{W}'(t)}_{\tilde{\mathbf{W}}'(t)}. \tag{3.80}$$

Let $n = \text{rank}(\mathbf{H})$ and $\mathbf{Q}(t)$ be the first n elements of the vector $\tilde{\mathbf{Q}}'(t)$ (for $\mathbf{Q} = \mathbf{Y}, \mathbf{X}$ and $\mathbf{W}$). It is obvious that (3.80) is equivalent to the following

$$\mathbf{Y}(t) = \mathbf{X}(t) + \mathbf{N}(t) \tag{3.81}$$

with the noise distributed as $N(\mathbf{0}, \mathbf{\Sigma})$ where $\mathbf{\Sigma} = \text{diag}\{\lambda_1^{-2}, \lambda_2^{-2}, \ldots, \lambda_n^{-2}\}$ and λ_i ($i \in [1:n]$) is the i^{th} singular value of $\mathbf{H}$. Therefore, the capacity of the deterministic channel in (3.79) is the same as the capacity of the additive non-white Gaussian noise channel in (3.81). It is assumed that the condition number of $\mathbf{H}$ is not unity, since in that case, it becomes equivalent to the scenario with identity channel matrix discussed in section 3.3. From now on, we consider $n = 2$.

Two possible changes of coordinates are as follows. Motivated by the elliptical symmetry of the noise, $\mathbf{X}$ and $\mathbf{Y}$ could be written in the following elliptical coordinates

$$\mathbf{Y} = R\boldsymbol{\Sigma}^{\frac{1}{2}}\mathbf{a}(\boldsymbol{\Psi}) \quad , \quad \mathbf{X} = P\boldsymbol{\Sigma}^{\frac{1}{2}}\mathbf{a}(\boldsymbol{\Theta}) \tag{3.82}$$

and using a similar approach as in section 3.3, the optimization problem becomes

$$C(u_p, u_a) = \sup_{F_{P,\Theta(\rho,\theta)}: P^2\mathbf{a}^T(\theta)\boldsymbol{\Sigma}\mathbf{a}(\theta)\leq u_p, E[P^2\mathbf{a}^T(\theta)\boldsymbol{\Sigma}\mathbf{a}(\theta)]\leq u_a} h(V, \Psi; F_{P,\Theta}) - \ln 2\pi e. \tag{3.83}$$

where $V = \frac{R^2}{2}$. The joint entropy of the output variables is given by

$$h(V, \Psi; F_{P,\Theta}) = \int_0^\infty \int_0^{2\pi} \tilde{h}_{V,\Psi}(\rho, \theta; F_{P,\Theta}) d^2F_{P,\Theta}(\rho, \theta) \tag{3.84}$$

where the joint marginal entropy density writes as

$$\tilde{h}_{V,\Psi}(\rho, \theta; F_{P,\Theta}) = -\int_0^\infty \int_0^{2\pi} K(v, \psi, \rho, \theta) \ln f_{V,\Psi}(v, \psi; F_{P,\Theta}) d\psi dv \tag{3.85}$$

in which

$$f_{V,\Psi}(v, \psi; F_{P,\Theta}) = \int_0^\infty \int_0^{2\pi} K(v, \psi, \rho, \theta) d^2F_{P,\Theta}(\rho, \theta) \tag{3.86}$$

and

$$K(v, \psi, \rho, \theta) = \frac{1}{2\pi} e^{-v - \frac{\rho^2}{2} + \rho\sqrt{2v}\cos(\psi - \theta)}. \tag{3.87}$$

Alternatively, due to the spherical symmetry of the constraint, the input and the output could be written in the spherical coordinates in which

$$C(u_p, u_a) = \sup_{F_{P,\Theta(\rho,\theta)}: P^2\leq u_p, E[P^2]\leq u_a} h(V, \Psi; F_{P,\Theta}) - \ln(2\pi e\sqrt{|\boldsymbol{\Sigma}|}). \tag{3.88}$$

(3.84) to (3.86) remain unchanged, while the kernel is given by

$$K(v, \psi, \rho, \theta) = \frac{1}{2\pi\sqrt{|\boldsymbol{\Sigma}|}} e^{-\frac{1}{2}\left[\sqrt{2v}\mathbf{a}(\psi) - \rho\mathbf{a}(\theta)\right]^T \boldsymbol{\Sigma}^{-1}\left[\sqrt{2v}\mathbf{a}(\psi) - \rho\mathbf{a}(\theta)\right]}. \tag{3.89}$$

Using neither of the above coordinates makes the separation of the magnitude and the phases possible as done in (3.17). This is due to the different symmetries of the noise (elliptical) and the peak power constraint (spherical). Since the conditions of compactness, convexity and continuity remain unchanged, we can only proceed up to

the point of writing the necessary and sufficient conditions for the joint cdf $F_{P,\Theta}(\rho,\theta)$ to be the optimal solution. By using the spherical coordinates, the necessary and sufficient conditions for the optimal input distribution is given by

$$\tilde{h}_{V,\Psi}(\rho,\theta;F^*_{P,\Theta}) \leq h(V,\Psi;F^*_{P,\Theta}) + \lambda(\rho^2-u_a)\ ,\ \forall \rho\in[0,\sqrt{u_p}],\ \forall\theta\in[0,2\pi) \tag{3.90}$$

$$\tilde{h}_{V,\Psi}(\rho,\theta;F^*_{P,\Theta}) = h(V,\Psi;F^*_{P,\Theta}) + \lambda(\rho^2-u_a)\ ,\ \forall (\rho,\theta)\in\epsilon^*_{P,\Theta}. \tag{3.91}$$

where $\epsilon^*_{P,\Theta}$ is the set of points of increase in $F^*_{P,\Theta}$.

To make the problem caused by the different symmetries of the noise and the constraint more clear, let's assume $\lambda_1=\lambda_2$ (i.e., as in the previous section with identity channel.) In this case, we rewrite the optimization problem as

$$C(u_p,u_a) = \sup_{F_{P,\Theta(\rho,\theta)}:P^2\leq u_p,\ E[P^2]\leq u_a} h(V,\Psi;F_{P,\Theta}) - \ln(2\pi e\lambda_1^2). \tag{3.92}$$

It is already known that the optimal solution must have independent phase and magnitude with the former being uniformly distributed on $[0,2\pi)$. This can alternatively be inferred from the above necessary and sufficient conditions as follows. Let $f^*_{P,\Theta}(\rho,\theta) = f^*_P(\rho)f^*_{\Theta|P}(\theta|\rho)$ denote the (unique) solution of (3.92) with $\epsilon^*_{P,\Theta}$ as its points of increase. Let the pdf $l^\epsilon_{P,\Theta}$ be defined as

$$l^\epsilon_{P,\Theta}(\rho,\theta) = f^*_P(\rho)f^*_{\Theta|P}(\theta-\epsilon|\rho) \tag{3.93}$$

where ϵ is a constant arbitrarily chosen from $(0,2\pi)$. Let $L^\epsilon_{P,\Theta}$ be the corresponding CDF. It can be easily verified that

$$f_{V,\Psi}(v,\psi;L^\epsilon_{P,\Theta}) = f_{V,\Psi}(v,\psi-\epsilon;F^*_{P,\Theta}) \tag{3.94}$$

and therefore,

$$h(V,\Psi;L^\epsilon_{P,\Theta}) = h(V,\Psi;F^*_{P,\Theta}). \tag{3.95}$$

Since $L^\epsilon_{P,\Theta}$ satisfies the constraints and the optimal solution is unique, it is concluded that

$$f^*_{P,\Theta}(\rho,\theta) = l^\epsilon_{P,\Theta}(\rho,\theta) \tag{3.96}$$

which in turn results in

$$f_{\Theta|P}(\theta|\rho) = f_{\Theta|P}(\theta - \epsilon|\rho). \tag{3.97}$$

Since $\epsilon \in (0, 2\pi)$ was chosen arbitrarily, we conclude that $f_{\Theta|P}(\theta|\rho) = f_{\Theta}(\theta) = \frac{1}{2\pi}$. The problem in the case when $\lambda_1 \neq \lambda_2$ is that if the elliptical domain is used, (3.94) remains true, but $L^{\epsilon}_{P,\Theta}$ does not satisfy the spherical constraints any more, and if the spherical domain is considered, $L^{\epsilon}_{P,\Theta}$ satisfies the constraints, but (3.94) does not hold any longer. Therefore, in what follows, we provide some upper bounds and lower bounds for the capacity of the deterministic channel.

1. Bounds based on the cubic constraints: For brevity, let

$$\mathbb{F}(\mathbf{a}, \mathbf{b}) = \{F_{\mathbf{X}}(\mathbf{x}) | F_{X_i}(x_i) = 0 \; x_i < 0, \; F_{X_i}(x_i) = 1 \; x_i^2 \geq a_i, \int_{\mathbb{R}^n} x_i^2 d^n F_{\mathbf{X}}(\mathbf{x}) \leq b_i \; , \forall i \in [1:n]\} \tag{3.98}$$

be the set of all CDFs with the cubic constraints defined by the vectors $\mathbf{a}$ and $\mathbf{b}$, respectively. By strengthening or weakening the constraints of (3.2), we have

$$\sup_{F_{\mathbf{X}}(\mathbf{x}) \in \mathbb{F}_1} I(\mathbf{X}; \mathbf{Y}) \leq C(u_p, u_a) \leq \sup_{F_{\mathbf{X}}(\mathbf{x}) \in \mathbb{F}_2} I(\mathbf{X}; \mathbf{Y}) \tag{3.99}$$

as long as $\mathbb{F}_1 \subseteq \{F_{\mathbf{X}}(\mathbf{x}) | F_{\mathbf{X}}(\mathbf{x}) = 1 \text{ for } \|\mathbf{x}\|^2 \geq u_p, \int_{\mathbb{R}^n} \|\mathbf{x}\|^2 d^n F_{\mathbf{X}}(\mathbf{x}) \leq u_a\} \subseteq \mathbb{F}_2$. One possible choice for $\mathbb{F}_2$ is obtained with the enhanced cubic constraints as follows

$$\mathbb{F}_2 = \mathbb{F}(u_p \mathbf{1}, u_a \mathbf{1}) \tag{3.100}$$

where $\mathbf{1}$ is the n-dimensional all-one vector. Also, a trivial option for $\mathbb{F}_1$ would be

$$\mathbb{F}_1 = \mathbb{F}(\frac{u_p}{n}\mathbf{1}, \frac{u_a}{n}\mathbf{1}). \tag{3.101}$$

Since the noise elements are independent, we have

$$\sum_{i=1}^{n} \sup_{F_{X_i}(x_i): |X_i|^2 \leq \frac{u_p}{n}, E[|X_i|^2] \leq \frac{u_a}{n}} I(X_i; Y_i) \leq C(u_p, u_a) \leq \sum_{i=1}^{n} \sup_{F_{X_i}(x_i): |X_i|^2 \leq u_p, E[|X_i|^2] \leq u_a} I(X_i; Y_i) \tag{3.102}$$

which leads to

$$\sum_{i=1}^{n} C_S(\frac{\lambda_i^2 u_p}{n}, \frac{\lambda_i^2 u_a}{n}) \leq C(u_p, u_a) \leq \sum_{i=1}^{n} C_S(\lambda_i^2 u_p, \lambda_i^2 u_a) \tag{3.103}$$

In which $C_S(.,.)$ is the capacity of a scalar AWGN channel under peak and average power constraints defined in [25]. The resources could alternatively be allocated according to the noise covariance matrix Σ such that the resource of each component is inversely proportional to its noise variance. Therefore, another possible set for obtaining a lower bound is

$$\mathbb{F}_1 = \mathbb{F}(u_p\mathbf{v}, u_a\mathbf{v}) \tag{3.104}$$

in which $v_i = \frac{\lambda_i^2}{\sum_{j=1}^{n}\lambda_j^2}$. We name this last set of constraints as modified cubic constraints.

2. Bounds based on the elliptical constraints: Another possible set of lower and upper bounds is obtained by strengthening or weakening the constraints in (3.83). By noting that

$$\min\{\lambda_1^{-2}, \lambda_2^{-2}, \ldots, \lambda_n^{-2}\} \leq \mathbf{a}^T(\theta)\mathbf{\Sigma}\mathbf{a}(\theta) \leq \max\{\lambda_1^{-2}, \lambda_2^{-2}, \ldots, \lambda_n^{-2}\} \tag{3.105}$$

we get the two following sets of constraints for the lower and the upper bounds of (3.83), respectively.

$$\mathbb{F}_1 = \{F_{P,\mathbf{\Theta}}(\rho,\theta) | P^2 \leq \min\{\lambda_1^2, \ldots, \lambda_n^2\}u_p \ , \ E[P^2] \leq \min\{\lambda_1^2, \ldots, \lambda_n^2\}u_a\} \tag{3.106}$$

$$\mathbb{F}_2 = \{F_{P,\mathbf{\Theta}}(\rho,\theta) | P^2 \leq \max\{\lambda_1^2, \ldots, \lambda_n^2\}u_p \ , \ E[P^2] \leq \max\{\lambda_1^2, \ldots, \lambda_n^2\}u_a\}. \tag{3.107}$$

Following the same approach as in the proof of the theorem, it can be verified that with these sets of constraints, the lower and the upper bounds results from the input distributions that have finite number of concentric hyper-ellipsoids as their support.

3. Bounds based on whitening the noise: Another trivial set of upper and lower bounds is obtained by whitening the noise and therefore, making it spherically symmetric. It is obvious that

$$\sup_{\Sigma = max\{\lambda_1^{-2},\ldots,\lambda_n^{-2}\}\mathbf{I}} I(\mathbf{X};\mathbf{Y}) \leq C(u_p,u_a) \leq \sup_{\Sigma = min\{\lambda_1^{-2},\ldots,\lambda_n^{-2}\}\mathbf{I}} I(\mathbf{X};\mathbf{Y}) \tag{3.108}$$

where the bounds are obtained by distributions that have finite number of concentric hyper-spheres as their support as in section 3.4. It can be easily verified that the bounds in 2) and 3) are actually the same, although the former is based on weakening or strengthening the constraint and the latter is based on whitening the noise.

4. Lower bound based on Entropy Power Inequality (EPI): The mutual information can be lower bounded as

$$\begin{aligned} I(\mathbf{X};\mathbf{Y}) &= h(\mathbf{Y}) - \frac{1}{2}\ln((2\pi e)^n|\mathbf{\Sigma}|) \\ &\geq \frac{n}{2}\ln\left(e^{\frac{2}{n}h(\mathbf{X})} + e^{\frac{1}{n}\ln((2\pi e)^n|\mathbf{\Sigma}|)}\right) - \frac{1}{2}\ln((2\pi e)^n|\mathbf{\Sigma}|) \end{aligned} \tag{3.109}$$

where in (3.109), vector EPI [35] has been used. In order to get a lower bound for the capacity, we notice that the maximization of $h(\mathbf{X})$ under the peak and average constraints could be written as

$$\begin{aligned} \sup_{F_{\mathbf{X}}(\mathbf{x}):\|\mathbf{X}\|^2\leq u_p,\ E(\|\mathbf{X}\|^2)\leq u_a} h(\mathbf{X}) = \sup_{F_P(\rho):P^2\leq u_p,\ E(P^2)\leq u_a} &- \int_0^\infty f_P(\rho)\ln\frac{f_P(\rho)}{\rho^{n-1}}d\rho \\ &+ \sum_{i=1}^{n-2}\ln\alpha_i + \ln 2\pi. \end{aligned} \tag{3.110}$$

By the change of variable $T = \frac{P^n}{n}$, we have

$$\sup_{F_P(\rho):P^2\leq u_p,\ E(P^2)\leq u_a} - \int_0^\infty f_P(\rho)\ln\frac{f_P(\rho)}{\rho^{n-1}}d\rho = \sup_{F_T(t):T\leq\frac{u_p^{\frac{n}{2}}}{n},\ E(T^{\frac{2}{n}})\leq\frac{u_a}{n^{\frac{2}{n}}}} h(T). \tag{3.111}$$

It can be verified that optimization theory guarantees a unique solution for (3.111) and the necessary and sufficient conditions for f_T^* to be the optimal pdf is the existence of a $\lambda \geq 0$ for which the following inequality holds for any $f_T(t)$ that has its support inside the interval $[0, \frac{u_p^{\frac{n}{2}}}{n}]$

$$\int_0^{\frac{u_p^{\frac{n}{2}}}{n}} (\ln f_T^*(t) + \lambda t^{\frac{2}{n}})(f_T^*(t) - f_T(t))dt \leq 0. \tag{3.112}$$

It is obvious that when $u_a \geq \frac{nu_p}{n+2}$, $\lambda = 0$ and the optimal distribution will be uniform. In the case $u_a < \frac{nu_p}{n+2}$, $\lambda \neq 0$ and the optimal distribution is given by

$$f_T^*(t) = ae^{-\lambda t^{\frac{2}{n}}} \ , \ t \in [0, \frac{u_p^{\frac{n}{2}}}{n}] \tag{3.113}$$

or equivalently

$$f_P^*(\rho) = a\rho^{n-1}e^{-\frac{\lambda\rho^2}{(\sqrt[n]{n})^2}} \ , \ \rho \in [0, \sqrt{u_p}] \tag{3.114}$$

since it satisfies (3.112) with equality. The two degrees of freedom a, λ are uniquely obtained by solving the two following equations:

$$\frac{\int_0^{\frac{u_p^{\frac{n}{2}}}{n}} t^{\frac{2}{n}} e^{-\lambda t^{\frac{2}{n}}} dt}{\int_0^{\frac{u_p^{\frac{n}{2}}}{n}} e^{-\lambda t^{\frac{2}{n}}} dt} = \frac{u_a}{n^{\frac{2}{n}}} \tag{3.115}$$

$$a = \left(\int_0^{\frac{u_p^{\frac{n}{2}}}{n}} e^{-\lambda t^{\frac{2}{n}}} dt \right)^{-1} . \tag{3.116}$$

It can be verified that the left-hand side of (3.115) is a strictly decreasing function of λ having the range $(0, \frac{nu_p}{(n+2)n^{\frac{2}{n}}}]$ and by continuity, there exists a unique $\lambda > 0$ that satisfies (3.115). Substituting this λ in (3.116) gives the value of a which results in

$$h(\mathbf{X}) = \frac{\lambda u_a}{(\sqrt[n]{n})^2} + \ln\left(\frac{2(\sqrt{\pi})^n}{a\Gamma(\frac{n}{2})}\right) \tag{3.117}$$

Substituting (3.117) in (3.109), we get the following lower bound for the capacity

$$C(u_p, u_a) \geq \frac{n}{2} \ln\left(\frac{2^{\frac{2}{n}}\pi}{(a\Gamma(\frac{n}{2}))^{\frac{2}{n}}} e^{\frac{2\lambda u_a}{n(\sqrt[n]{n})^2}} + 2\pi e \sqrt[n]{|\Sigma|} \right) - \frac{1}{2}\ln((2\pi e)^n |\Sigma|) \tag{3.118}$$

A visual representation of some of the bounds is shown in figure 3.1 for $n = 2$, $\lambda_1^2 = 2\lambda_2^2$ and $u_a \geq u_p$. It is obvious that the figures inside the circle (which shows the peak power constraint for the 2-dimensional channel) strengthen the constraint and those outside the circle weaken it. In figure 3.1(a), the two ellipsoids are obtained from (3.105). In other words the inner and the outer ellipsoids are given by

$$a^T(\theta)\mathbf{\Sigma a}(\theta) = \min\{\lambda_1^{-2}, \lambda_2^{-2}\}$$

and

$$a^T(\theta)\mathbf{\Sigma}\mathbf{a}(\theta) = \max\{\lambda_1^{-2}, \lambda_2^{-2}\},$$

respectively. The inner and outer squares in figure 3.1(b) are $[-\sqrt{\frac{u_p}{2}}, \sqrt{\frac{u_p}{2}}]^2$ and $[-\sqrt{u_p}, \sqrt{u_p}]^2$, respectively. The modified cubic constraint in figure 3.1(c) is based on resource allocation according to the channel gains (i.e.,λ_1 and λ_2). Channels 1 and 2 have the peak power of $\frac{\lambda_1^2}{\lambda_1^2+\lambda_2^2}u_p (= \frac{2}{3}u_p$ in this example) and $\frac{\lambda_2^2}{\lambda_1^2+\lambda_2^2}u_p (= \frac{1}{3}u_p$ in this example), respectively.

3.6 Numerical results

As stated in Theorem 3.1, the magnitude of the optimal input distribution has a finite number of mass points and the phases are distributed according to (3.27). The algorithm [8] for finding the number, the positions and the probabilities of the optimal mass points is exactly the same as that explained in [24]. When the average power constraint is relaxed, Figures 3.2 to 3.6 show the capacity of the channel in (3.2) along with the capacity-achieving input distribution for different values of n. In these figures, black, red and green points have their probabilities in the intervals $[0.7, 1]$, $[0.3, 0.7]$ and $[0, 0.3]$, respectively. These points represent the optimal input mass points.

Figure 3.7 shows the capacity of the four dimensional channel versus u_p along with the optimal input for a fixed average power $u_a = 10$. It is obvious that the capacity saturates at its conventional value given in (3.34). This saturation shows the near-optimal performance of the discrete input for the conventional unbounded scenario. For example, when $n = 4$ and $u_a = 10$ the capacity of the channel with unbounded input (i.e., $C_G = 2.5055$) which is achieved by a generalized Rayleigh distributed P, can also be achieved with good approximation (i.e., $I(\mathbf{X};\mathbf{Y}) = 2.5052$) by a pmf having only three mass points below $\sqrt{30}$.

Figure 3.8 shows the capacity versus the average power constraint for a fixed value of the peak power ($u_p = 20$). It is obvious that for $u_a \geq u_p$, the average constraint becomes inactive and the capacity is determined only by u_p. We have already shown that when the peak power is very small (i.e., $u_p \ll 1$) and $u_a \geq u_p$, the optimal input has only one

[8] The codes for this section are available at http://www.ee.ic.ac.uk/bruno.clerckx/Research.html .

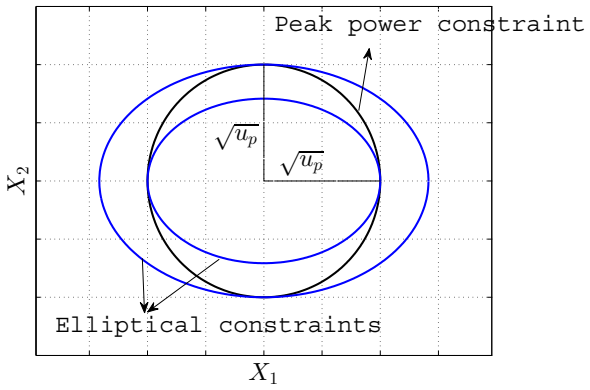

(a) Elliptical Constraints

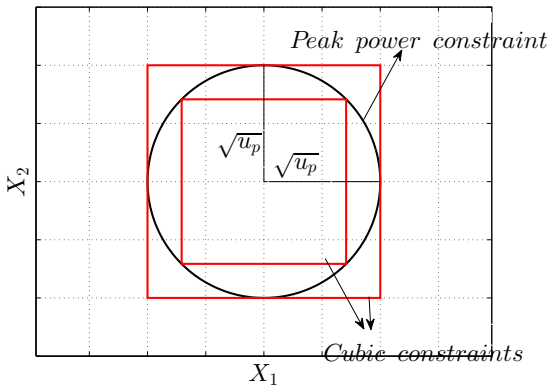

(b) Cubic Constraints

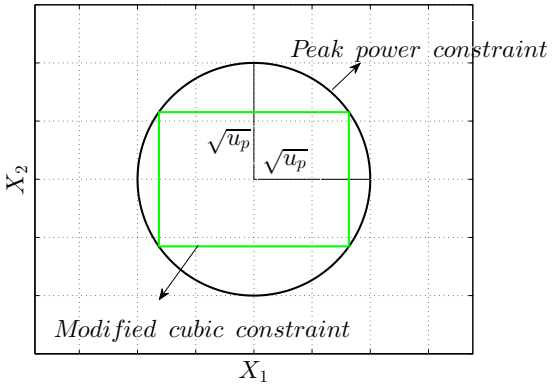

(c) Modified Cubic Constraint

FIGURE 3.1: Weakening or strengthening the peak power constraint for $n = 2$ and $\lambda_1^2 = 2\lambda_2^2$.

mass point at $\rho = \sqrt{u_p}$. Let F_{P_1} denote the cdf of this optimal input. Therefore,

$$f_V(v; F_{P_1}) = K_n(v, \sqrt{u_p}) \tag{3.119}$$

$$\tilde{h}_V(\rho; F_{P_1}) = -\int_0^\infty K_n(v, \rho) \ln(K_n(v, \sqrt{u_p}))dv. \tag{3.120}$$

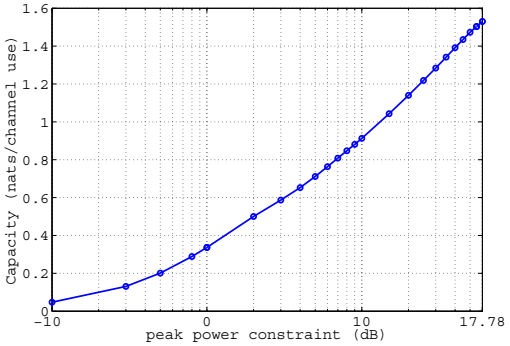

(a) Capacity

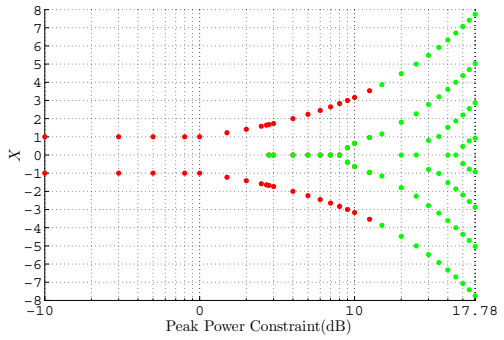

(b) Optimal Input Distribution

FIGURE 3.2: Capacity vs. u_p for $n = 1$ ($u_a \geq u_p$), and the optimal input mass points.

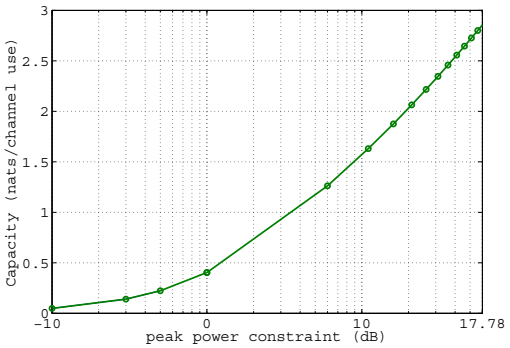

(a) Capacity

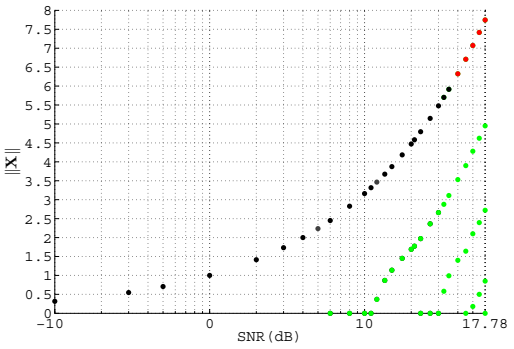

(b) Optimal Input Distribution

FIGURE 3.3: Capacity vs. u_p for $n = 2$ ($u_a \geq u_p$), and the optimal input mass points.

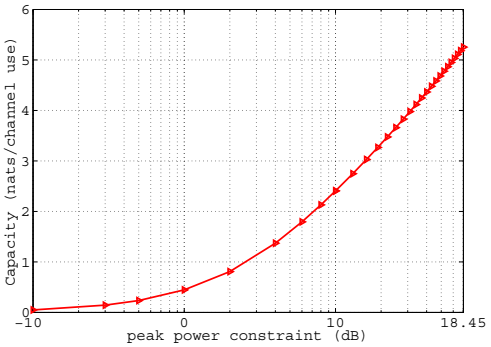

(a) Capacity

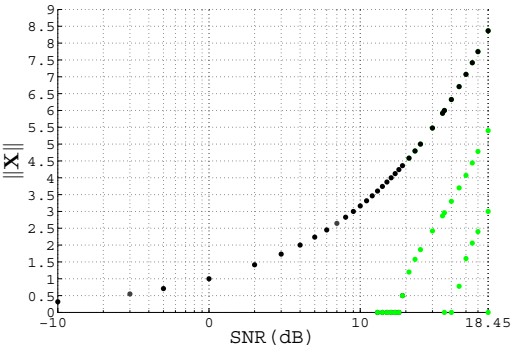

(b) Optimal Input Distribution

FIGURE 3.4: Capacity vs. u_p for $n = 4$ ($u_a \geq u_p$), and the optimal input mass points.

When $u_p \ll 1$, the above marginal entropy density is a convex and increasing function of ρ and satisfies the equality of (3.39) (with $\lambda = 0$) at $\rho = \sqrt{u_p}$ and the inequality of (3.38) at all other points. As u_p increases, F_{P_1} remains optimal until it violates the necessary and sufficient conditions. By observing the behavior of $\tilde{h}_V(\rho, F_{P_1})$, it is concluded that

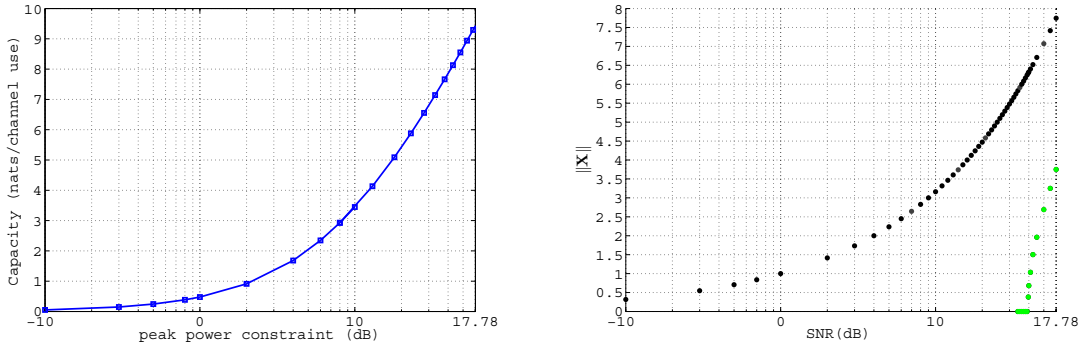

(a) Capacity (b) Optimal Input Distribution

FIGURE 3.5: Capacity vs. u_p for $n = 10$ ($u_a \geq u_p$), and the optimal input mass points.

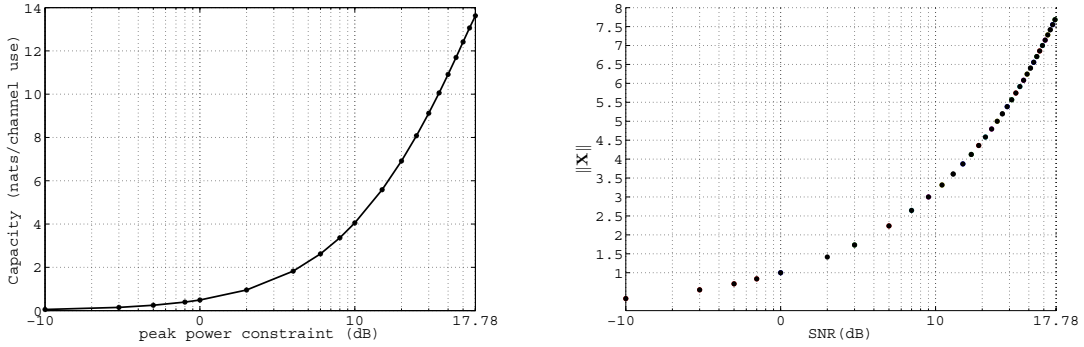

(a) Capacity (b) Optimal Input Distribution

FIGURE 3.6: Capacity vs. u_p for $n = 20$ ($u_a \geq u_p$), and the optimal input mass points.

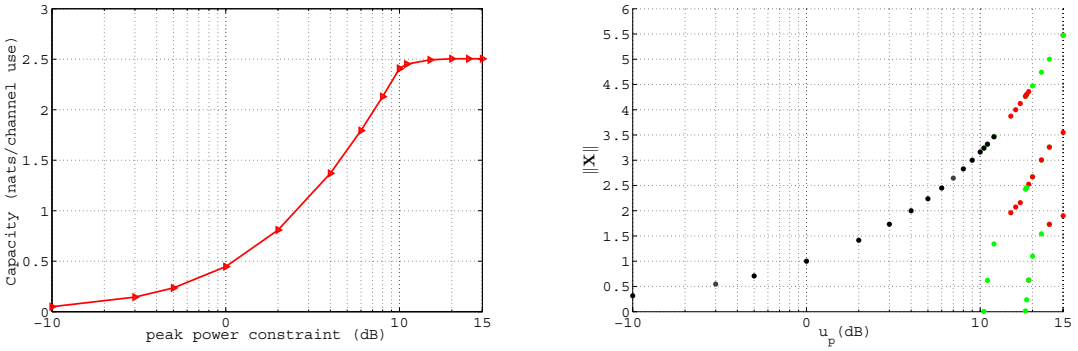

(a) Capacity (b) Optimal Input Distribution

FIGURE 3.7: Capacity vs. u_p for $n = 4$ ($u_a = 10$), and the optimal input mass points.

as u_p increases, the first point to violate the necessary and sufficient conditions will happen at $\rho = 0$. Therefore, the peak power threshold u_p^t for which F_{P_1} remains optimal

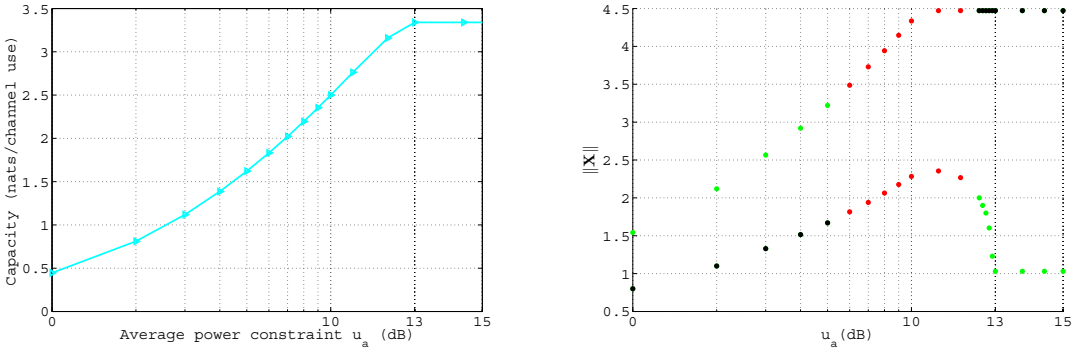

(a) Capacity (b) Optimal Input Distribution

FIGURE 3.8: Capacity vs. u_a for $n = 4$ ($u_p = 20$), and the optimal input mass points.

(when $u_a \geq u_p$) is obtained by solving the following equation for u_p^t

$$\tilde{h}_V(0; F_{P_1}) = h(V; F_{P_1}). \tag{3.121}$$

By solving (3.121) numerically, the values of the peak power threshold are obtained for different values of n as shown in figure 3.9. For example, for $n = 4$, $u_p^t \approx 12.81$ which means that when the peak power is below 12.81, the support of the optimal input has only one hyper-sphere, and at this threshold it gets another mass point at zero as already shown in figure 3.4. For $n = 20$, when $u_p \leq 66$, constant amplitude signaling is optimal which is consistent with figure 3.6. From figure 3.9, it can be observed that the ratio $\frac{u_p}{n}$ does not necessarily need to be vanishingly small to guarantee the optimality of F_{P_1}. Specifically, for the ratios of $\frac{u_p}{n}$ below (approximately) 3.4, F_{P_1} remains optimal.

It has already been shown that when the number of antennas is above a certain threshold, constant amplitude signaling at the peak power (i.e., $\|\mathbf{X}\| = \sqrt{u_p}$) becomes optimal. Figure 3.10 compares the achievable rate of the constant amplitude signaling [9]at the peak power with the capacity of the channel (with the constraint $\|\mathbf{X}\|^2 \leq u_p$) and the unbounded Gaussian input having an average power of u_p. As it can be observed, when the number of antennas is sufficiently large, constant amplitude signaling is not

[9]The rate has been obtained by numerical evaluation of

$$\sup_{F_{\mathbf{X}}(\mathbf{x}):\|\mathbf{X}\|^2=u_p} I(\mathbf{X};\mathbf{Y}) = -\int_0^\infty e^{-\frac{(\sqrt[n]{nv})^2+u_p}{2}} \frac{I_{\frac{n}{2}-1}(\sqrt{u_p}\sqrt[n]{nv})}{(\sqrt{u_p}\sqrt[n]{nv})^{\frac{n}{2}-1}} \ln\left(e^{-\frac{(\sqrt[n]{nv})^2+u_p}{2}} \frac{I_{\frac{n}{2}-1}(\sqrt{u_p}\sqrt[n]{nv})}{(\sqrt{u_p}\sqrt[n]{nv})^{\frac{n}{2}-1}}\right) dv - \frac{n}{2}\ln(2e) + \ln 2.$$

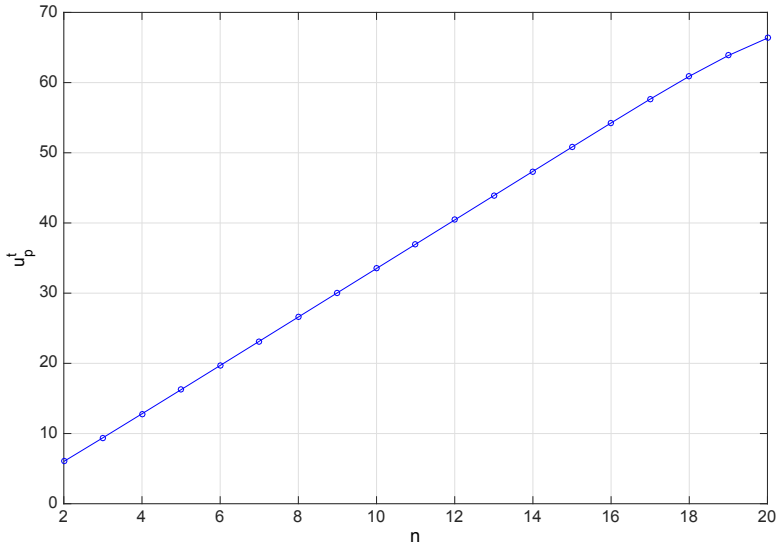

FIGURE 3.9: The peak power threshold for which F_{P_1} remains optimal versus n ($u_a \geq u_p$).

only optimal but also it has a performance close to that of the unbounded Gaussian signaling.

Figures 3.11 and 3.12 demonstrate the bounds for the deterministic MIMO channel in (3.79) for two values of the condition number of the channel. It can be observed that the gap between the elliptical lower and upper bound increases with the condition number. This is intuitively justified by noting that the elliptical bounds converge to the actual capacity of the channel when the condition number approaches unity. For large values of the condition number, the lower bound obtained by modified cubic constraints performs better than the equal resource allocation at small values of the peak power. Finally, it is important to note that although the lower bound obtained by EPI is loose in these two figures, it becomes asymptotically tight for large values of u_p. It can be easily verified by the fact that when the average power constraint is relaxed, we have $\lambda = 0$ and $a = \frac{n}{u_p^2}$ in (3.117). When $u_p \to \infty$ the lower bound in (3.118) gets arbitrarily close to $h(\mathbf{X})$ in (3.117) which is obviously an upper bound for the capacity. This justifies the asymptotic tightness of the bound resulted from EPI at large values of u_p.

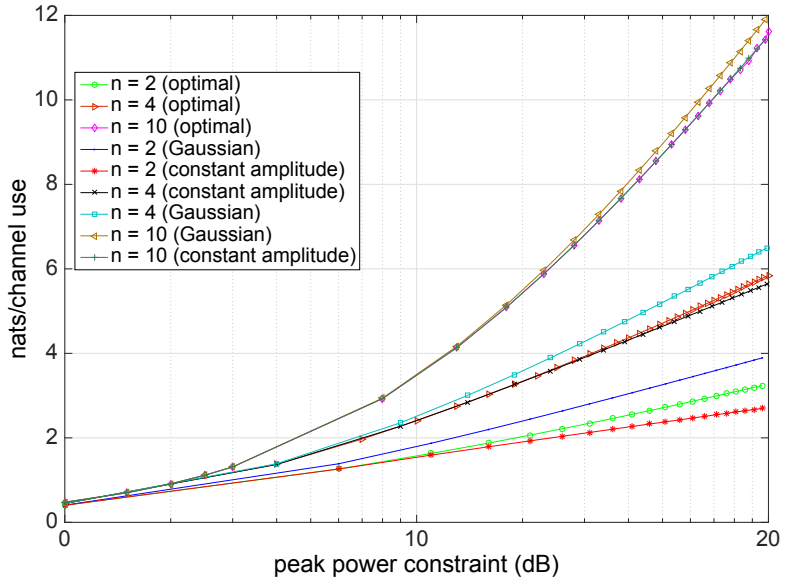

FIGURE 3.10: Achievable rate by the constant amplitude signaling at the peak power (i.e., $\|\mathbf{X}\| = \sqrt{u_p}$) when the average power constraint is relaxed.

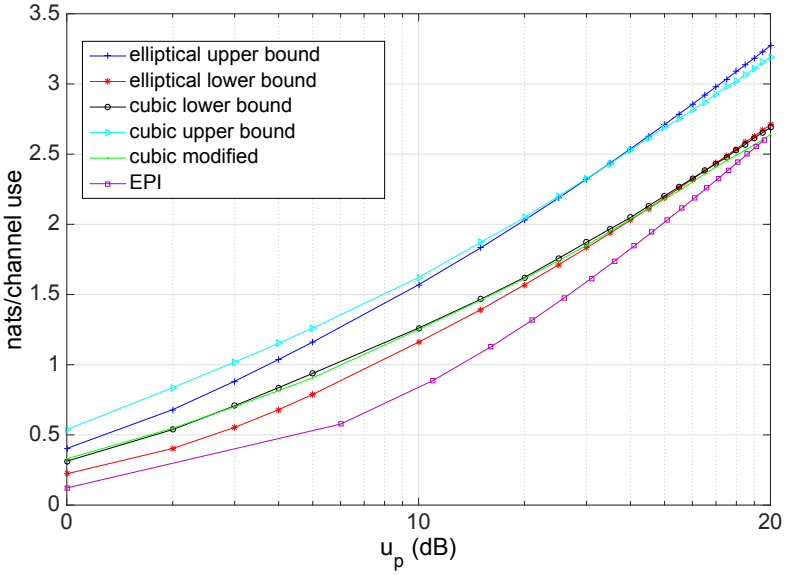

FIGURE 3.11: Bounds for the capacity of the deterministic MIMO channel ($\lambda_2^2 = 2\lambda_1^2 = 1$).

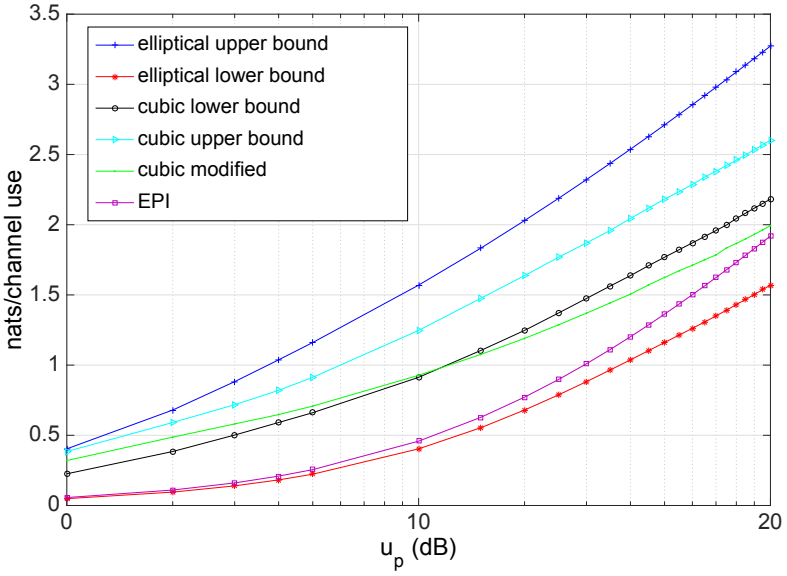

FIGURE 3.12: Bounds for the capacity of the deterministic MIMO channel ($\lambda_2^2 = 10\lambda_1^2 = 1$).

Chapter 4

A Tighter Bound for the Capacity of the Amplitude-Constrained Scalar AWGN Channel

4.1 Overview

This chapter slightly improves the upper bound in Thangaraj et al. on the capacity of the amplitude-constrained scalar AWGN channel. This improvement makes the upper bound within 0.002 bits of the capacity for $\frac{E_b}{N_0} \leq 2.5$ dB.

4.2 Introduction

The capacity of the point-to-point communication system subject to amplitude and variance (or equivalently, peak and average power) constraints was investigated in [25] for the scalar Gaussian channel where it was shown that the capacity-achieving distribution is unique and has a probability mass function with a finite number of mass points. Consequently, the capacity and its achieving distribution can be evaluated numerically where the number, position and probabilities of the mass points are obtained numerically.

In [36], an analytic upper bound is provided on the capacity which reduces the computational burden of numerical methods significantly. Recently, the bound in [36] was

refined in [37]. In this chapter, this bound is further refined by means of increasing the optimization parameters.

This chapter is organized as follows. Section 4.3 provides some preliminaries helpful for the following sections. The main result is given as a theorem in section 4.4. A comparison of the bounds is provided in section 4.5.

4.3 Preliminaries

For a memoryless channel with input X, output Y, input Cumulative Distribution Function (CDF) $F_X(x)$ with support $\mathbb{S}$ and the channel density $f_{Y|X}(y|x)$, we have (as in [37])

$$\begin{aligned} C &= \sup_{F_X(x)} I(X;Y) \\ &= \sup_{F_X(x)} \int D(f_{Y|X}(y|x)||f_Y(y))dF_X(x) && (4.1) \\ &\leq \sup_{F_X(x)} \int D(f_{Y|X}(y|x)||q_Y(y))dF_X(x) && (4.2) \\ &\leq \sup_{x\in\mathbb{S}} D(f_{Y|X}(y|x)||q_Y(y)) && (4.3) \end{aligned}$$

where in (4.1), $D(a||b)$ denotes the relative entropy between the densities a and b. The inequality in (4.2) is a direct consequence of the non-negativity of relative entropy, i.e. $D(f_Y(y)||q_Y(y)) \geq 0$ in which $q_Y(y)$ is an arbitrary test density. Note that, the more similar $q_Y(y)$ is to $f_Y(y)$, the tighter becomes the upper bound in (4.2).

For the scalar AWGN channel, we have

$$Y = X + N \tag{4.4}$$

where $N \sim N(0,1)$ is a Gaussian noise independent of the input. The amplitude-constrained capacity of this channel is

$$C = \max_{F_X(x):|X|\leq A} I(X;Y) \tag{4.5}$$

where A denotes the amplitude constraint.

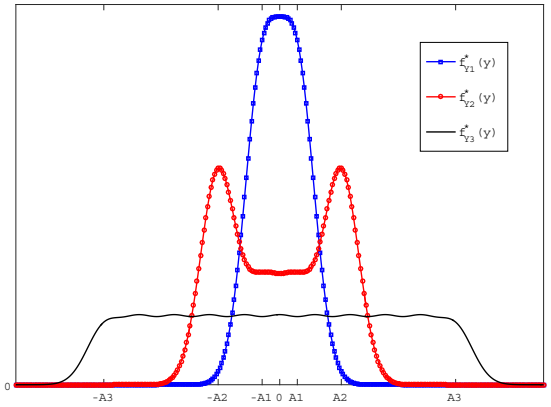

FIGURE 4.1: The optimal output density as A increases.

It was shown in [25] that the capacity-achieving distribution $F^*_X(x)$ has a finite number of mass points in $[-A, A]$. McKellips proposed an analytic upper bound for C based on bounding the entropy of Y in [36]. In [37], the upper bound for the capacity is further refined. The main idea is to find a simple test density $q_Y(y)$ that looks quite similar to the optimal output density $f^*_Y(y)$, which results from the optimal input $F^*_X(x)$, and plug it into (4.2) to get a tight upper bound. Since, as mentioned before, the more similar $q_Y(y)$ is to $f_Y(y)$, the tighter becomes the upper bound in (4.2).

Figure 4.1 shows the optimal output density $f^*_Y(y)$ for three values of the amplitude constraint ($A_1 < A_2 < A_3$). As it can be observed, it is intuitive to take a test density $q_Y(y)$ which is uniform on $[-A, A]$ and has Gaussian tails towards infinity[1].

The following functions are frequently used throughout this chapter

$$\psi(x) = \frac{1}{\sqrt{2\pi}} e^{-\frac{x^2}{2}}$$
$$Q(x) = \int_x^{+\infty} \psi(t)dt$$
$$g(u) \triangleq u^2 Q(u) - u\psi(u).$$

For the capacity in (4.5), a trivial upper bound is the capacity with average power constraint, i.e. $\frac{1}{2}\log(1+P)$ in which $P = A^2$. Therefore, the bounds proposed in

[1] According to Figure 4.1, this choice of test density is more acceptable in small or very large values of A.

literature have the general form of

$$C \leq \min\left\{\mathcal{T}(P), \frac{1}{2}\log(1+P)\right\} \tag{4.6}$$

where in [36], we have

$$\mathcal{T}(P) = \log\left(1+\sqrt{\frac{2P}{\pi e}}\right) \tag{4.7}$$

and in [37], it was tightened further for $P \leq 6.303$ dB as[2]

$$\mathcal{T}(P) = \beta(P)\log\sqrt{\frac{2P}{\pi e}} + H(\beta(P)) \tag{4.8}$$

in which $\beta(P) = \frac{1}{2} - Q(2\sqrt{P})$ and $H(x) = -x\log(x) - (1-x)\log(1-x)$.[3]

In the following section, we further tighten $\mathcal{T}(P)$ for the whole SNR regime.

4.4 Main results

Theorem 4.1. *The capacity in (4.5) has the following upper bound*

$$C \leq \min\left\{R(P) + W(P), \frac{1}{2}\log(1+P)\right\} \tag{4.9}$$

where

$$W(P) = \frac{1}{2}\left(\log\sigma^2(P) + \frac{1}{\sigma^2(P)} - 1\right)\left(\frac{1}{2} + Q(2\sqrt{P})\right) + \frac{g(2\sqrt{P})}{2\sigma^2(P)} \tag{4.10}$$

in which

$$\sigma^2(P) = 1 + \frac{2g(2\sqrt{P})}{1+2Q(2\sqrt{P})}, \tag{4.11}$$

and

$$R(P) = \begin{cases} \log\left(1+\sqrt{\frac{2P}{\pi e}}\right) & P \geq 6.303dB \\ \beta(P)\log\sqrt{\frac{2P}{\pi e}} + H(\beta(P)) & otherwise \end{cases}. \tag{4.12}$$

Note that in the very small/large SNR regimes (i.e., $P \ll 0.1$ or $P \gg 0.5$), $\sigma^2(P) \approx 1$ and $g(2\sqrt{P}) \approx 0$ which makes the bound boil down to (4.7) and (4.8).

[2] This is the RHS of (17) in [37].
[3] The logarithms are in base e.

Proof. Consider the following family of test densities

$$q_Y(y) = \begin{cases} \frac{\beta}{2A} & |y| \leq A \\ \frac{1-\beta}{\sqrt{2\pi\sigma^2}} e^{-\frac{(y-A)^2}{2\sigma^2}} & |y| > A \end{cases} \tag{4.13}$$

where σ^2 and $\beta (\in [0,1])$ are parameters to be optimized. With this choice of test density, the relative entropy in (4.3) is evaluated as

$$\begin{aligned} D(f_{Y|X}(y|x)||q_Y(y)) &= \int_{-\infty}^{+\infty} \psi(y-x) \log \frac{\psi(y-x)}{q_Y(y)} dy \\ &= \log \frac{2A}{\beta\sqrt{2\pi e}} + \log \frac{\beta\sqrt{2\pi e}}{(1-\beta)2A} \left[Q(A-x) + Q(A+x)\right] \\ &\quad + \frac{1}{2}\left(\log \sigma^2 + \frac{1}{\sigma^2} - 1\right) \left[Q(A-x) + Q(A+x)\right] \\ &\quad + \frac{1}{2\sigma^2}[g(A-x) + g(A+x)] \end{aligned} \tag{4.14}$$

We first find the maximum of (4.14) over $x \in [-A, A]$ and then minimize this maximum value over the parameters β and σ^2. In other words,

$$C \leq \min_{\beta,\sigma^2} \max_{-A \leq x \leq A} D(f_{Y|X}(y|x)||q_Y(y)). \tag{4.15}$$

As it can be observed, (4.14) is an even function of x which makes the region of interest as $x \in [0, A]$. Also, the optimization of the first two terms in (4.14) was done in [37]. Therefore, we focus on the remaining terms.

Lemma. The following inequality holds for $\forall x \in [0, A]$

$$g(A-x) + g(A+x) \leq g(2A). \tag{4.16}$$

Proof. The proof is provided in Appendix H. □

It can be easily verified that $Q(A-x) + Q(A+x)$ is an increasing function of $x \in [0, A]$ and $\log x + \frac{1}{x} - 1 \geq 0$ for $x > 0$. Therefore, we can write

$$\begin{aligned} &\frac{1}{2}\left(\log \sigma^2 + \frac{1}{\sigma^2} - 1\right) \left[Q(A-x) + Q(A+x)\right] + \frac{1}{2\sigma^2}[g(A-x) + g(A+x)] \\ &\leq \frac{1}{2}\left(\log \sigma^2 + \frac{1}{\sigma^2} - 1\right) \left(\frac{1}{2} + Q(2A)\right) + \frac{1}{2\sigma^2} g(2A). \end{aligned} \tag{4.17}$$

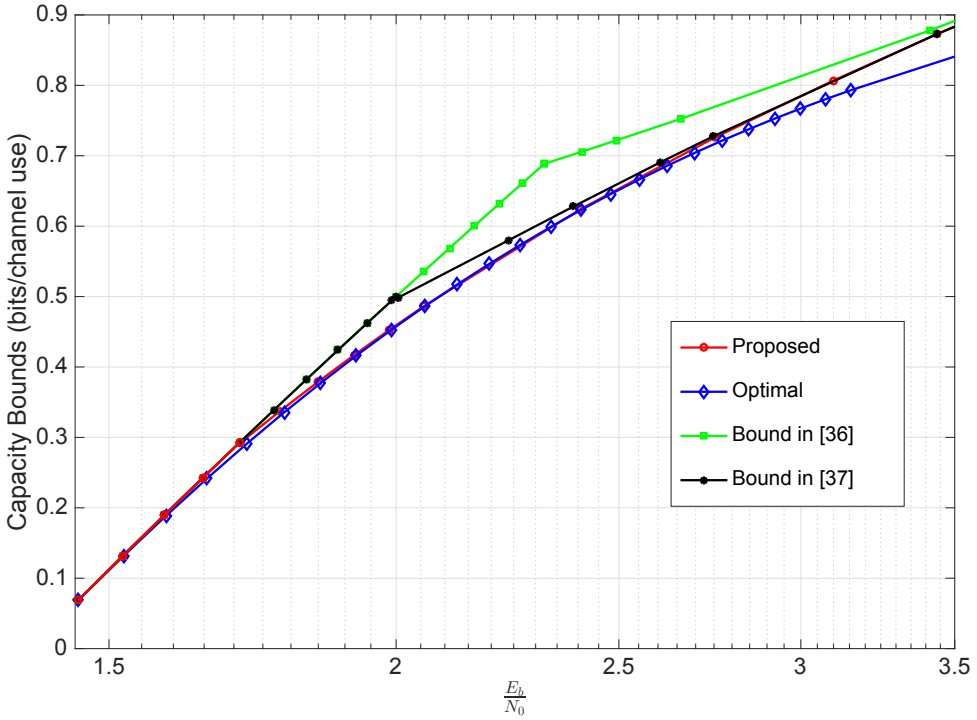

FIGURE 4.2: Comparison of the bounds.

The RHS of (4.17) is minimized by setting σ^2 as in (4.11) and the minimum is equal to $W(P)$ in (4.10). This completes the proof. □

Note that the lemma is the key part in allowing to add σ^2 to the optimization parameters, since if the trivial upper bound of zero is used instead of (4.16), the optimal value of σ^2 would be one (as used in [36] and [37]).

4.5 Numerical results

Figure 4.2 compares the bounds in literature with the one proposed in this chapter. We observe that the addition of σ^2 to the optimization problem results in the tightest bound. This small improvement is mainly visible in the range $[-1.5, 2.5]$ dB (SNR per bit) as shown in the figure.

Chapter 5

Constant Envelope Signaling in parallel Channels

5.1 Overview

The capacity of the point-to-point vector Gaussian channel under the peak power constraint is not known in general. In this chapter, we consider a simpler scenario in which the input signal vector is forced to have a constant envelope (or norm). The capacity-achieving distribution for the non-identity 2×2 parallel when the input vector lies on a circle in $\mathbb{R}^2$ is obtained and is shown to have a finite number of mass points on the circle. Subsequently, it is shown that the degrees of freedom (DoF) of a full-rank n by n channel with constant envelope signaling is $n-1$ and it can be achieved by a uniform distribution over the surface of the hypersphere whose radius is defined by the constant envelope.

5.2 Introduction

The capacity of the Gaussian MIMO with identity channel under the peak and average power constraints is shown in chapter 3 (and in [38]) where the support of the optimal input distribution is a finite set of hyper-spheres with mutually independent phases and amplitude in the spherical domain. However, the capacity of the general point-to-point Gaussian MIMO channel under the peak power constraint is an open problem. In this

chapter, we address a simpler problem in which the input is forced to have a constant envelope (i.e., for any codeword $\mathbf{x}^n(m)$ where m denotes the message index, instead of the peak power constraint which is equivalent to $\|\mathbf{x}_i(m)\| \leq R\ ,\ \forall i \in [1:n]$, a stronger condition, which is $\|\mathbf{x}_i(m)\| = R\ ,\ \forall i \in [1:n]$, must be satisfied). A 2 by 2 non-identity channel matrix is considered. The capacity of this channel under constant-norm inputs is obtained and it is shown that the capacity achieving distribution has a finite number of mass points on the circle defined by the constraint. Although the capacity does not have a closed form solution, lower and upper bounds can be obtained for it which are sufficient to give the optimal degrees of freedom (DoF). As a result, it is shown that the degrees of freedom (DoF) of a full-rank n by n channel with constant envelope signaling is $n-1$ and it can be achieved by a uniform distribution over the surface of the hypersphere whose radius is defined by the constant envelope.

The steps for proving the finiteness of the support of the optimal input is similar to that in [25] which is based on contradiction. More precisely, first, it is assumed that the optimal input has an infinite number of mass points. By using some tools in real and complex analysis, this assumption leads to an equality (involving a probability density function) which must be satisfied on a set. The last part of the proof is showing that this equality does not hold, and therefore disproving the first assumption of an infinite number of points for the optimal input distribution. In [25] and [24] this contradiction is obtained by directly solving for the probability density function (by means of Fourier and Laplace transforms) and showing that either it is not a legitimate pdf or it cannot be induced by the input. Hermite polynomials and its properties were used in [39] to solve for the probability density function and get the contradiction. The application of these methods and solving for the pdf is not straightforward for the problem considered in this chapter. Therefore, knowing that the right hand side of the aforementioned equality is a constant, we obtain the contradiction by showing that the left hand side of this equality can become unbounded with its parameter.

This chapter is organized as follows. Section 5.3 explains the system model under consideration. Section 5.4 states the main result of this chapter through a theorem whose detailed proof is given in section 5.5. The asymptotic behavior of the capacity-achieving input distribution for small values of SNR along with the degrees of freedom under constant envelope signaling are presented in section 5.6 . In section 5.7, the problem

is analyzed in the polar coordinates and the notations of this section will be used in section 5.8 which shows the numerical results.

5.3 System model

We consider a 2×2 discrete-time memoryless vector Gaussian channel given by

$$\mathbf{Y}_i = \mathbf{H}\mathbf{X}_i + \mathbf{W}_i \tag{5.1}$$

in which i denotes the channel use. $\mathbf{H} = \text{diag}\{\lambda, 1\}$ ($|\lambda| \neq 1$) is the deterministic channel matrix and $\{\mathbf{W}_i\}$ is an i.i.d. noise vector process with $\mathbf{W}_i \sim N(\mathbf{0}, \mathbf{I}_2)$ (and independent of $\mathbf{X}_i$) for every transmission $i \in [1 : n]$. The assumption of $|\lambda| \neq 1$ is to exclude the identity channel matrix for which the capacity-achieving distribution under a fixed transmission power is already known in [40] (i.e., the optimal input has uniform phase on the circle defined by the constant norm). It can be easily verified that it is sufficient to consider only the case $\lambda > 1$. [1]

The capacity of this channel under a fixed transmission power (i.e., constant norm) is

$$C(R) = \sup_{F_{\mathbf{X}}(\mathbf{x}):\|\mathbf{X}\| \overset{a.s.}{=} R} I(\mathbf{X};\mathbf{Y}) = \sup_{F_{\mathbf{X}}(\mathbf{x}):\|\mathbf{X}\| \overset{a.s.}{=} R} h(\mathbf{Y}) - \ln(2\pi e) \tag{5.2}$$

where R denotes the constant envelope and the capacity is in $\frac{\text{nats}}{\text{channel use}}$. $F_{\mathbf{X}}(\mathbf{x})$ denotes the CDF of the input over which the optimization is done. The pdf of the output determined by the input is given by

$$f_{\mathbf{Y}}(\mathbf{y}; F_{\mathbf{X}}) = \iint_{\|\mathbf{x}\|=R} \frac{1}{2\pi} e^{-\frac{(y_1-\lambda x_1)^2}{2} - \frac{(y_2-x_2)^2}{2}} d^2F_{\mathbf{X}}(\mathbf{x}) \tag{5.3}$$

where the notation $f_{\mathbf{Y}}(\mathbf{y}; F_{\mathbf{X}})$ is to emphasize that $\mathbf{Y}$ has been resulted by $F_{\mathbf{X}}$. Due to the symmetry of noise and constant amplitude of the input, it suffices to consider the input distributions that satisfy the following

$$d^2F_{\mathbf{X}}(\mathbf{x}) = (dF_{X_1}(x_1)).\left[\frac{1}{2}\delta(x_2 - \sqrt{R^2 - x_1^2}) + \frac{1}{2}\delta(x_2 + \sqrt{R^2 - x_1^2})\right] dx_2 \tag{5.4}$$

[1] This can be justified by a simple normalization and symmetry of the noise.

where $\delta(\cdot)$ is the Dirac-delta function. In other words, any other input distribution that does not take the form in (5.4), cannot be an optimal distribution and hence is excluded from our consideration.

Substituting (5.4) in (5.3), we get the output pdf as

$$f_{\mathbf{Y}}(\mathbf{y}; F_{X_1}) = \int_{-R}^{R} K(y_1, y_2, x) dF_{X_1}(x) \tag{5.5}$$

where the kernel is [2]

$$K(y_1, y_2, x) = \frac{1}{2\pi} e^{-\frac{(y_1-\lambda x)^2}{2}} \left[\frac{1}{2} e^{-\frac{(y_2-\sqrt{R^2-x^2})^2}{2}} + \frac{1}{2} e^{-\frac{(y_2+\sqrt{R^2-x^2})^2}{2}} \right]. \tag{5.6}$$

The marginal entropy density of the output variables induced by the input is defined as [25]

$$\tilde{h}_{\mathbf{Y}}(x; F_{X_1}) = -\int_{-\infty}^{\infty}\int_{-\infty}^{\infty} K(y_1, y_2, x) \ln f_{\mathbf{Y}}(\mathbf{y}; F_{X_1}) d\mathbf{y} \tag{5.7}$$

which satisfies the following (which in turn justifies why it is named density)

$$h(\mathbf{Y}; F_{X_1}) = \int_{-R}^{R} \tilde{h}_{\mathbf{Y}}(x; F_{X_1}) dF_{X_1}(x). \tag{5.8}$$

Finally, the optimization problem in (5.2) becomes equivalent to

$$C(R) = \sup_{F_{X_1}(x): X_1 \in [-R,R]} h(\mathbf{Y}; F_{X_1}) - \ln(2\pi e) \tag{5.9}$$

where $X_1 \in [-R, R]$ is in $a.s.$ sense.

5.4 Main results

Let ϵ_X^* denote the set of points of increase of the optimal input distribution.[3]

[2] The kernel function is the same as the conditional pdf of the output given the input i.e., $f_{\mathbf{Y}|X}(\mathbf{y}|x)$.

[3] A point P is said to be a point of increase of a distribution if for any open set Γ containing P, we have $\Pr\{\Gamma\} > 0$.

Theorem 5.1. *The optimization problem in (5.9) has a unique solution (denoted by $F^*_{X_1}(x)$) which satisfies the following necessary and sufficient conditions*

$$\tilde{h}_{\mathbf{Y}}(x; F^*_{X_1}) = h(\mathbf{Y}; F^*_{X_1}) \quad \forall x \in \epsilon^*_X \tag{5.10}$$

$$\tilde{h}_{\mathbf{Y}}(x; F^*_{X_1}) < h(\mathbf{Y}; F^*_{X_1}) \quad \forall x \in [-R, R] - \epsilon^*_X. \tag{5.11}$$

Further, ϵ^*_X consists of a finite number of mass points in the interval $[-R, R]$ (i.e., $|\epsilon^*_X| < \infty$).

5.5 Proof of Theorem 5.1

The steps of the proof are as follows. The uniqueness of the solution along with the necessary and sufficient conditions are obtained through the convex optimization problem. The finite cardinality of ϵ^*_X is proved by contradiction. In other words, it is shown that infinite number of mass points for the optimal input is not possible.

Let $\mathbb{F}_R$ denote the set of all cumulative distribution functions having their support in the interval $[-R, R]$, i.e.

$$\mathbb{F}_R = \{F_{X_1}(x) | F_{X_1}(x) = 0 \ \forall x < -R \ , \ F_{X_1}(x) = 1 \ \forall x \geq R\}. \tag{5.12}$$

Proposition 1. The metric space $(\mathbb{F}_R, d_L)$ is convex and compact where d_L denotes the Levy metric [41].

Proof. The proof is the same as that in [42] and [26, Appendix I]. □

Proposition 2. The differential entropy $h(\mathbf{Y}; F_{X_1}) : \mathbb{F}_R \to \mathbb{R}$ is continuous.

Proof. The proof is the same as that in [42], [24, Proposition 3], [26, Appendix I] and [29, Proposition 1]. □

Proposition 3. The differential entropy $h(\mathbf{Y}; F_{X_1}) : \mathbb{F}_R \to \mathbb{R}$ is strictly concave and weakly differentiable.

Proof. The proof is the same as that in [42], [24, Proposition 4], [26, Appendix II] and [29, Proposition 2]. □

The weak derivative of $h(\mathbf{Y}; F_{X_1})$ at $F^0_{X_1}$ is given by

$$\begin{aligned}
&h'_{F^0_{X_1}}(\mathbf{Y}; F_{X_1}) \\
&= \lim_{\zeta \to 0} \frac{h(\mathbf{Y}; (1-\zeta)F^0_{X_1} + \zeta F_{X_1}) - h(\mathbf{Y}; F^0_{X_1})}{\zeta} \\
&= \lim_{\zeta \to 0} \frac{\int_{-R}^{R} \tilde{h}_{\mathbf{Y}}\left(x; (1-\zeta)F^0_{X_1} + \zeta F_{X_1}\right) d\left((1-\zeta)F^0_{X_1}(x) + \zeta F_{X_1}(x)\right) - \int_{-R}^{R} \tilde{h}_{\mathbf{Y}}\left(x; F^0_{X_1}\right) dF^0_{X_1}(x)}{\zeta} \\
&= \lim_{\zeta \to 0} \frac{(1-\zeta)\int_{-R}^{R} \tilde{h}_{\mathbf{Y}}(x; F^0_{X_1}) dF^0_{X_1}(x) + \zeta \int_{-R}^{R} \tilde{h}_{\mathbf{Y}}(x; F^0_{X_1}) dF_{X_1}(x) - \int_{-R}^{R} \tilde{h}_{\mathbf{Y}}\left(x; F^0_{X_1}\right) dF^0_{X_1}(x)}{\zeta} \\
&= \int_{-R}^{R} \tilde{h}_{\mathbf{Y}}(x; F^0_{X_1}) dF_{X_1}(x) - h(\mathbf{Y}; F^0_{X_1}) \quad , \quad \forall F_{X_1} \in \mathbb{F}_R. \qquad (5.13)
\end{aligned}$$

Since $h(\mathbf{Y}; F_{X_1})$ is a concave map from $\mathbb{F}_R$ to $\mathbb{R}$, Lagrangian optimization [43] guarantees a unique solution for (5.9) and the necessary and sufficient condition for the maximizer $F^*_{X_1}$ is

$$\int_{-R}^{R} \tilde{h}_{\mathbf{Y}}(x; F^*_{X_1}) dF_{X_1}(x) \leq h(\mathbf{Y}; F^*_{X_1}) \quad , \quad \forall F_{X_1} \in \mathbb{F}_R. \qquad (5.14)$$

It can be shown that (5.14) is equivalent to (5.10) and (5.11) (as in [25, Corollary 1]). The marginal entropy density can be extended to the complex domain, i.e.

$$\tilde{h}_{\mathbf{Y}}(z; F_{X_1}) = -\int_{-\infty}^{\infty}\int_{-\infty}^{\infty} K(y_1, y_2, z) \ln f_{\mathbf{Y}}(\mathbf{y}; F_{X_1}) d\mathbf{y} \quad , \quad z \in \mathbb{C}. \qquad (5.15)$$

Let $\mathbb{D} = \mathbb{C} - \{(-\infty, -R] \cup [R, +\infty)\}$.

Proposition 4. The kernel $K(y_1, y_2, z)$ is holomorphic on $\mathbb{D}$.

Proof. This can be verified[4] by the fact that the real and imaginary parts of $K(y_1, y_2, z = x + jy)$ have continuous partial derivatives and satisfy the Cauchy-Riemann equations on $\mathbb{D}$. As a result, by Cauchy's theorem, for every rectifiable closed curve γ in $\mathbb{D}$,

$$\int_{\gamma} K(y_1, y_2, z) dz = 0. \qquad (5.16)$$

□

[4] Alternatively, it can be verified by noting that $\mathbb{D}$ is the domain where $\log(R^2 - z^2)$ is holomorphic.

Proposition 5. The marginal entropy density $\tilde{h}_{\mathbf{Y}}(z; F_{X_1})$ is holomorphic on $\mathbb{D}$.

Proof. First, we show the continuity of $\tilde{h}_{\mathbf{Y}}(z; F_{X_1})$ on $\mathbb{D}$. Let $\{z_m\}_1^\infty$ be a sequence of complex numbers in $\mathbb{D}$ converging to $z_0 \in \mathbb{D}$. Since $K(y_1, y_2, z)$ is holomorphic on this domain, it is continuous. Therefore,

$$\lim_{m\to\infty} K(y_1, y_2, z_m) \ln f_{\mathbf{Y}}(\mathbf{y}; F_{X_1}) = K(y_1, y_2, z_0) \ln f_{\mathbf{Y}}(\mathbf{y}; F_{X_1}). \tag{5.17}$$

By the application of Lebesgue's dominated convergence theorem, the continuity and boundedness of the kernel guarantees the continuity of $f_{\mathbf{Y}}(\mathbf{y}; F_{X_1})$ given in (5.5). This allows us to write

$$\min_{x\in[-R,R]} K(y_1, y_2, x) \le f_{\mathbf{Y}}(\mathbf{y}; F_{X_1}) \le \max_{x\in[-R,R]} K(y_1, y_2, x). \tag{5.18}$$

Therefore,

$$\frac{1}{2\pi} e^{-\frac{y_1^2+y_2^2}{2} - \frac{\lambda^2 R^2}{2} - \lambda R|y_1|} \le f_{\mathbf{Y}}(\mathbf{y}; F_{X_1}) \le \frac{1}{2\pi} e^{-\frac{y_1^2+y_2^2}{2} - \frac{R^2}{2} + \lambda R|y_1|} \cosh Ry_2 \tag{5.19}$$

which results in

$$|\ln f_{\mathbf{Y}}(\mathbf{y}; F_{X_1})| \le \ln(2\pi) + \frac{y_1^2+y_2^2}{2} + \frac{\lambda^2 R^2}{2} + \lambda R|y_1| + \ln(\cosh Ry_2). \tag{5.20}$$

It can be verified that

$$\begin{aligned}
&|\tilde{h}_{\mathbf{Y}}(z_m; F_{X_1})| \\
&\le \int_{-\infty}^{\infty}\int_{-\infty}^{\infty} |K(y_1, y_2, z_m)||\ln f_{\mathbf{Y}}(\mathbf{y}; F_{X_1})| d\mathbf{y} \\
&\le |\frac{1}{2\pi} e^{-\frac{(\lambda^2-1)z_m^2}{2}}| e^{-\frac{R^2}{2}} \int_{-\infty}^{\infty}\int_{-\infty}^{\infty} e^{-\frac{y_1^2+y_2^2}{2}} |e^{\lambda y_1 z_m}||\cosh(y_2\sqrt{R^2 - z_m^2})||\ln f_{\mathbf{Y}}(\mathbf{y}; F_{X_1})| d\mathbf{y} \\
&\le |\frac{1}{2\pi} e^{-\frac{(\lambda^2-1)z_m^2}{2}}| e^{-\frac{R^2}{2}} \int_{-\infty}^{\infty}\int_{-\infty}^{\infty} e^{-\frac{y_1^2+y_2^2}{2}} e^{\lambda y_1 \mathrm{Re}(z_m)} e^{|y_2|\sqrt{R^2+|z_m|^2}} |\ln f_{\mathbf{Y}}(\mathbf{y}; F_{X_1})| d\mathbf{y} \qquad (5.21) \\
&< \infty \qquad (5.22)
\end{aligned}$$

where in (5.21), we have used the fact that $|e^z| = e^{\mathrm{Re}(z)}$, $|\cosh(z)| \le \cosh(\mathrm{Re}(z))$ and $\cosh(x) \le e^{|x|} (x \in \mathbb{R})$. (5.22) is due to the upper bound in (5.20) and the term $e^{-\frac{y_1^2+y_2^2}{2}}$ in the integration. Since the absolute value of the integrand of $\tilde{h}_{\mathbf{Y}}(z_m; F_{X_1})$ is integrable,

by Lebesgue's dominated convergence theorem, we have

$$\begin{aligned}\lim_{m\to\infty}\tilde{h}_{\mathbf{Y}}(z_m;F_{X_1}) &= -\lim_{m\to\infty}\int_{-\infty}^{\infty}\int_{-\infty}^{\infty}K(y_1,y_2,z_m)\ln f_{\mathbf{Y}}(\mathbf{y};F_{X_1})d\mathbf{y}\\ &= -\int_{-\infty}^{\infty}\int_{-\infty}^{\infty}\lim_{m\to\infty}K(y_1,y_2,z_m)\ln f_{\mathbf{Y}}(\mathbf{y};F_{X_1})d\mathbf{y}\\ &= -\int_{-\infty}^{\infty}\int_{-\infty}^{\infty}K(y_1,y_2,z_0)\ln f_{\mathbf{Y}}(\mathbf{y};F_{X_1})d\mathbf{y}\\ &= \tilde{h}_{\mathbf{Y}}(z_0;F_{X_1}) \qquad (5.23)\end{aligned}$$

which proves the continuity of $\tilde{h}_{\mathbf{Y}}(z;F_{X_1})$. Let ∂T denote an arbitrary triangle in $\mathbb{D}$. We can write,

$$\begin{aligned}\int_{\partial T}\tilde{h}_{\mathbf{Y}}(z;F_{X_1})dz &= -\int_{\partial T}\int_{-\infty}^{\infty}\int_{-\infty}^{\infty}K(y_1,y_2,z)\ln f_{\mathbf{Y}}(\mathbf{y};F_{X_1})d\mathbf{y}dz\\ &= -\int_{-\infty}^{\infty}\int_{-\infty}^{\infty}\int_{\partial T}K(y_1,y_2,z)dz\ln f_{\mathbf{Y}}(\mathbf{y};F_{X_1})d\mathbf{y} \qquad (5.24)\\ &= 0 \qquad (5.25)\end{aligned}$$

where (5.24) is allowed by Fubini's theorem, because for a given rectifiable triangle ∂T,

$$\int_{\partial T}|\tilde{h}_{\mathbf{Y}}(z;F_{X_1})|dz<\infty. \qquad (5.26)$$

(5.25) is due to the holomorphy of $K(y_1,y_2,z)$ (see (5.16)). Therefore, by Morera's theorem (with weakened hypothesis) [44], it is concluded that $\tilde{h}_{\mathbf{Y}}(z;F_{X_1})$ is holomorphic on $\mathbb{D}$. □

If ϵ_X^* has an infinite number of points, since it is bounded in $[-R,R]$, it must have an accumulation point by Bolzano-Weierstrass theorem. If the accumulation point is in $(-R,R)$, it is also in the domain where the marginal entropy density is holomorphic (i.e., $\mathbb{D}=\mathbb{C}-\{(-\infty,-R]\cup[R,+\infty)\}$). Therefore, by using the identity theorem of holomorphic functions of one complex variable, the following must be satisfied

$$\tilde{h}_{\mathbf{Y}}(z;F_{X_1}^*)=h(\mathbf{Y};F_{X_1}^*) \quad , \quad \forall z\in\mathbb{D}. \qquad (5.27)$$

If the accumulation point is on the boundary (i.e. it is $\pm R$) where the holomorphy fails to hold (and the usage of identity theorem is not allowed), we can still show that (5.27) must hold. The reason is as follows. Note that an accumulation point of P ($\in[-R,R]$)

on the x_1 axis is equivalent to an accumulation point of $\sqrt{R^2-P^2}$ ($\in[-R,R]$) on the x_2 axis and vice versa. Therefore, if there is an accumulation point of $\pm R$ on x_1 axis, there is an accumulation point of 0 on x_2 axis. By using an alternative representation of the input distribution in (5.4), we can write

$$d^2F_{\mathbf{X}}(\mathbf{x}) = (dF_{X_2}(x_2)).\left[\frac{1}{2}\delta(x_1-\sqrt{R^2-x_2^2})+\frac{1}{2}\delta(x_1+\sqrt{R^2-x_2^2})\right]dx_1 \tag{5.28}$$

which results in an equivalent optimization problem as

$$C(R) = \sup_{F_{X_2}(x):X_2\in[-R,R]} h(\mathbf{Y};F_{X_2}) - \ln(2\pi e) \tag{5.29}$$

with the following modified terms

$$f_{\mathbf{Y}}(\mathbf{y};F_{X_2}) = \int_{-R}^{R} K'(y_1,y_2,x)dF_{X_2}(x) \tag{5.30}$$

$$\tilde{h}_{\mathbf{Y}}(x;F_{X_2}) = -\int_{-\infty}^{\infty}\int_{-\infty}^{\infty} K'(y_1,y_2,x)\ln f_{\mathbf{Y}}(\mathbf{y};F_{X_2})d\mathbf{y} \tag{5.31}$$

$$K'(y_1,y_2,x) = \frac{1}{2\pi}e^{-\frac{(y_2-x)^2}{2}}\left[\frac{1}{2}e^{-\frac{(y_1-\lambda\sqrt{R^2-x^2})^2}{2}}+\frac{1}{2}e^{-\frac{(y_1+\lambda\sqrt{R^2-x^2})^2}{2}}\right]. \tag{5.32}$$

By using the same tools in analysis, an accumulation point of $\pm R$ on x_1 axis (which is equivalent to an accumulation point of 0 on x_2 axis) results in

$$\tilde{h}_{\mathbf{Y}}(z;F^*_{X_2}) = h(\mathbf{Y};F^*_{X_2}) \quad , \quad \forall z\in\mathbb{D}. \tag{5.33}$$

This also means that all the points on the x_2 axis in the interval $(-R,R)$ are points of increase of $F^*_{X_2}$. Hence, all the points on the x_1 axis in the interval $(-R,R)-\{0\}$ are points of increase of $F^*_{X_1}$ which in turn results in having an accumulation point ($\neq\pm R$) on the x_1 axis. Therefore, regardless of having the accumulation point on x_1 axis in the interior or the boundary of $[-R,R]$, the assumption of having an infinite number of mass points in ϵ^*_X results in (5.27). In what follows, the equality in (5.27) is disproved. Rewriting (5.27), we have

$$-\frac{1}{2\pi}\int_{-\infty}^{\infty}\int_{-\infty}^{\infty} e^{-\frac{(y_1-\lambda z)^2}{2}}\left[\frac{1}{2}e^{-\frac{(y_2-\sqrt{R^2-z^2})^2}{2}}+\frac{1}{2}e^{-\frac{(y_2+\sqrt{R^2-z^2})^2}{2}}\right]\ln f_{\mathbf{Y}}(\mathbf{y};F^*_{X_1})d\mathbf{y} = c, \quad \forall z\in\mathbb{D} \tag{5.34}$$

where $c(= h(\mathbf{Y}; F^*_{X_1}))$ is a constant. Let $z = x + i\epsilon$ ($\epsilon \neq 0$). For any given $x < \infty$, (5.34) implies

$$\lim_{\epsilon \to 0} -\frac{1}{2\pi} \int_{-\infty}^{\infty}\int_{-\infty}^{\infty} e^{-\frac{(y_1-\lambda(x+i\epsilon))^2}{2}} \left[\frac{1}{2} e^{-\frac{(y_2-\sqrt{R^2-(x+i\epsilon)^2})^2}{2}} + \frac{1}{2} e^{-\frac{(y_2+\sqrt{R^2-(x+i\epsilon)^2})^2}{2}}\right] \times \ln f_{\mathbf{Y}}(\mathbf{y}; F^*_{X_1}) d\mathbf{y} = c. \tag{5.35}$$

Since the absolute value of the integrand in (5.35) is integrable, by the application of Lebesgue's dominated convergence theorem, we can take the limit inside the integrals and obtain

$$-\frac{1}{2\pi} \int_{-\infty}^{\infty}\int_{-\infty}^{\infty} e^{-\frac{(y_1-\lambda x)^2}{2}} \left[\frac{1}{2} e^{-\frac{(y_2-\sqrt{R^2-x^2})^2}{2}} + \frac{1}{2} e^{-\frac{(y_2+\sqrt{R^2-x^2})^2}{2}}\right] \ln f_{\mathbf{Y}}(\mathbf{y}; F^*_{X_1}) d\mathbf{y} = c, \quad \forall x \in \mathbb{R}. \tag{5.36}$$

In the sequel, it is shown that (5.36) does not hold. More precisely, it is shown that the left hand side of (5.36) becomes unbounded as x goes to infinity and therefore it cannot be a constant on the whole real line. We rewrite $f_{\mathbf{Y}}(\mathbf{y}; F^*_{X_1})$ as

$$f_{\mathbf{Y}}(\mathbf{y}; F^*_{X_1}) = \frac{1}{2\pi} e^{-\frac{y_1^2+y_2^2}{2} - \frac{R^2}{2}} g(\mathbf{y}; F^*_{X_1}) \tag{5.37}$$

where

$$g(\mathbf{y}; F^*_{X_1}) = \int_{-R}^{R} e^{-\frac{(\lambda^2-1)x^2}{2} + \lambda y_1 x} \cosh(y_2 \sqrt{R^2 - x^2}) dF^*_{X_1}(x). \tag{5.38}$$

By substituting (5.37) in (5.36), we obtain

$$\ln(2\pi) + R^2 + 1 + \frac{\lambda^2 - 1}{2} x^2 - \underbrace{\int_{-\infty}^{\infty}\int_{-\infty}^{\infty} K(y_1, y_2, x) \ln g(\mathbf{y}; F^*_{X_1}) dy_2 dy_1}_{I} = c \quad , \quad \forall x \in \mathbb{R}. \tag{5.39}$$

The double integral in (5.39) at large values of x can be written as (note that we make use of the equality $\cosh(ix) = \cos(x)$)

$$I = e^{-\frac{(\lambda^2-1)}{2}x^2} \int_{-\infty}^{\infty}\int_{-\infty}^{\infty} e^{\frac{-y_1^2-y_2^2+2\lambda y_1 x}{2}} \cos(y_2\sqrt{x^2 - R^2}) \ln g(\mathbf{y}; F^*_{X_1}) dy_2 dy_1 \tag{5.40}$$

$$= \lim_{a,b,c,d \to +\infty} e^{-\frac{(\lambda^2-1)}{2}x^2} \int_{-a}^{b}\int_{-c}^{d} e^{\frac{-y_1^2-y_2^2+2\lambda y_1 x}{2}} \cos(y_2\sqrt{x^2 - R^2}) \ln g(\mathbf{y}; F^*_{X_1}) dy_2 dy_1. \tag{5.41}$$

If it can be shown that $|I| \leq O(x)$ (i.e., the growth of I with x is at most linearly), then

the proof is complete by observing that the left hand side of (5.39) does not converge to any real number as x increases and therefore it cannot be a constant on the whole real line.

Let M, K be two sufficiently large numbers satisfying $K \gg M$ and define $I(M)$ as

$$I(M) = I_{-\infty}^{-K} + I_{-K}^{K} + I_{K}^{+\infty} \tag{5.42}$$

in which

$$I_a^b \triangleq e^{-\frac{(\lambda^2-1)}{2}x^2} \int_a^b \int_{-M}^{M} e^{\frac{-y_1^2-y_2^2+2\lambda y_1 x}{2}} \cos(y_2\sqrt{x^2-R^2}) \ln g(\mathbf{y}; F_{X_1}^*) dy_2 dy_1, \quad a, b \in \mathbb{R} \cup \{-\infty, +\infty\}. \tag{5.43}$$

In what follows, we find upper bounds for each of the terms in (5.42) when x is sufficiently large.

$$\begin{aligned}
&\lim_{x\to+\infty} |I_{-K}^{K}| \\
&\leq \lim_{x\to+\infty} e^{-\frac{(\lambda^2-1)}{2}x^2} \int_{-K}^{K}\int_{-M}^{M} e^{\frac{-y_1^2-y_2^2+2\lambda y_1 x}{2}} |\cos(y_2\sqrt{x^2-R^2})||\ln g(\mathbf{y}; F_{X_1}^*)| dy_2 dy_1 \\
&\leq \lim_{x\to+\infty} e^{-\frac{(\lambda^2-1)}{2}x^2} \int_{-K}^{K}\int_{-M}^{M} e^{\frac{-y_1^2-y_2^2+2\lambda y_1 x}{2}} |\ln g(\mathbf{y}; F_{X_1}^*)| dy_2 dy_1 \\
&\leq \lim_{x\to+\infty} e^{-\frac{(\lambda^2-1)}{2}x^2} \int_{-K}^{K}\int_{-M}^{M} e^{\frac{-y_1^2-y_2^2+2\lambda y_1 x}{2}} R(\lambda|y_1| + |y_2|) dy_2 dy_1 \qquad (5.44) \\
&= 0 \qquad (5.45)
\end{aligned}$$

where in (5.44), we use the following upper bound for $g(\mathbf{y}; F_{X_1}^*)$ defined in (5.38)

$$g(\mathbf{y}; F_{X_1}^*) \leq e^{R(\lambda|y_1|+|y_2|)}. \tag{5.46}$$

Similarly, for the term $I_{-\infty}^{-K}$, we can write

$$\begin{aligned}
\lim_{x\to+\infty} |I_{-\infty}^{-K}| &\leq \lim_{x\to+\infty} e^{-\frac{(\lambda^2-1)}{2}x^2} \int_{-\infty}^{-K}\int_{-M}^{M} e^{\frac{-y_1^2-y_2^2+2\lambda y_1 x}{2}} R(\lambda|y_1| + |y_2|) dy_2 dy_1 \qquad (5.47) \\
&= 0. \qquad (5.48)
\end{aligned}$$

Bounding $I_K^{+\infty}$ is more involved. First, according to the boundary of integration in $I_K^{+\infty}$, we have $y_1 \geq K \gg M \geq |y_2|$. By rewriting $g(\mathbf{y}; F_{X_1}^*)$ in this regime, we get

$$g(\mathbf{y}; F_{X_1}^*) = \int_{-R}^{R} e^{-\frac{(\lambda^2-1)x^2}{2}+\lambda y_1 x} \cosh(y_2\sqrt{R^2-x^2}) dF_{X_1}^*(x)$$

$$\begin{aligned}
&= \int_{-R}^{R} \left[\frac{1}{2}e^{-\frac{(\lambda^2-1)x^2}{2}+\lambda y_1 x+y_2\sqrt{R^2-x^2}} + \frac{1}{2}e^{-\frac{(\lambda^2-1)x^2}{2}+\lambda y_1 x-y_2\sqrt{R^2-x^2}}\right] dF_{X_1}^*(x) \\
&\approx \int_{-R}^{R} \left[\frac{1}{2}e^{\lambda y_1 x} + \frac{1}{2}e^{\lambda y_1 x}\right] dF_{X_1}^*(x) \qquad (5.49) \\
&= \int_{-R}^{R} e^{\lambda y_1 x} dF_{X_1}^*(x) \qquad (5.50)
\end{aligned}$$

where (5.49) is due to the fact that $y_1 \geq K \gg M \geq \max\{|y_2|, R\}$ and this approximation gets better when $M \to \infty$ and K grows faster than M. Therefore,

$$\begin{aligned}
&\lim_{M\to+\infty: x\gg K\gg M} |I_K^{+\infty}| \qquad (5.51) \\
&= \lim_{M\to+\infty: x\gg K\gg M} \left| e^{-\frac{(\lambda^2-1)}{2}x^2} \int_K^{\infty}\int_{-M}^{M} e^{\frac{-y_1^2-y_2^2+2\lambda y_1 x}{2}} \cos(y_2\sqrt{x^2-R^2}) \ln g(\mathbf{y}; F_{X_1}^*) dy_2 dy_1 \right| \\
&\approx \lim_{M\to+\infty: x\gg K\gg M} \left| e^{-\frac{(\lambda^2-1)}{2}x^2} \int_K^{\infty} e^{\frac{-y_1^2+2\lambda y_1 x}{2}} \int_{-M}^{M} e^{-\frac{y_2^2}{2}} \cos(y_2\sqrt{x^2-R^2}) dy_2 \right. \\
&\qquad \left. \times \ln\left(\int_{-R}^{R} e^{\lambda y_1 x} dF_{X_1}^*(x)\right) dy_1 \right| \\
&= \lim_{K\to+\infty: x\gg K} \left| \sqrt{2\pi} e^{-\frac{\lambda^2}{2}x^2+\frac{R^2}{2}} \int_K^{\infty} e^{\frac{-y_1^2+2\lambda y_1 x}{2}} \ln\left(\int_{-R}^{R} e^{\lambda y_1 x} dF_{X_1}^*(x)\right) dy_1 \right| \qquad (5.52) \\
&\leq \lim_{K\to+\infty: x\gg K} \sqrt{2\pi} e^{-\frac{\lambda^2}{2}x^2+\frac{R^2}{2}} \int_K^{\infty} e^{\frac{-y_1^2+2\lambda y_1 x}{2}} R\lambda y_1 dy_1 \\
&= \lim_{K\to+\infty: x\gg K} \sqrt{2\pi} R\lambda e^{\frac{R^2}{2}} \int_K^{\infty} e^{-\frac{(y_1-\lambda x)^2}{2}} y_1 dy_1 \\
&= \lim_{K\to+\infty: x\gg K} \sqrt{2\pi} R\lambda e^{\frac{R^2}{2}} \left(e^{-\frac{(K-\lambda x)^2}{2}} + \sqrt{2\pi}\lambda x Q(K-\lambda x)\right) \qquad (5.53) \\
&= \lim_{x\to+\infty} 2\pi R e^{\frac{R^2}{2}} \lambda^2 x \qquad (5.54)
\end{aligned}$$

where in (5.52), we have used the equality $\int_{-\infty}^{+\infty} e^{-\beta x^2} \cos bx dx = \sqrt{\frac{\pi}{\beta}} e^{-\frac{b^2}{4\beta}}$ $(\mathrm{Re}\{\beta\} > 0)$ and this approximation becomes better as M grows. In (5.53), $Q(a) = \int_a^{\infty} \frac{e^{-\frac{t^2}{2}}}{\sqrt{2\pi}} dt$. The

limit of the left hand side of (5.39) is

$$\begin{aligned}
&\lim_{x\to+\infty} \ln(2\pi) + R^2 + 1 + \frac{\lambda^2-1}{2}x^2 - I \\
&= \lim_{M\to+\infty:x\gg K\gg M} \ln(2\pi) + R^2 + 1 + \frac{\lambda^2-1}{2}x^2 - I(M) \qquad (5.55)\\
&= \lim_{M\to+\infty:x\gg K\gg M} \ln(2\pi) + R^2 + 1 + \frac{\lambda^2-1}{2}x^2 - I_{-\infty}^{-K} - I_{-K}^{K} - I_{K}^{+\infty} \\
&\geq \lim_{M\to+\infty:x\gg K\gg M} \ln(2\pi) + R^2 + 1 + \frac{\lambda^2-1}{2}x^2 - |I_{-\infty}^{-K}| - |I_{-K}^{K}| - |I_{K}^{+\infty}| \\
&\geq \lim_{x\to+\infty} \ln(2\pi) + R^2 + 1 + \frac{\lambda^2-1}{2}x^2 - 2\pi R e^{\frac{R^2}{2}}\lambda^2 x \\
&= +\infty. \qquad (5.56)
\end{aligned}$$

Note that the assumption of $\lambda > 1$ is crucial for all of the bounds specially in (5.56). Therefore, (5.39) does not hold on the whole real line (and in turn (5.27) does not hold on $\mathbb{D}$) which makes the assumption of infinite number of mass points incorrect. This completes the proof.

5.6 Asymptotic behavior

Corollary 1. For $\lambda \geq 1$, when the norm of the input vector is very small, we have

$$C(R) \approx \frac{\lambda^2 R^2}{2} \quad , \quad R \to 0 \qquad (5.57)$$

and the asymptotically optimal input distribution is given by

$$F_{\mathbf{X}}^{\text{asym}}(\mathbf{x}) = \left[\frac{1}{2}u(x_1 - R) + \frac{1}{2}u(x_1 + R)\right] u(x_2) \qquad (5.58)$$

where $u(.)$ is the unit step function.

Proof. From (5.2), we can write

$$\begin{aligned}
C(R) &\leq \sup_{F_{\mathbf{X}}(\mathbf{x}):E[\|X\|^2]\leq R^2} I(\mathbf{X};\mathbf{Y}) \\
&= \frac{1}{2}\ln(1+\lambda^2 P_1^*) + \frac{1}{2}\ln(1+P_2^*) \qquad (5.59)
\end{aligned}$$

where the solutions of the water filling algorithm are given by

$$(P_1^*, P_2^*) = \begin{cases} (R^2, 0) & R^2 \leq 1 - \frac{1}{\lambda^2} \\ (\frac{R^2+1-\frac{1}{\lambda^2}}{2}, \frac{R^2-1+\frac{1}{\lambda^2}}{2}) & \text{o.w.} \end{cases}. \tag{5.60}$$

When R is vanishingly small, from (5.59) and (5.60), we have

$$\lim_{R\to 0} C(R) \leq \lim_{R\to 0} \frac{1}{2}\ln(1+\lambda^2 R^2) = \frac{\lambda^2 R^2}{2}. \tag{5.61}$$

In what follows, we show that the distribution in (5.58) achieves the upper bound in (5.79) asymptotically. The pdf of the output induced by this input distribution is

$$f_{\mathbf{Y}}(\mathbf{y}; F_{\mathbf{X}}^{\text{asym}}) = \frac{1}{2\pi} e^{-\frac{y_2^2}{2}} \left(\frac{1}{2} e^{-\frac{(y_1-\lambda R)^2}{2}} + \frac{1}{2} e^{-\frac{(y_1+\lambda R)^2}{2}} \right). \tag{5.62}$$

When R is small,

$$\begin{aligned} h(\mathbf{Y}; F_{\mathbf{X}}^{\text{asym}}) &= \lim_{R\to 0} -\int_{-\infty}^{\infty}\int_{-\infty}^{\infty} f_{\mathbf{Y}}(\mathbf{y}; F_{\mathbf{X}}^{\text{asym}}) \ln f_{\mathbf{Y}}(\mathbf{y}; F_{\mathbf{X}}^{\text{asym}}) d\mathbf{y} \\ &= \lim_{R\to 0} \int_{-\infty}^{\infty}\int_{-\infty}^{\infty} \frac{1}{2\pi} e^{-\frac{y_2^2}{2}} \left(\frac{1}{2} e^{-\frac{(y_1-\lambda R)^2}{2}} + \frac{1}{2} e^{-\frac{(y_1+\lambda R)^2}{2}} \right) \\ &\quad \times \left(\ln 2\pi + \frac{y_2^2}{2} + \frac{y_1^2}{2} + \frac{\lambda^2 R^2}{2} - \ln\cosh(\lambda R y_1) \right) d\mathbf{y} \\ &= \lim_{R\to 0} \int_{-\infty}^{\infty}\int_{-\infty}^{\infty} \frac{1}{2\pi} e^{-\frac{y_2^2}{2}} \left(\frac{1}{2} e^{-\frac{(y_1-\lambda R)^2}{2}} + \frac{1}{2} e^{-\frac{(y_1+\lambda R)^2}{2}} \right) \\ &\quad \times \left(\ln 2\pi + \frac{y_2^2}{2} + \frac{y_1^2}{2} + \frac{\lambda^2 R^2}{2} - \frac{\lambda^2 R^2 y_1^2}{2} \right) d\mathbf{y} \qquad (5.63) \\ &= \lim_{R\to 0} 1 + \ln 2\pi + \frac{\lambda^2 R^2}{2} \qquad (5.64) \end{aligned}$$

where in (5.63), we have used the approximations $\cosh x \approx 1 + \frac{x^2}{2}$ and $\ln(1+x) \approx x$ for $x \ll 1$ and in (5.64), we have dropped the higher order terms of R. Therefore, when the norm of the input is very small, the mutual information resulted by the input distribution $F_{\mathbf{X}}^{\text{asym}}(\mathbf{x})$ is

$$\lim_{R\to 0} h(\mathbf{Y}; F_{\mathbf{X}}^{\text{asym}}) - \ln 2\pi e = \frac{\lambda^2 R^2}{2} \tag{5.65}$$

which confirms that the upper bound in (5.79) is asymptotically tight.

The asymptotic optimality of the distribution in (5.58) can alternatively be proved by inspecting the behavior of the marginal entropy density $\tilde{h}_{\mathbf{Y}}(x; F_{X_1})$ when R is sufficiently

small. From (5.19), we have

$$f_{\mathbf{Y}}(\mathbf{y}; F_{X_1}) \overset{R\to 0}{\longrightarrow} \frac{1}{2\pi} e^{-\frac{y_1^2+y_2^2}{2}}. \tag{5.66}$$

Therefore,

$$\begin{aligned}
\tilde{h}_{\mathbf{Y}}(x; F_{X_1}) &= -\int_{-\infty}^{\infty}\int_{-\infty}^{\infty} K(y_1, y_2, x) \ln f_{\mathbf{Y}}(\mathbf{y}; F_{X_1}) d\mathbf{y} && (5.67)\\
&\to \int_{-\infty}^{\infty}\int_{-\infty}^{\infty} \frac{1}{2\pi} e^{-\frac{(y_1-\lambda x)^2}{2}} \left[\frac{1}{2} e^{-\frac{(y_2-\sqrt{R^2-x^2})^2}{2}} + \frac{1}{2} e^{-\frac{(y_2+\sqrt{R^2-x^2})^2}{2}}\right] \\
&\quad \times (\ln 2\pi + \frac{y_1^2+y_2^2}{2}) d\mathbf{y} && (5.68)\\
&= 1 + \ln 2\pi + \frac{R^2}{2} + \frac{\lambda^2-1}{2} x^2 && (5.69)
\end{aligned}$$

which is a strictly convex (and even) function. Hence, the necessary and sufficient conditions in (5.10) and (5.11) are satisfied if and only if the input is distributed as (5.58)[5]. Note that in contrast to the optimal distribution, the asymptotically optimal distribution is not unique. As a special case, when $\lambda = 1$, the distribution in (5.58) with two mass points is still asymptotically optimal. However, the optimal input distribution has an infinite number of mass points uniformly distributed on the circle with radius R (as shown in [40]). □

Corollary 2. For high SNR values, we have

$$\lim_{R\to\infty} \frac{C(R)}{\ln R} = 1. \tag{5.70}$$

In other words, the constant envelope signaling in a 2 by 2 channel has only one degree of freedom.

[5]It can alternatively be verified that when $R \ll 1$, $\tilde{h}_{\mathbf{Y}}(x; F_{X_2})$ becomes strictly concave and one mass point at zero on the x_2 axis is optimal which is equivalent to (5.58).

Proof. By writing the input of the channel in polar coordinates as $\mathbf{X} = R[\cos\Theta\ ,\ \sin\Theta]^T$, the differential entropy of the input in polar coordinates is given by

$$\begin{aligned} h(\mathbf{X}) &= -\int_{\|\mathbf{x}\|=R} f_{\mathbf{X}}(\mathbf{x}) \ln f_{\mathbf{X}}(\mathbf{x}) d\mathbf{x} \\ &= -\int_0^{2\pi} f_{\mathbf{X}}(\mathbf{x}(R,\theta)) \ln f_{\mathbf{X}}(\mathbf{x}(R,\theta)) |\frac{\partial \mathbf{x}}{\partial(R,\theta)}| d\theta \\ &= -\int_0^{2\pi} f_{\Theta}(\theta) \ln \frac{f_{\Theta}(\theta)}{|\frac{\partial \mathbf{x}}{\partial(R,\theta)}|} d\theta \\ &= h(\Theta) + \ln R \\ &\leq \ln 2\pi R \end{aligned} \tag{5.71}$$

where $\frac{\partial \mathbf{x}}{\partial(R,\theta)} = R$ is the Jacobian of the transform and the maximum in (5.71) is achieved iff the $\Theta \sim U[0, 2\pi)$. The capacity is bounded below as follows.

$$\begin{aligned} C(R) &= \sup_{F_{\mathbf{X}}(\mathbf{x}):\|\mathbf{X}\|=R} h(\mathbf{Y}; F_{\mathbf{X}}) - \ln(2\pi e) \\ &\geq \sup_{F_{\mathbf{X}}(\mathbf{x}):\|\mathbf{X}\|=R} \ln\left(e^{h(\mathbf{HX})} + e^{h(\mathbf{W})}\right) - \ln(2\pi e) \qquad (5.72) \\ &= \sup_{F_{\mathbf{X}}(\mathbf{x}):\|\mathbf{X}\|=R} \ln\left(e^{\ln|\det(\mathbf{H})|+h(\mathbf{X})} + 2\pi e\right) - \ln(2\pi e) \\ &= \ln(2\pi\lambda R + 2\pi e) - \ln(2\pi e) \qquad (5.73) \end{aligned}$$

where (5.72) is due to the vector entropy-power inequality (EPI) and in (5.73) the upper bound in (5.71) is used.

The capacity is bounded above as follows.

$$\begin{aligned} C(R) &= \sup_{F_{\mathbf{X}}(\mathbf{x}):\|\mathbf{X}\|=R} h(\mathbf{HX} + \mathbf{W}; F_{\mathbf{X}}) - \ln(2\pi e) \\ &\leq \sup_{F_{\mathbf{X}}(\mathbf{x}):\|\mathbf{X}\|=R} h(\mathbf{HX}, \mathbf{W}; F_{\mathbf{X}}) - \ln(2\pi e) \\ &\leq \sup_{F_{\mathbf{X}}(\mathbf{x}):\|\mathbf{X}\|=R} h(\mathbf{HX}; F_{\mathbf{X}}) + h(\mathbf{W}) - \ln(2\pi e) \\ &= \ln(2\pi R) + \ln\lambda. \end{aligned} \tag{5.74}$$

Combining (5.73) and (5.74), we have

$$\ln(2\pi\lambda R + 2\pi e) - \ln(2\pi e) \leq C(R) \leq \ln(2\pi R) + \ln\lambda. \tag{5.75}$$

Dividing by $\ln R$ and letting $R \to \infty$ results in (5.70). □

The analysis can be readily generalized to the n-dimensional full rank channels by noting that

$$h(\mathbf{X}) \leq \ln\left(\frac{2\pi^{\frac{n}{2}} R^{n-1}}{\Gamma(\frac{n}{2})}\right) \tag{5.76}$$

which is tight iff the distribution of the phase vector of $\mathbf{X}$ in the spherical coordinates is as follows

$$f_{\mathbf{\Theta}}(\theta) = \frac{1}{2\pi} \prod_{i=1}^{n-2} \alpha_i^{-1} \sin^{n-i-1}\theta_i \tag{5.77}$$

where $\alpha_i = \frac{\sqrt{\pi}\Gamma(\frac{n-i}{2})}{\Gamma(\frac{n-i+1}{2})}$. Therefore, we have

$$\frac{n}{2}\ln\left((\frac{2R^{n-1}\pi^{\frac{n}{2}}|\det(\mathbf{H})|}{\Gamma(\frac{n}{2})})^{\frac{2}{n}} + 2\pi e\right) - \frac{n}{2}\ln(2\pi e) \leq C(R) \leq \ln\left(\frac{2\pi^{\frac{n}{2}} R^{n-1}}{\Gamma(\frac{n}{2})}\right) + \ln|\det(\mathbf{H})| \tag{5.78}$$

which results in

$$\lim_{R\to\infty} \frac{C(R)}{\ln R} = n - 1. \tag{5.79}$$

Intuitively, that loss of 1 degree of freedom is due to the fact that for a constant norm n-dimensional vector, given its $n-1$ elements, the remaining element has the uncertainty of at most 1 bit which does not scale with R as it goes to infinity. Finally, note that the phase distribution in (5.77) is equivalent to uniform distribution on the surface of the hypersphere with radius R which is optimal in the DoF sense[6].

5.7 Analysis in polar coordinates

In this section, the problem in (5.2) is analyzed in polar coordinates. Also, in the numerical section, we adopt the notations used in this section. By writing the input and output of the channel in polar coordinates, we have

$$\mathbf{X} = R[\cos\Theta\ ,\ \sin\Theta]^T\ \ ,\ \ \mathbf{Y} = P[\cos\Psi\ ,\ \sin\Psi]^T \quad \Theta, \Psi \in [0, 2\pi)\ , P \in [0, \infty). \tag{5.80}$$

[6] It is important to note that the DoF-achieving distribution is not unique in contrast to the capacity-achieving distribution.

Therefore,

$$h(\mathbf{Y}) = -\int_{\mathbb{R}^2} f_{\mathbf{Y}}(\mathbf{y}) \ln f_{\mathbf{Y}}(\mathbf{y}) d\mathbf{y} \tag{5.81}$$

$$= -\int_0^{\infty}\int_0^{2\pi} f_{\mathbf{Y}}(\mathbf{y}(\rho,\psi)) \ln f_{\mathbf{Y}}(\mathbf{y}(\rho,\psi)) |\frac{\partial \mathbf{y}}{\partial(\rho,\psi)}| d\psi d\rho \tag{5.82}$$

$$= -\int_0^{\infty}\int_0^{2\pi} f_{P,\Psi}(\rho,\psi) \ln \frac{f_{P,\Psi}(\rho,\psi)}{|\frac{\partial \mathbf{y}}{\partial(\rho,\psi)}|} d\psi d\rho \tag{5.83}$$

$$= h(P,\Psi) + \int_0^{\infty} f_P(\rho) \ln \rho d\rho \tag{5.84}$$

$$= h(V,\Psi) \tag{5.85}$$

where $\frac{\partial \mathbf{y}}{\partial(\rho,\psi)} = \rho$ is the Jacobian of the transform and $V = \frac{P^2}{2}$. It can be easily verified that

$$f_{V,\Psi}(v,\psi;F_\Theta) = \int_0^{2\pi} \tilde{K}(v,\psi,\theta) dF_\Theta(\theta) \tag{5.86}$$

where the kernel function is given by

$$\tilde{K}(v,\psi,\theta) = \frac{1}{2\pi} e^{-\frac{\lambda^2-1}{2}R^2\cos^2\theta - \frac{R^2}{2} + R\sqrt{2v}(\lambda\cos\psi\cos\theta + \sin\psi\sin\theta) - v}. \tag{5.87}$$

The marginal entropy density of the output variables induced by the input distribution is defined as

$$\tilde{h}_{V,\Psi}(\theta;F_\Theta) = -\int_0^{\infty}\int_0^{2\pi} \tilde{K}(v,\psi,\theta) \ln f_{V,\Psi}(v,\psi;F_\Theta) d\psi dv \tag{5.88}$$

which satisfies the following

$$h(V,\Psi;F_\Theta) = \int_0^{2\pi} \tilde{h}_{V,\Psi}(\theta;F_\Theta) dF_\Theta(\theta). \tag{5.89}$$

Finally, the optimization problem in (5.2) becomes

$$C(R) = \sup_{F_\Theta(\theta)} h(V,\Psi;F_\Theta) - \ln(2\pi e) \tag{5.90}$$

Let ϵ_θ^* denote the set of points of increase for the optimal input phase distribution $F_\Theta^*(\theta)$. Analogous to the proof of the theorem in Cartesian coordinates, Lagrangian optimization

gives the necessary and sufficient condition for the unique maximizer $F_\Theta^*(\theta)$ as

$$\begin{aligned}\tilde{h}_{V,\Psi}(\theta;F_\Theta^*) &= h(V,\Psi;F_\Theta^*) \quad \forall\theta\in\epsilon_\theta^*\\ \tilde{h}_{V,\Psi}(\theta;F_\Theta^*) &< h(V,\Psi;F_\Theta^*) \quad \forall\theta\in[0,2\pi)-\epsilon_\theta^*.\end{aligned} \tag{5.91}$$

For the second part of the proof (i.e., showing that $|\epsilon_\theta^*|<\infty$), the difference between investigating the problem in the Cartesian and polar coordinates is in the extension to complex domain. In other words, the kernel and marginal entropy density are entire functions (i.e., holomorphic on the whole complex plane) in polar coordinates. This helps us avoid the consideration of checking the position of accumulation point (see the paragraph below (5.27)). Therefore, the assumption of an infinite number of points of increase results in

$$\tilde{h}_{V,\Psi}(z;F_\Theta^*) = h(V,\Psi;F_\Theta^*) \quad , \quad \forall z\in\mathbb{C} \tag{5.92}$$

or equivalently

$$-\frac{1}{2\pi}e^{-\frac{R^2}{2}}\int_0^\infty\int_0^{2\pi} e^{-\frac{\lambda^2-1}{2}R^2\cos^2 z+R\sqrt{2v}(\lambda\cos\psi\cos z+\sin\psi\sin z)-v}\ln f_{V,\Psi}(v,\psi;F_\Theta^*)d\psi dv = c, \quad \forall z\in\mathbb{C} \tag{5.93}$$

where c is a constant ($=h(V,\Psi;F_\Theta^*)$). Taking z on the imaginary line, we have

$$\cos z = t\ (t\geq 1) \quad , \quad \sin z = i\sqrt{t^2-1}. \tag{5.94}$$

By replacing (5.94) in (5.93), we get

$$-\frac{1}{2\pi}e^{-\frac{R^2}{2}}\int_0^\infty\int_0^{2\pi} e^{-\frac{\lambda^2-1}{2}R^2t^2+R\sqrt{2v}(\lambda\cos\psi t+i\sin\psi\sqrt{t^2-1})-v}\ln f_{V,\Psi}(v,\psi;F_\Theta^*)d\psi dv = c\ ,\ \forall t\geq 1. \tag{5.95}$$

Finally, by separating the real and imaginary parts of the left-hand side of (5.95), the following is resulted

$$-\frac{1}{2\pi}e^{-\frac{R^2}{2}}\int_0^\infty\int_0^{2\pi} e^{-\frac{\lambda^2-1}{2}R^2t^2+R\sqrt{2v}\lambda\cos\psi t-v}\cos\left(\sin\psi R\sqrt{2v(t^2-1)}\right) \times\ln f_{V,\Psi}(v,\psi;F_\Theta^*)d\psi dv = c \tag{5.96}$$

$$-\frac{1}{2\pi}e^{-\frac{R^2}{2}}\int_0^\infty\int_0^{2\pi} e^{-\frac{\lambda^2-1}{2}R^2t^2+R\sqrt{2v}\lambda\cos\psi t-v}\sin\left(\sin\psi R\sqrt{2v(t^2-1)}\right) \times\ln f_{V,\Psi}(v,\psi;F_\Theta^*)d\psi dv = 0. \tag{5.97}$$

It is easy to verify that the integrand of (5.97) is an odd function with respect to $\psi = \pi$ which is a consequence of the symmetry of the additive noise. Therefore, (5.97) is always true. The way to show that (5.96) does not hold is similar to that for disproving (5.36).

5.8 Numerical results

The theorem in section 5.4 states that the optimal input has a finite number of mass points on the circle defined by the constraint. The algorithm for finding the number, the positions and the probabilities of these points is the same as that explained in [24] where we start with two points for very small R and then increase R by some step and check the necessary and sufficient conditions. At any stage that these conditions are violated, we increase the number of points, do the optimization to find the position and probabilities of the points, check the conditions and keep repeating this process.

The support of the capacity achieving input and the marginal entropy densities induced by them are shown in Figures 5.1 to 5.4 for $\lambda = 2$ and different values of R. Here, we have performed the optimization in polar coordinates. The optimality of the points in the left subfigures is guaranteed by the necessary and sufficient conditions in (5.91) which can also be verified through right subfigures. As it can be observed, the points of increase of the optimal input, which correspond to the peaks in the marginal entropy densities, have a finite number.

Let $F^1_{X_1}(x)$ be defined as

$$F^1_{X_1}(x) = \frac{1}{2}\left[u(x-R) + u(x+R)\right]. \tag{5.98}$$

According to section 5.6, we know that this CDF is optimal for sufficiently small values of R. As R increases, $F^1_{X_1}(x)$ remains optimal until it violates the necessary and sufficient conditions. By observing the behavior of $\tilde{h}_{\mathbf{Y}}(x; F^1_{X_1})$, it is concluded that as R increases, the first point to violate the necessary and sufficient conditions will happen at $x = 0$ (which is equivalent to $(0, R)$ and $(0, -R)$ on the circle).

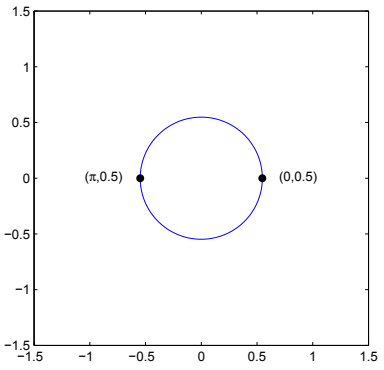

(a) Support

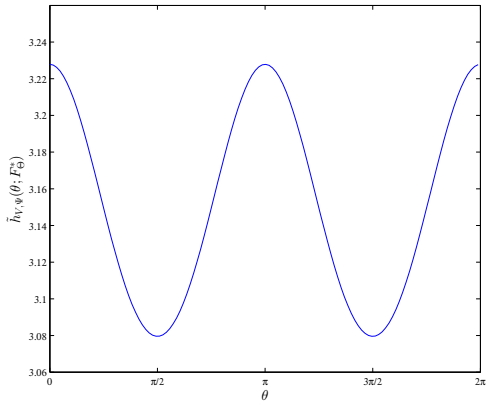

(b) Marginal Entropy Density

FIGURE 5.1: The support of the optimal input (a) and the marginal entropy density induced by it (b) for $R = 0.5477$ and $\lambda = 2$. In (a), the pairs represent the phase and its probability as in $(\theta, P_\Theta(\theta))$.

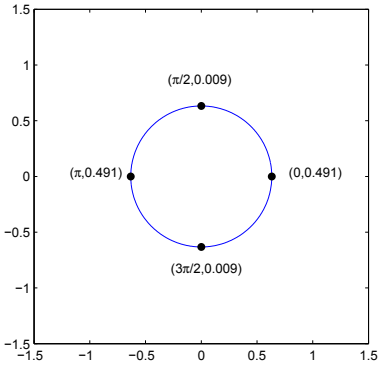

(a) Support

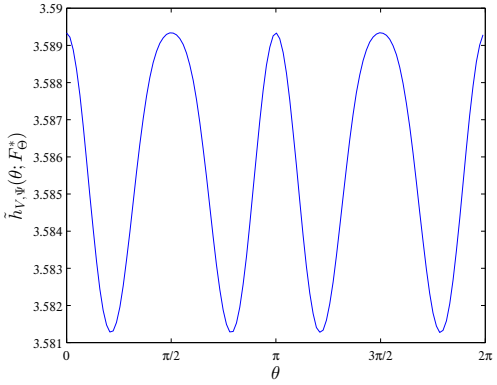

(b) Marginal Entropy Density

FIGURE 5.2: The support of the optimal input (a) and the marginal entropy density induced by it (b) for $R = 0.6325$ and $\lambda = 2$. In (a), the pairs represent the phase and its probability as in $(\theta, P_\Theta(\theta))$.

This is shown in figure 5.5 for $\lambda = 10$. Therefore, the norm threshold (R^t) for which $F^1_{X_1}(x)$ remains optimal is obtained by solving the following equation for R^t

$$\tilde{h}_{\mathbf{Y}}(0; F^1_{X_1}) = \tilde{h}_{\mathbf{Y}}(R; F^1_{X_1}) \tag{5.99}$$

which, after some manipulation, becomes equivalent to

$$\frac{1}{\sqrt{2\pi}} \int_{-\infty}^{+\infty} (e^{-\frac{(y-\lambda R)^2}{2}} - e^{-\frac{y^2}{2}}) \ln \cosh(\lambda R y) dy = \frac{(\lambda^2 - 1)}{2} R^2. \tag{5.100}$$

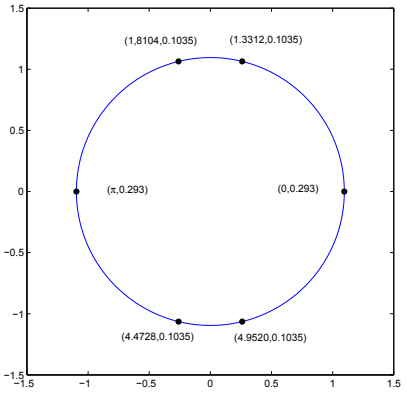

(a) Support

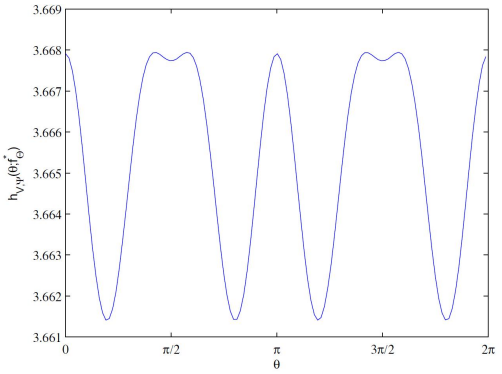

(b) Marginal Entropy Density

FIGURE 5.3: The support of the optimal input (a) and the marginal entropy density induced by it (b) for $R = 1.0954$ and $\lambda = 2$. In (a), the pairs represent the phase and its probability as in $(\theta, P_\Theta(\theta))$.

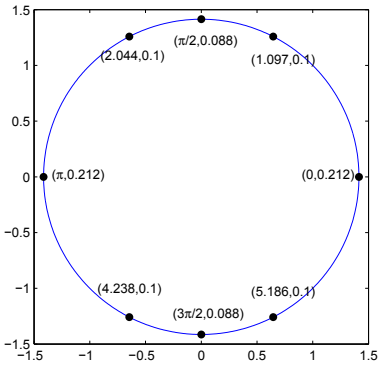

(a) Support

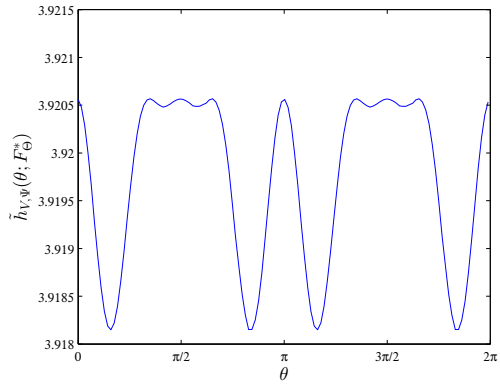

(b) Marginal Entropy Density

FIGURE 5.4: The support of the optimal input (a) and the marginal entropy density induced by it (b) for $R = \sqrt{2}$ and $\lambda = 2$. In (a), the pairs represent the phase and its probability as in $(\theta, P_\Theta(\theta))$.

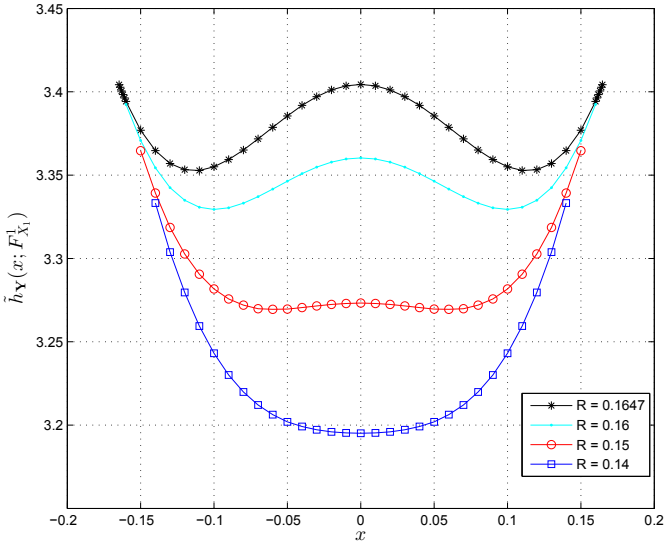

FIGURE 5.5: For small values of R, when R increases, the first point to become a mass point is $x = 0$. (here $\lambda = 10$).

By solving (5.100) numerically, the values of R^t are obtained for different values of λ. For example, for $\lambda = 10$, $R^t = 0.1647$ which means that when the norm R is below 0.1647 the support of the optimal input has only two equiprobable mass points at $(R, 0)$ and $(-R, 0)$, and at this threshold it gets another mass point at zero as already shown in figure 5.5.

Chapter 6

Conclusion and Future Works

In this thesis, we tried to address some of the communication limits in MIMO wireless networks. The main focus was on the effect of two practical constraints: 1) Imperfect channel state information at the transmitter and 2) Transmission with peak power constraint.

In Chapter 2, given the marginal probabilities of CSIT, an outer bound was derived for the DoF region of the K-user MISO BC with alternating/hybrid CSIT . This outer bound was shown to be achievable by specific CSIT patterns in certain regions. A set of inequalities was provided based on the joint CSIT distribution which shows that in general, the DoF region of the K-user MISO BC (when $K \geq 3$) cannot be characterized completely by the marginal probabilities. Afterwards, an outer bound for the DoF region of a two user MIMO BC in which the CSIT of a user is either perfect or unknown was derived which was shown to be tight in some scenarios. Finally, an alternative proof for the DoF of a K-user MIMO BC was proposed which was used to obtain the capacity region of certain types of channels.

In Chapter 3, we have shown that the capacity-achieving distribution of the vector Gaussian channel with identity channel matrix under the peak and average power constraints has a finite number of mass points for its amplitude and the points are uniformly distributed on the hyper-spheres determined by the amplitude mass points. It was shown that when the peak power is the only active constraint, constant amplitude signaling at the peak power is optimal when the number of dimensions is above a threshold. Finally, some upper and lower bounds were given for the general deterministic channel and their

performance was evaluated numerically as a function of the condition number of the channel.

The results of this chapter could be applied to the MIMO communication systems with only one single RF chain at the transmitter which is of great interest and necessitate the peak power constraint. The importance of the results becomes more pronounced in the massive MIMO settings, where it was shown that the capacity has a closed form solution and no computer program is needed to find the optimal input distribution.

In Chapter 4, the capacity of a scalar AWGN with amplitude-constrained input was considered and a further refinement of the previous bounds in literature was proposed.

In Chapter 5, constant envelope signaling in point-to-point Gaussian parallel channels was considered. For a 2 by 2 channel, we showed that the capacity-achieving input distribution has a finite number of mass points on the circle defined by the constant norm. In this setting, the optimal DoF of a full rank n by n channel was shown to be $n-1$ which is achieved by a uniform distribution over the surface of the hypersphere defined by the constant envelope.

There are many open and challenging problems related to the topics mentioned in this thesis. Some of them are

- Characterization of the DoF region of the 3-user MISO BC with alternating/hybrid CSIT. It is important to note that even for some fixed CSIT patterns, the DoF region is not known.
- The capacity of the 2 by 2 deterministic MIMO channel with peak power constraint.
- The capacity region of a SISO BC with peak power constraint. Although the channel is degraded and superposition coding is optimal, the region is not explicitly known.

Appendix A

Derivation of (3.22)

The following lemma is useful in the sequel.

Lemma. Let a and b be two real numbers with $a > 0$. Also, let $\mathcal{N}_0$ be the set of non-negative integers. Then,

$$\int_{-1}^{1} I_n(a\sqrt{1-u^2})(\sqrt{1-u^2})^n e^{-bu}du = \sqrt{2\pi}a^n \frac{I_{n+\frac{1}{2}}(\sqrt{a^2+b^2})}{(\sqrt{a^2+b^2})^{n+\frac{1}{2}}}, \quad n = \frac{k}{2} \ \forall k \in \mathcal{N}_0. \tag{A.1}$$

Proof. By using [45, pp. 698], (A.1) could be shown for $n = 0$. Also, by some manipulation, (A.1) holds true for $n = \frac{1}{2}, 1, \frac{3}{2}$. For general n, we use induction as follows. Denote the left-hand side of (A.1) by Q_n. It is shown that if (A.1) is true for n, it will also be true for $n + \frac{1}{2}$. In other words, if

$$Q_n = \sqrt{2\pi}a^n \frac{I_{n+\frac{1}{2}}(\sqrt{a^2+b^2})}{(\sqrt{a^2+b^2})^{n+\frac{1}{2}}} \quad (n \geq \frac{3}{2}) \tag{A.2}$$

then

$$Q_{n+\frac{1}{2}} = \sqrt{2\pi}a^{n+\frac{1}{2}} \frac{I_{n+1}(\sqrt{a^2+b^2})}{(\sqrt{a^2+b^2})^{n+1}}. \tag{A.3}$$

By using the recursive identity for the bessel function (i.e., $I_\alpha(z) = I_{\alpha-2}(z) - \frac{2(\alpha-1)}{z} I_{\alpha-1}(z)$), we have

$$\begin{aligned} Q_{n+\frac{1}{2}} &= \int_{-1}^{1} I_{n-\frac{3}{2}}(a\sqrt{1-u^2})(\sqrt{1-u^2})^{n+\frac{1}{2}} e^{-bu} du \\ &\quad - \frac{2(n-\frac{1}{2})}{a} \int_{-1}^{1} I_{n-\frac{1}{2}}(a\sqrt{1-u^2})(\sqrt{1-u^2})^{n-\frac{1}{2}} e^{-bu} du \\ &= \int_{-1}^{1} I_{n-\frac{3}{2}}(a\sqrt{1-u^2})(\sqrt{1-u^2})^{n+\frac{1}{2}} e^{-bu} du - 2(n-\frac{1}{2})\sqrt{2\pi} a^{n-\frac{3}{2}} \frac{I_n(\sqrt{a^2+b^2})}{(\sqrt{a^2+b^2})^n} \end{aligned} \tag{A.4}$$

where in (A.4), we have used (A.2). From (A.2), we have

$$Q_{n-\frac{1}{2}} = \sqrt{2\pi} a^{n-\frac{1}{2}} \frac{I_n(\sqrt{a^2+b^2})}{(\sqrt{a^2+b^2})^n}. \tag{A.5}$$

By taking the derivative of (A.5) with respect to a and using the identity $I'_\alpha(z) = \frac{1}{2}(I_{\alpha-1}(z) + I_{\alpha+1}(z))$ for $\alpha \neq 0$, we have

$$\int_{-1}^{1} I_{n-\frac{3}{2}}(a\sqrt{1-u^2})(\sqrt{1-u^2})^{n+\frac{1}{2}} e^{-bu} du + Q_{n+\frac{1}{2}} = 2\sqrt{2\pi} \frac{\partial}{\partial a} \left\{ a^{n-\frac{1}{2}} \frac{I_n(\sqrt{a^2+b^2})}{(\sqrt{a^2+b^2})^n} \right\}. \tag{A.6}$$

Solving for $Q_{n+\frac{1}{2}}$ in (A.4) and (A.6) results in

$$\begin{aligned} Q_{n+\frac{1}{2}} &= \sqrt{2\pi} a^{n-\frac{1}{2}} \frac{\partial}{\partial a} \left\{ \frac{I_n(\sqrt{a^2+b^2})}{(\sqrt{a^2+b^2})^n} \right\} \\ &= \sqrt{2\pi} a^{n+\frac{1}{2}} \frac{I_{n+1}(\sqrt{a^2+b^2})}{(\sqrt{a^2+b^2})^{n+1}} \end{aligned} \tag{A.7}$$

where in (A.7), we have used the identity $\frac{d}{dx}\{\frac{I_n(x)}{x^n}\} = \frac{I_{n+1}(x)}{x^n}$. □

(3.22) is equivalent to

$$\underbrace{\int_0^\pi \cdots \int_0^\pi}_{n-2 \text{ times}} \int_0^{2\pi} \frac{1}{(\sqrt{2\pi})^n} e^{x\mathbf{a}^T(\theta)\mathbf{a}(\psi)} \prod_{i=1}^{n-2} \sin^{n-i-1}\psi_i d\psi_{n-1} \ldots d\psi_1 = \begin{cases} \frac{I_{\frac{n}{2}-1}(x)}{(x)^{\frac{n}{2}-1}} & x \neq 0 \\ \frac{1}{\Gamma(\frac{n}{2}) 2^{\frac{n}{2}-1}} & x = 0 \end{cases}$$

$$\forall n \geq 2. \tag{A.8}$$

If $x = 0$, it is obvious that the left-hand side of (A.8) is the hyper-surface area of an n-sphere with unit radius ($= \frac{2\pi^{\frac{n}{2}}}{\Gamma(\frac{n}{2})}$) divided by $(\sqrt{2\pi})^n$ which results in the value shown

on the right-hand side. Therefore, we consider $x \neq 0$. It is obvious that (A.8) is valid for $n = 2$. Denote the left-hand side of (A.8) by W_n and assume it is valid for $n \geq 2$. It can be verified that

$$\begin{aligned} W_{n+1} &= \int_0^{\pi} \frac{I_{\frac{n}{2}-1}(x \sin\theta \sin\psi)}{\sqrt{2\pi}(x \sin\theta \sin\psi)^{\frac{n}{2}-1}} \sin^{n-1}\psi e^{x\cos\theta\cos\psi} d\psi \\ &= \int_{-1}^{1} \frac{I_{\frac{n}{2}-1}(x \sin\theta\sqrt{1-u^2})}{\sqrt{2\pi}(x\sin\theta)^{\frac{n}{2}-1}} (\sqrt{1-u^2})^{\frac{n}{2}-1} e^{-x\cos\theta u} du \qquad \text{(A.9)} \\ &= \frac{I_{\frac{n-1}{2}}(x)}{(x)^{\frac{n-1}{2}}} \qquad \text{(A.10)} \end{aligned}$$

where in (A.9), $u = -\cos\psi$ and in (A.10), we have used the lemma.

Appendix B

Appendix B

Proposition. Let X be a non-negative random variable and $m \in \mathcal{R}^+$. The following optimization problem

$$\sup_{f_X(x):E[X^m]\leq A} H(X) \tag{B.1}$$

has a unique solution. Further, the maximum is

$$\frac{\Gamma(\frac{m+1}{m})}{\Gamma(\frac{1}{m})} - \ln\left(\frac{m\sqrt[m]{\frac{\Gamma(\frac{m+1}{m})}{\Gamma(\frac{1}{m})A}}}{\Gamma(\frac{1}{m})}\right) \tag{B.2}$$

and is achieved by the following distribution

$$f_{X^*}(x) = \frac{m\sqrt[m]{\frac{\Gamma(\frac{m+1}{m})}{\Gamma(\frac{1}{m})A}}}{\Gamma(\frac{1}{m})} e^{-\frac{\Gamma(\frac{m+1}{m})}{A\Gamma(\frac{1}{m})}x^m}. \tag{B.3}$$

Proof. Let Ω denote the set of all probability density functions on the non-negative real line. It can be shown that Ω is convex and compact in the Levy metric. Further, the following function

$$L(f_X(x)) = H(X) - \lambda(\int_0^\infty x^m f_X(x)dx - A) \tag{B.4}$$

is for $\lambda \geq 0$, a continuous, weakly differentiable and strictly concave function of $f_X(x)$ having the weak derivative at $f_X^0(x)$ as

$$L'_{f_X^0(x)}(f_X(x)) = \int_0^\infty (\ln f_X^0(x) + \lambda x^m)(f_X^0(x) - f_X(x))dx. \tag{B.5}$$

Therefore, the Lagrangian optimization guarantees a unique solution for (B.1) and the necessary and sufficient condition for $f_{X^*}(x)$ to be the optimal solution is the existence of a $\lambda \geq 0$ for which $L'_{f_{X^*}(x)}(f_X(x)) \leq 0 \quad \forall f_X(x) \in \Omega$. It can be verified that for $\lambda = \frac{\Gamma(\frac{m+1}{m})}{A\Gamma(\frac{1}{m})}$, the distribution in (B.3) results in $L'_{f_{X^*}(x)}(f_X(x)) = 0$ which satisfies the necessary and sufficient conditions. Hence, the pdf in (B.3), which has the differential entropy in (B.2), is the unique solution of (B.1). □

Appendix C

Proof of Theorem 3.1

Let $\mathbb{F}_{u_p}$ denote the space of all cumulative distribution functions satisfying the peak power constraint, i.e.

$$\mathbb{F}_{u_p} = \{F_P(\rho) | F_P(\rho) = 0 \ \forall \rho < 0 \ , \ F_P(\rho) = 1 \ \forall \rho \geq \sqrt{u_p}\}. \tag{C.1}$$

The metric space $(\mathbb{F}_{u_p}, d_L)$ is convex and compact ([42], [26, Appendix I]) where d_L denotes the Levy metric [41] (note that the proof of the compactness in [26] relies only on the average power constraint). The differential entropy $h(V; F_P) : \mathbb{F}_{u_p} \rightarrow \mathbb{R}$ is continuous ([42], [24, Proposition 3], [26, Appendix I], [29, Proposition 1]) (note that the proof of continuity in [29] is more general in the sense that it does not rely on the Schwartz properties), strictly concave and weakly differentiable ([42], [24, Proposition 4], [26, Appendix II], [29, Proposition 2]) and has the weak derivative at F_P^0 given by

$$\begin{aligned} h'_{F_P^0}(V; F_P) &= \lim_{\zeta \rightarrow 0} \frac{h(V; (1-\zeta)F_P^0 + \zeta F_P) - h(V; F_P^0)}{\zeta} \\ &= \int_0^{\sqrt{u_p}} \tilde{h}_V(\rho; F_P^0) dF_P(\rho) - h(V; F_P^0) \quad , \forall F_P \in \mathbb{F}_{u_p}. \end{aligned} \tag{C.2}$$

The average power constraint is denoted by

$$G(F_P) = \int_0^{\sqrt{u_p}} \rho^2 dF_P(\rho) - u_a \leq 0. \tag{C.3}$$

It is obvious that $G : \mathbb{F}_{u_p} \rightarrow \mathbb{R}$ is linear and weakly differentiable having the weak derivative at F_P^0 given by

$$G'_{F_P^0}(F_P) = G(F_P) - G(F_P^0) \quad , \forall F_P \in \mathbb{F}_{u_p}. \tag{C.4}$$

Since $h(V; F_P)$ and $G(F_P)$ are concave maps from $\mathbb{F}_{u_p}$ to $\mathbb{R}$, Lagrangian optimization [43] guarantees a unique solution for (3.31) and the necessary and sufficient condition for F_{P^*} to be the optimal solution is the existence of a $\lambda(\geq 0)$ such that

$$\int_0^{\sqrt{u_p}} (\tilde{h}_V(\rho; F_{P^*}) - \lambda\rho^2) dF_P(\rho) \leq h(V; F_{P^*}) - \lambda u_a \quad , \quad \forall F_P \in \mathbb{F}_{u_p}. \tag{C.5}$$

It can be shown that (C.5) is equivalent to (3.38) and (3.39) ([25, Corollary 1]). In order to show the finiteness of the cardinality of ϵ_{P^*}, we extend the marginal entropy density in (3.35) to the complex domain i.e.,

$$\tilde{h}_V(z; F_P) = -\int_0^{\infty} K_n(v, z) \ln f_V(v; F_P) dv \quad , \quad z \in \mathbb{C}. \tag{C.6}$$

Proposition 1. The kernel $K_n(v, z)$ is an entire function in z for every v.

Proof. This can be verified by the fact that the real and imaginary parts of $K(v, z = x + jy)$ have continuous partial derivatives and satisfy the Cauchy-Riemann equations which leads to its holomorphy over the complex plane. As a result, by Cauchy's theorem, for every rectifiable closed curve γ in $\mathbb{C}$,

$$\int_\gamma K_n(v, z) dz = 0. \tag{C.7}$$

□

Proposition 2. The marginal entropy density $\tilde{h}_V(z; F_P)$ is an entire function.

Proof. First, we show the continuity of $\tilde{h}_V(z; F_P)$. Let $\{z_m\}_1^\infty$ be a sequence of complex numbers converging to z_0. Since $K_n(v, z)$ is holomorphic (see Proposition 1), it is continuous. Therefore,

$$\lim_{m\to\infty} K_n(v, z_m) \ln f_V(v; F_P) = K_n(v, z_0) \ln f_V(v; F_P). \tag{C.8}$$

Because the kernel is continuous and $K_n(v,+\infty)=0$, it is also bounded (i.e., $0\leq K_n(v,\rho)<\infty$ for all $\rho\in\mathbb{R}_{\geq 0}$.) The continuity and boundedness of the kernel guarantees the continuity of $f_V(v;F_P)$ given in (3.20) by the application of Lebesgue's dominated convergence theorem. This allows us to write

$$\begin{aligned}0<e^{-\frac{(\sqrt[n]{nv})^2+u_p}{2}}\frac{1}{\Gamma(\frac{n}{2})2^{\frac{n}{2}-1}}&\leq \min_{\rho\in[0,\sqrt{u_p}]}K_n(v,\rho)\leq f_V(v;F_P)\\ &\leq \max_{\rho\in[0,\sqrt{u_p}]}K_n(v,\rho)\leq e^{-\frac{(\sqrt[n]{nv})^2}{2}}\frac{I_{\frac{n}{2}-1}(u_p\sqrt[n]{nv})}{(u_p\sqrt[n]{nv})^{\frac{n}{2}-1}}<\infty \qquad \text{(C.9)}\end{aligned}$$

since $\frac{I_n(x)}{x^n}(x>0)$ is a strictly increasing function. Therefore,

$$\begin{aligned}|\ln f_V(v;F_P)|&\leq \frac{(\sqrt[n]{nv})^2+u_p}{2}+|\ln(\frac{I_{\frac{n}{2}-1}(u_p\sqrt[n]{nv})}{(u_p\sqrt[n]{nv})^{\frac{n}{2}-1}})|\\ &\leq \frac{(\sqrt[n]{nv})^2+u_p}{2}+u_p\sqrt[n]{nv}+\ln(\Gamma(\frac{n}{2})2^{\frac{n}{2}-1}) \qquad \text{(C.10)}\\ &\leq \frac{(\sqrt[n]{nv})^2}{2}(1+u_p)+u_p+\ln(\Gamma(\frac{n}{2})2^{\frac{n}{2}-1}) \qquad \text{(C.11)}\end{aligned}$$

where in (C.10), we have used the inequality

$$\frac{I_\nu(x)}{x^\nu}<\frac{\cosh x}{2^\nu\Gamma(\nu+1)}\overset{x>0}{<}\frac{e^x}{2^\nu\Gamma(\nu+1)} \qquad \text{(C.12)}$$

which was proved in [46]. From (C.11), it can be verified that

$$\begin{aligned}|\tilde{h}_V(z_m;F_P)|&\leq\int_0^\infty|e^{-\frac{(\sqrt[n]{nv})^2+z_m^2}{2}}||\frac{I_{\frac{n}{2}-1}(z_m\sqrt[n]{nv})}{(z_m\sqrt[n]{nv})^{\frac{n}{2}-1}}||\ln f_V(v;F_P)|dv \qquad \text{(C.13)}\\ &\leq|e^{-\frac{z_m^2}{2}}|\int_0^\infty e^{-\frac{(\sqrt[n]{nv})^2}{2}}\frac{I_{\frac{n}{2}-1}(|z_m|\sqrt[n]{nv})}{(|z_m|\sqrt[n]{nv})^{\frac{n}{2}-1}}|\ln f_V(v;F_P)|dv \qquad \text{(C.14)}\\ &\leq|e^{\frac{|z_m|^2-z_m^2}{2}}|\left(\frac{(|z_m|^2+n)}{2}(1+u_p)+u_p+\ln(\Gamma(\frac{n}{2})2^{\frac{n}{2}-1})\right) \qquad \text{(C.15)}\\ &<\infty \qquad \text{(C.16)}\end{aligned}$$

where in (C.14), we have used the fact that $|I_n(z)|\leq I_n(|z|)$ and in (C.15) the upper bound in (C.11) has been used. Since the absolute value of the integrand of $\tilde{h}_V(z_n;F_P)$ is integrable, by Lebesgue's dominated convergence theorem, we have

$$\begin{aligned}\lim_{m\to\infty}\tilde{h}_V(z_m;F_P)&=\lim_{m\to\infty}\int_0^\infty K_n(v,z_m)\ln f_V(v;F_P)dv \qquad \text{(C.17)}\\ &=\int_0^\infty\lim_{m\to\infty}K_n(v,z_m)\ln f_V(v;F_P)dv \qquad \text{(C.18)}\end{aligned}$$

$$= \int_0^\infty K_n(v, z_0) \ln f_V(v; F_P) dv \tag{C.19}$$

$$= \tilde{h}_V(z_0; F_P) \tag{C.20}$$

which proves the continuity of $\tilde{h}_V(z, F_P)$. Let ∂T denote an arbitrary triangle in the complex plane. We can write,

$$\begin{aligned}\int_{\partial T} \tilde{h}_V(z; F_P) dz &= -\int_{\partial T} \int_0^\infty K_n(v, z) \ln f_V(v; F_P) dv dz \\ &= -\int_0^\infty \int_{\partial T} K_n(v, z) dz \ln f_V(v; F_P) dv \qquad \text{(C.21)} \\ &= 0 \qquad \text{(C.22)}\end{aligned}$$

where (C.21) is allowed by Fubini's theorem, because for a given rectifiable triangle ∂T

$$\int_{\partial T} |\tilde{h}_V(z; F_P)| dz < \infty. \tag{C.23}$$

(C.22) is due to the holomorphy of $K_n(v, z)$ (see (C.7)). Therefore, by Morera's theorem (with weakened hypothesis), it is concluded that $\tilde{h}_V(z; F_P)$ is holomorphic on the entire complex plane.

Alternatively, the holomorphy of the marginal entropy density can be proved as follows. The following integral

$$\tilde{h}_V(z; F_P) = -\int_0^\infty K_n(v, z) \ln f_V(v; F_P) dv \tag{C.24}$$

is uniformly convergent for all $z \in \mathbb{K}$ (where $\mathbb{K}$ is a compact subset of $\mathbb{C}$) in the sense that for $\forall \delta > 0$, there exists some real number L_0 such that

$$\left| -\int_{L_1}^{L_2} K_n(v, z) \ln f_V(v; F_P) dv \right| < \delta \tag{C.25}$$

for $\forall L_1, L_2$ satisfying $L_0 < L_1 < L_2$. Therefore, by the differentiation lemma [44], $\tilde{h}_V(z; F_P)$ is holomorphic on the complex plane. □

If ϵ_{P^*} has infinite number of points, since it is a bounded subset of the real line ($\subseteq [0, \sqrt{u_p}]$), it has an accumulation point in $\mathbb{R}$ by Bolzano-Weierstrass theorem [47]. Hence, according to (3.39), the two holomorphic functions $\tilde{h}_V(z; F_{P^*})$ and $h(V; F_{P^*}) + \lambda(z^2 - u_a)$ become equal on an infinite set that has an accumulation point in $\mathbb{C}$. Therefore, by

the identity theorem for holomorphic functions of one complex variable [44], the two functions are equal on the whole complex plane, i.e.

$$\tilde{h}_V(z; F_{P^*}) = h(V; F_{P^*}) + \lambda(z^2 - u_a) \quad , \quad \forall z \in \mathbb{C} \tag{C.26}$$

which results in

$$\tilde{h}_V(\rho; F_{P^*}) = h(V; F_{P^*}) + \lambda(\rho^2 - u_a) \quad , \quad \forall \rho \in \mathbb{R}. \tag{C.27}$$

In the following, we show that (C.27) leads to a contradiction.

1. $\lambda = 0$. In this case, in which the average power constraint is relaxed, (C.27) results in

$$f_V(v; F_P) = e^{-h(V;F_{P^*})} \tag{C.28}$$

which is a constant and is guaranteed by the invertibility of (3.35) to be the only solution. The uniform distribution in (C.28) cannot be a legitimate pdf for V on the non-negative real line. This contradiction can be observed in an alternative way. By noting that from (C.28) and (3.20), if $f_V(v; F_P)$ is to be constant (shown by C), then

$$f_P(\rho) = C\rho^{n-1} \quad \rho \geq 0 \tag{C.29}$$

which is the only solution for $f_P(\rho)$ by the invertibility of (3.20). Again, it is not a legitimate pdf for ρ and obviously violates the peak power constraint.

2. $\lambda > 0$. In this case (C.27) holds iff

$$f_V(v; F_P) = \frac{2(\sqrt{\lambda})^n}{\Gamma(\frac{n}{2})} e^{-\lambda(\sqrt[n]{nv})^2} \tag{C.30}$$

which also holds iff

$$f_P(\rho) = \left(\sqrt{\frac{\lambda}{1-2\lambda}}\right)^n \frac{\rho^{n-1} e^{-\frac{\lambda}{1-2\lambda}\rho^2}}{\Gamma(\frac{n}{2})} \tag{C.31}$$

with $\lambda = \frac{\Gamma(\frac{n}{2}+1)}{\Gamma(\frac{n}{2})(u_a+\frac{n}{2})}$. It is obvious that for $0 < \lambda < \frac{1}{2}$, the solution in (C.31) violates the peak power constraint and for $\lambda > \frac{1}{2}$, no legitimate $f_P(\rho)$ results in (C.30). For $\lambda = \frac{1}{2}$, $f_P(\rho) = \delta(\rho)$ which implies a unit mass point at zero. This, of

course, contradicts the first assumption of F_{P^*} having infinite points of increase and also results in $C(u_p, u_a) = 0$.

Therefore, the magnitude of the optimal input has a finite number of mass points. This completes the proof of the theorem.

Appendix D

Two Invertible Transforms

In this section, we show that the two following integral transforms are invertible (i.e., one-to-one),

$$q(v) = \int_0^\infty K_n(v,\rho)t(\rho)d\rho \tag{D.1}$$

$$w(\rho) = \int_0^\infty K_n(v,\rho)g(v)dv \tag{D.2}$$

where t is allowed to have at most an exponential order and g a polynomial with a finite degree, so that the transforms exist. The invertibility of (D.1) and (D.2) is equivalent to the invertibility of (3.20) and (3.35), respectively. The following lemma will be helpful in the sequel.

Lemma. The kernel function $K_n(v,\rho)$ satisfies the two following equations,

$$\int_0^\infty K_n(v,\rho)\rho^{n-1}e^{-s\rho^2}d\rho = \frac{e^{-\frac{s}{2s+1}(\sqrt[n]{nv})^2}}{(\sqrt{2s+1})^n} \tag{D.3}$$

$$\int_0^\infty K_n(v,\rho)e^{-s(\sqrt[n]{nv})^2}dv = \frac{e^{-\frac{s}{2s+1}\rho^2}}{(\sqrt{2s+1})^n} \tag{D.4}$$

where $s \geq 0$.

Proof. From the properties of probability density functions,

$$\int_{R^n} \frac{1}{(\sqrt{2\pi\sigma^2})^n} e^{-\frac{\|\mathbf{y}-\mathbf{x}\|^2}{2\sigma^2}} d\mathbf{y} = 1. \tag{D.5}$$

By writing $\mathbf{y}$ and $\mathbf{x}$ in spherical coordinates (i.e., $\mathbf{y} \equiv (r, \psi)$ and $\mathbf{x} \equiv (\rho, \theta)$), and by substituting $\beta = \frac{1}{2\sigma^2}$ and $\alpha = \frac{\rho}{\sigma^2}$, we get

$$\int_0^\infty \underbrace{\int_0^\pi \dots \int_0^\pi}_{n-2 \text{ times}} \int_0^{2\pi} e^{-\beta r^2 + \alpha r \mathbf{a}^T(\theta)\mathbf{a}(\psi)} r^{n-1} \prod_{i=1}^{n-2} \sin^{n-i-1}\psi_i d\psi_{n-1} d\psi_{n-2} \dots d\psi_1 dr$$

$$= (\sqrt{\frac{\pi}{\beta}})^n e^{\frac{\alpha^2}{4\beta}}. \quad \text{(D.6)}$$

By using (D.6) and by change of variables, (D.3) and (D.4) are obtained. □

In order to show the invertibility of (D.1), it is sufficient to show that the following

$$\int_0^\infty K_n(v, \rho) t(\rho) d\rho = 0 \quad \text{(D.7)}$$

results in $t(\rho) = 0$. From (D.7), we have

$$\int_0^\infty \int_0^\infty K_n(v, \rho) t(\rho) d\rho e^{-s(\sqrt[n]{nv})^2} dv = 0 \quad s \geq 0. \quad \text{(D.8)}$$

By changing the order of integration, which is allowed here by Fubini's theorem, and by (D.4)

$$\int_0^\infty t(\rho) \frac{e^{-\frac{s}{2s+1}\rho^2}}{(\sqrt{2s+1})^n} d\rho = 0 \quad s \geq 0. \quad \text{(D.9)}$$

which results in

$$\int_0^\infty \frac{t(\sqrt{x})}{\sqrt{x}} e^{-\mu x} dx = 0 \quad \mu \in [0, \frac{1}{2}). \quad \text{(D.10)}$$

Again, by extending μ to the complex domain, it is easy to verify that the left-hand side of (D.10) is holomorphic on the complex plane. Since this holomorphic function is zero on an infinite set ($[0, \frac{1}{2})$) which has an accumulation point in $\mathbb{C}$, it is zero on the whole complex plane and consequently the real line by the identity theorem. Therefore,

$$\int_0^\infty \frac{t(\sqrt{x})}{\sqrt{x}} e^{-\mu x} dx = 0 \quad \mu \in \mathbb{R} \quad \text{(D.11)}$$

which results in $t(\rho) = 0$. The uniqueness of this solution results from the invertibility of Laplace transform (by considering the non-negative values for μ). It is obvious that the same approach can be carried out to show the invertibility of the transform (D.2).

Alternatively, the following property of the kernel function

$$K_n(v,\rho) = K_n(\frac{\rho^n}{n},\ \sqrt[n]{nv}) \tag{D.12}$$

could be used in (D.1) to show the invertibility of (D.2).

Appendix E

Appendix E

From [48] and [49], we have[1]

$$\Gamma(x+1) < \sqrt{\pi}(\frac{x}{e})^x(8x^3+4x^2+x+\frac{1}{30})^{\frac{1}{6}}. \tag{E.1}$$

Let $f(n) \triangleq 2e\left[\frac{(n-1)}{2}\Gamma(\frac{n-1}{2})\right]^{\frac{2}{n-1}}$. From (3.67), we can write

$$\begin{aligned} C_G &\geq \frac{n-1}{2}\log\left(1+\frac{u_p}{f(n)}\right) \\ &\geq \frac{n-1}{2}\log\left(1+\frac{u_p}{F(n)}\right) \end{aligned} \tag{E.2}$$

in which $F(n)$ is an upper bound for $f(n)$ and is obtained from (E.1) as

$$F(n) = 2e\left[\frac{(n-1)}{2}\sqrt{\pi}\left(\frac{n-3}{2e}\right)^{\frac{n-3}{2}}\left(8(\frac{n-3}{2})^3+4(\frac{n-3}{2})^2+\frac{n-3}{2}+\frac{1}{30}\right)^{\frac{1}{6}}\right]^{\frac{2}{n-1}}. \tag{E.3}$$

The behavior of $F(n)$ as n goes to infinity can be obtained as follows.

$$\begin{aligned} \lim_{n\to\infty}\ln\frac{F(n)}{2e} &= \lim_{n\to\infty}\frac{n-3}{n-1}\ln(\frac{n-3}{2e}) \\ &\quad + \underbrace{\lim_{n\to\infty}\frac{2}{n-1}\ln\left[\frac{(n-1)}{2}\sqrt{\pi}\left(8(\frac{n-3}{2})^3+4(\frac{n-3}{2})^2+\frac{n-3}{2}+\frac{1}{30}\right)^{\frac{1}{6}}\right]}_{=0} \\ &= +\infty. \end{aligned} \tag{E.4}$$

[1] Tighter bounds for Gamma function can be found in [50].

Therefore, $\frac{u_p}{F(n)}$ goes to zero with n, and from the expansion of $\ln(1+x)$ when $x \ll 1$, we can write

$$\begin{aligned}\lim_{n\to\infty} \frac{n-1}{2} \ln\left(1+\frac{u_p}{F(n)}\right) &= \lim_{n\to\infty} \frac{u_p(n-1)}{2F(n)} \\ &\geq \lim_{n\to\infty} \frac{u_p(n-1)}{2(n+25)} \end{aligned} \tag{E.5}$$

where in (E.5), we have used the fact that for $n \leq 10^{10}$, it can be verified that $n < F(n) < n+25$. The gap between C_G and constant amplitude signaling can be written as

$$\lim_{n\to\infty} C_G - \lim_{n\to\infty} \sup_{F_{\mathbf{X}}(\mathbf{x}):\|\mathbf{X}\|^2=u_p} I(\mathbf{X};\mathbf{Y}) \leq \lim_{n\to\infty} \frac{u_p}{2}\left(1-\frac{n-1}{n+25}\right) \tag{E.6}$$

$$= \frac{13u_p}{n+25} \tag{E.7}$$

which completes the proof.

Appendix F

Proof of (3.69)

We have

$$C(u_p, u_a) \leq C(\infty, u_a) = \frac{n}{2}\ln(1+\frac{u_a}{n}) \tag{F.1}$$

and

$$\lim_{u_a \to 0} C(u_p, u_a) \leq \frac{u_a}{2}. \tag{F.2}$$

The CDF $F_P^{**}(\rho) = (1-\frac{u_a}{u_p})u(\rho) + \frac{u_a}{u_p}u(\rho - \sqrt{u_p})$ induces the following output pdf

$$f_V(v; F_P^{**}) = (1-\frac{u_a}{u_p})K_n(v,0) + \frac{u_a}{u_p}K_n(v, \sqrt{u_p}) \tag{F.3}$$

$$= (1-\frac{u_a}{u_p})\frac{e^{-\frac{(\sqrt[n]{nv})^2}{2}}}{\Gamma(\frac{n}{2})2^{\frac{n}{2}-1}} + \frac{u_a}{u_p}e^{-\frac{(\sqrt[n]{nv})^2+u_p}{2}}\frac{I_{\frac{n}{2}-1}(\sqrt{u_p}\sqrt[n]{nv})}{(\sqrt{u_p}\sqrt[n]{nv})^{\frac{n}{2}-1}} \tag{F.4}$$

$$= (1-\frac{u_a}{u_p})\frac{e^{-\frac{(\sqrt[n]{nv})^2}{2}}}{\Gamma(\frac{n}{2})2^{\frac{n}{2}-1}}\left[1 + \frac{u_a}{u_p-u_a}\frac{e^{-\frac{u_p}{2}}\Gamma(\frac{n}{2})2^{\frac{n}{2}-1}I_{\frac{n}{2}-1}(\sqrt{u_p}\sqrt[n]{nv})}{(\sqrt{u_p}\sqrt[n]{nv})^{\frac{n}{2}-1}}\right]. \tag{F.5}$$

When u_a is small,

$$\lim_{u_a\to 0} h(V; F_P^{**}) = \lim_{u_a \to 0} -\int_0^\infty f_V(v; F_P^{**})\ln f_V(v; F_P^{**})dv \tag{F.6}$$

$$= \lim_{u_a\to 0}\int_0^\infty \left\{(1-\frac{u_a}{u_p})\frac{e^{-\frac{(\sqrt[n]{nv})^2}{2}}}{\Gamma(\frac{n}{2})2^{\frac{n}{2}-1}} + \frac{u_a}{u_p}e^{-\frac{(\sqrt[n]{nv})^2+u_p}{2}}\frac{I_{\frac{n}{2}-1}(\sqrt{u_p}\sqrt[n]{nv})}{(\sqrt{u_p}\sqrt[n]{nv})^{\frac{n}{2}-1}}\right\}\times$$
$$\left\{\frac{(\sqrt[n]{nv})^2}{2} + \ln\left(\frac{\Gamma(\frac{n}{2})2^{\frac{n}{2}-1}}{(1-\frac{u_a}{u_p})}\right) - \frac{u_a}{u_p-u_a}\frac{e^{-\frac{u_p}{2}}\Gamma(\frac{n}{2})2^{\frac{n}{2}-1}I_{\frac{n}{2}-1}(\sqrt{u_p}\sqrt[n]{nv})}{(\sqrt{u_p}\sqrt[n]{nv})^{\frac{n}{2}-1}}\right\}dv \tag{F.7}$$

$$= \lim_{u_a \to 0} \frac{n}{2}(1 - \frac{u_a}{u_p}) + (1 - \frac{u_a}{u_p}) \ln \left(\frac{\Gamma(\frac{n}{2}) 2^{\frac{n}{2}-1}}{(1 - \frac{u_a}{u_p})} \right) - \frac{u_a}{u_p} + \frac{u_a}{u_p}(\frac{n + u_p}{2})$$

$$+ \frac{u_a}{u_p} \ln \left(\frac{\Gamma(\frac{n}{2}) 2^{\frac{n}{2}-1}}{(1 - \frac{u_a}{u_p})} \right) - \frac{u_a^2}{u_p - u_a} \underbrace{\gamma(u_p)}_{\text{constant}} \tag{F.8}$$

$$= \frac{n}{2} + \frac{u_a}{2} + \ln \left(\Gamma(\frac{n}{2}) 2^{\frac{n}{2}-1} \right) \tag{F.9}$$

where the six terms in (F.8) are obtained by multiplying the terms in the brackets of (F.7) in order. In (F.9), we have neglected the last higher order term in (F.8) and have used the approximation $\ln(1 - x) \approx -x$ when $x \ll 1$. Therefore,

$$\lim_{u_a \to 0} h(V; F_P^{**}) + \sum_{i=1}^{n-2} \ln \alpha_i + (1 - \frac{n}{2}) \ln 2\pi - \frac{n}{2} = \frac{u_a}{2}. \tag{F.10}$$

(F.10) and (F.2) show the asymptotic optimality of the distribution in (3.69).

Appendix G

Appendix G

Since $\sqrt{z}$ is holomorphic on the complex plane excluding the non-positive real line (i.e., the domain where the principal branch of the complex logarithm function is holomorphic), $g(\sqrt{x})$ has the following power series expansion about $\epsilon > 0$

$$g(\sqrt{x}) = \sum_{m=0}^{\infty} g_m (x-\epsilon)^m = \sum_{m=0}^{\infty} \tilde{g}_m x^m \tag{G.1}$$

where its interval of convergence is $(0, \infty)$. Assuming infinite number of mass points, with the constraint in (3.71), (C.27) changes to

$$\tilde{h}_V(\rho; F_{P^*}) = h(V; F_{P^*}) + \lambda(g(\rho) - u_a) \quad , \quad \forall \rho \in \mathbb{R} \tag{G.2}$$

or equivalently

$$-\int_0^{\infty} K_n(v,\rho) \ln f_V(v; F_P^*) dv = \lambda g(\rho) + h(V; F_P^*) - \lambda u_a \ , \ \forall \rho \in \mathbb{R}. \tag{G.3}$$

Multiplying both sides of (G.3) by $\rho^{n-1} e^{-s\rho^2}$ $(s \geq 0)$ and integrating with respect to ρ gives

$$-\int_0^{\infty} \ln f_V(v; F_P^*) \frac{e^{-\frac{s}{2s+1}(\sqrt[n]{nv})^2}}{(\sqrt{2s+1})^n} dv = \int_0^{\infty} [\lambda g(\rho) + h(V; F_P^*) - \lambda u_a] \rho^{n-1} e^{-s\rho^2} d\rho \tag{G.4}$$

where we have used the transform in (D.3). By a change of variables as $v = \frac{t^{\frac{n}{2}}}{n}$ and $x = \rho^2$, we have

$$-\int_0^\infty \ln f_V(\frac{t^{\frac{n}{2}}}{n}; F_P^*) t^{\frac{n}{2}-1} \frac{e^{-\frac{s}{2s+1}t}}{(\sqrt{2s+1})^n} dt = \int_0^\infty [\lambda g(\sqrt{x}) + h(V; F_P^*) - \lambda u_a] x^{\frac{n}{2}-1} e^{-sx} dx. \tag{G.5}$$

By substituting (G.1) in (G.5), we get

$$-\int_0^\infty \ln f_V(\frac{t^{\frac{n}{2}}}{n}; F_P^*) t^{\frac{n}{2}-1} \frac{e^{-\frac{s}{2s+1}t}}{(\sqrt{2s+1})^n} dt = \sum_{m=1}^\infty \frac{\tilde{g}_m \Gamma(\frac{n}{2}+m)}{s^{\frac{n}{2}+m}} + \frac{[h(V; F_P^*) - \lambda u_a + \lambda \tilde{g}_0]\Gamma(\frac{n}{2})}{s^{\frac{n}{2}}}. \tag{G.6}$$

Taking the inverse transform gives the unique solution as

$$\ln f_V(\frac{t^{\frac{n}{2}}}{n}; F_P^*) = \sum_{m=0}^\infty c_m t^m \tag{G.7}$$

where the coefficients are obtained from the following set of equations

$$\begin{cases} -\sum_{m=0}^\infty \frac{c_m \Gamma(\frac{n}{2}+m)(2s+1)^m}{s^{\frac{n}{2}+m}} \equiv \sum_{m=1}^\infty \frac{\tilde{g}_m \Gamma(\frac{n}{2}+m)}{s^{\frac{n}{2}+m}} + \frac{[h(V;F_P^*) - \lambda u_a + \lambda \tilde{g}_0]\Gamma(\frac{n}{2})}{s^{\frac{n}{2}}} \\ h(V; F_P^*) = -\int_0^\infty f_V(v; F_P^*) \ln f_V(v; F_P^*) dv \end{cases}. \tag{G.8}$$

If there is no solution satisfying (G.8), (G.2) does not hold, which is the desired contradiction. However, in the case of having a solution for the coefficients in (G.8), we have

$$f_V(v; F_P^*) = e^{\sum_{m=0}^\infty c_m (\sqrt[n]{nv})^{2m}}. \tag{G.9}$$

In the case $c_m = 0$ $(m \geq 1)$, f_V becomes a constant on the non-negative real line which cannot be a probability density function. The case $c_m = 0$ $(m \geq 2)$ does not result in a legitimate pdf, either (see (C.30) and its following discussion.) For the remaining case of having at least one non-zero $c_m (m \geq 3)$, (G.9) leads to a contradiction as follows. Let $m^* = \max_m \{m | c_m \neq 0\}$. If $c_{m^*} > 0$, (G.9) is not integrable over the non-negative real line, hence, it is not a pdf. However, if $c_{m^*} < 0$, no $F_P(\rho)$ can result in f_V, since from (C.9),

$$f_V^{-1}(v; F_P) = O(e^{\frac{(\sqrt[n]{nv})^2}{2}}) \tag{G.10}$$

while the behavior of the inverse of (G.9) is different from (G.10) as v goes to infinity. Therefore, it is concluded that (G.9) cannot be resulted by any $F_P(\rho)$ due to its behavior at large v. This implies that the discrete nature of the magnitude of the optimal input distribution does not change when the average constraint is generalized to (3.71).

Appendix H

Proof of Lemma

Let

$$f_A(x) \triangleq g(A-x) + g(A+x) \quad , \quad x \in [0, A].$$

For the function g, we can obtain the following properties

$$g(u) \leq 0 \quad , \quad u \geq 0 \tag{H.1}$$

$$g'(u) \geq 0 \quad , \quad u \geq 1. \tag{H.2}$$

(H.1) is obtained as

$$\begin{aligned} g(u) &= u^2 Q(u) - u\psi(u) \\ &< u\psi(u) - u\psi(u) \\ &= 0 \end{aligned}$$

where we have used the inequality $xQ(x) < \psi(x)$. (H.2) is obtained as

$$\begin{aligned} g'(u) &= 2uQ(u) - \psi(u) \\ &> \frac{u^2-1}{u^2+1}\psi(u) \\ &\geq 0 \quad , \quad \text{for } u \geq 1 \end{aligned}$$

where we have used the inequality $Q(x) > \frac{x\psi(x)}{1+x^2}$.

Therefore, for $A \geq 1$, we have

$$f_A(x) < g(A+x) \tag{H.3}$$
$$< g(2A) \tag{H.4}$$

where (H.3) and (H.4) are due to (H.1) and (H.2), respectively.

For $A \leq 1$, we proceed as follows. The fourth derivative of g is given by

$$\frac{d^4}{du^4} g(u) = u(5-u^2)\psi(u)$$

Hence, for $u \in [0, \sqrt{5})$, $\frac{d^4}{du^4} g(u) > 0$ which indicates that $\frac{d^3}{du^3} g(u)$ is strictly increasing. This results in

$$\frac{d^3}{dx^3} f_A(x) = \frac{d^3}{du^3} g(A+x) - \frac{d^3}{dx^3} g(A-x) \geq 0 \tag{H.5}$$

for $A \leq 1$. (H.5) results in

$$\begin{aligned} f''_A(x) &\geq f''_A(0) \\ &= 2g''(A) \\ &= 2[2Q(A) - A\psi(A)] \\ &> \frac{2A(1-A^2)}{1+A^2}\psi(A) \end{aligned} \tag{H.6}$$

where in (H.6), we have used the inequality $Q(x) > \frac{x\psi(x)}{1+x^2}$. Therefore, for $A \leq 1$, we have $f''_A(x) > 0$ which results in $f'_A(x) > f'_A(0) = 0$. Finally, having an increasing $f_A(x)$ confirms

$$f_A(x) < f_A(A) = g(2A).$$

This completes the proof.

Bibliography

[1] B. Clerckx and C. Oestges, *MIMO Wireless Networks, 2nd Edition*. United Kingdom: Academic Press, 2013.

[2] M. Maddah-Ali and D. Tse, "Completely stale transmitter channel state information is still very useful," *IEEE Trans. Inf. Theory*, vol. 58, no. 7, pp. 4418–4431, July 2012.

[3] S. Yang, M. Kobayashi, D. Gesbert, and X. Yi, "Degrees of freedom of time correlated MISO broadcast channel with delayed CSIT," *IEEE Trans. Inf. Theory*, vol. 59, no. 1, pp. 315–328, January 2013.

[4] T. Gou and S. Jafar, "Optimal use of current and outdated channel state information: Degrees of freedom of the MISO BC with mixed CSIT," *IEEE Comms. Letters*, vol. 16, no. 7, pp. 1084 –1087, July 2012.

[5] J. Chen and P. Elia, "Degrees-of-freedom region of the MISO broadcast channel with general mixed-CSIT," available on arxiv:1205.3474.

[6] P. de Kerret, X. Yi, and D. Gesbert, "On the degrees of freedom of the K-user time correlated broadcast channel with delayed CSIT," in *ISIT 2013, IEEE International Symposium on Information Theory, July 7-12, 2013, Istanbul, Turkey*, Istanbul, TURKEY, July 2013. [Online]. Available: http://www.eurecom.fr/publication/4000

[7] C. Hao and B. Clerckx, "Imperfect and unmatched CSIT is still useful for the frequency correlated MISO broadcast channel," in *IEEE ICC*, Budapest, Hungary, June 2013, pp. 3181–3186.

[8] ——, "MISO broadcast channel with imperfect and (un)matched CSIT in the frequency domain: DoF region and transmission strategies," in *IEEE PIMRC*, Sep. 2013, pp. 1–6.

[9] R. Tandon, S. Jafar, S. Shamai Shitz, and H. Poor, "On the synergistic benefits of alternating CSIT for the MISO broadcast channel," *IEEE Trans. Inf. Theory.*, vol. 59, no. 7, pp. 4106–4128, July 2013.

[10] K. Mohanty and M. Varanasi, "On the DoF region of the K-user MISO broadcast channel with hybrid CSIT." available on arXiv:1312.1309.

[11] S. Amuru, R. Tandon, and S. Shamai, "On the degrees-of-freedom of the 3-user MISO broadcast channel with hybrid CSIT," in *IEEE ISIT*, 2014, pp. 2137–2141.

[12] S. Lashgari, R. Tandon, and S. Avestimehr, "MISO broadcast channel with hybrid CSIT: Beyond two users," available on arXiv:1504.04615.

[13] N. Lee and R. Heath Jr., "Space-time interference alignment and degrees of freedom regions for the MISO broadcast channel with periodic CSI feedback," *IEEE Trans. Inf. Theory.*, vol. 60, no. 1, pp. 515–528, Jan. 2014.

[14] N. Lee, R. Tandon, and R. Heath Jr., "Distributed space-time interference alignment with moderately delayed CSIT," *IEEE Trans. Wireless Comm.*, vol. 14, no. 2, pp. 1048–1059, Feb. 2015.

[15] T. M. Cover and J. A. Thomas, *Elements of Information Theory, second edition.* New York: Wiley-Intersicence, 2006.

[16] A. Gamal, "The feedback capacity of degraded broadcast channels (corresp.)," *IEEE Trans. Inf. Theory*, vol. 24, no. 3, pp. 379 – 381, May 1978.

[17] A. Davoodi and S. Jafar, "Aligned image sets under channel uncertainty: Settling a conjecture by Lapidoth, Shamai and Wigger on the collapse of degrees of freedom under finite precision CSIT," available on arxiv:1403.1541.

[18] X. Yi, S. Yang, D. Gesbert, and M. Kobayashi, "The degree of freedom region of temporally correlated MIMO networks with delayed CSIT," *IEEE Trans. Inf. Theory*, vol. 60, no. 1, pp. 494 –514, Jan. 2014.

[19] C. Huang, S. Jafar, and S. Shamai, "Multiuser MIMO degrees of freedom without CSIT," presented at the Inf. Theory Appl. Workshop, San Diego, CA, Feb. 2009.

[20] C. Huang, S. Jafar, S. Shamai, and S. Vishwanath, "On degrees of freedom region of MIMO networks without channel state information at transmitters," *IEEE Trans. Inf. Theory*, vol. 58, no. 2, pp. 849 –857, feb. 2012.

[21] C. Vaze and M. Varanasi, "The degree-of-freedom regions of MIMO broadcast, interference, and cognitive radio channels with no CSIT," *IEEE Trans. Inf. Theory,*, vol. 58, no. 8, pp. 5354 –5374, aug. 2012.

[22] E. Telatar, "Capacity of multi-antenna Gaussian channels," *European Trans. on Telecommunications*, vol. 10, no. 6, pp. 585 –595, 1999.

[23] D. Tse and P. Viswanath, *Fundamentals of Wireless Communication, 1st Edition.* Cambridge University Press, 2005.

[24] S. Shamai and I. Bar-David, "The capacity of average and peak-power-limited quadrature gaussian channels," *IEEE Trans. Inf. Theory*, vol. 41, no. 4, pp. 1060–1071, July 1995.

[25] J. Smith, "The information capacity of amplitude and variance constrained scalar gaussian channels," *Inform. Contr.*, vol. 18, pp. 203–219, 1971.

[26] I. Abou-Faycal, M. Trott, and S. Shamai, "The capacity of discrete-time memoryless Rayleigh-fading channels," *IEEE Trans. Inf. Theory*, vol. 47, no. 4, pp. 1290–1300, May 2001.

[27] M. Katz and S. Shamai(Shitz), "On the capacity-achieving distribution of the discrete-time noncoherent and partially coherent AWGN channels," *IEEE Trans. Inf. Theory*, vol. 50, no. 10, pp. 2257–2270, October 2004.

[28] M. Gursoy, H. Poor, and S. Verdú, "The noncoherent Rician fading channel-parti: Structure of the capacity-achieving input," *IEEE Trans. Wireless Comm.*, vol. 4, no. 5, pp. 2193–2206, September 2005.

[29] A. Tchamkerten, "On the discreteness of capacity-achieving distributions," *IEEE Trans. Inf. Theory*, vol. 50, no. 11, pp. 2773–2778, November 2004.

[30] B. Mamandipoor, K. Moshkar, and A. Khandani, "Capacity-achieving distributions in Gaussian multiple access channel with peak power constraints," *IEEE Trans. Inf. Theory*, vol. 60, no. 10, pp. 6080–6092, October 2014.

[31] M. A. Sedaghat, R. R. Mueller, and G. Fischer, "A novel single-RF transmitter for massive MIMO," in *18th International ITG Workshop on Smart Antennas (WSA)*. VDE, 2014, pp. 1–8.

[32] R. Palanki, "On the capacity achieving distributions of some fading channels," in *Proc., 40th Annu. Allerton Conf. Communication, Control, and Computing*, Monticello, IL, Oct. 2002, pp. 337–346.

[33] S. Chan, S. Hranilovic, and F. Kschischang, "Capacity-achieving probability measure for conditionally Gaussian channels with bounded inputs," *IEEE Trans. Inf. Theory*, vol. 51, no. 6, pp. 2073–2088, June 2005.

[34] J. Sommerfeld, I. Bjelaković, and H. Boche, "On the boundedness of the support of optimal input measures for rayleigh fading channels," in *IEEE International Symposium on Information Theory (ISIT)*, July 2008, pp. 1208–1212.

[35] A. E. Gamal and Y.-H. Kim, *Network Information Theory*. United Kingdom: Cambridge University Press, 2012.

[36] A. McKellips, "Simple tight bounds on capacity for the peak-limited discrete-time channel," in *IEEE International Symposium on Information Theory (ISIT)*, June 2004, pp. 348–348.

[37] A. Thangaraj, G. Kramer, and G. Böcherer, "Capacity bounds for discrete-time, amplitude-constrained, additive white Gaussian noise channels," *arXiv:1511.08742*, Nov. 2015.

[38] B. Rassouli and B. Clerckx, "On the capacity of vector Gaussian channels with bounded inputs," *Available on arxiv*.

[39] J. Fahs and I. Abou-Faycal, "Using Hermite bases in studying capacity-achieving distributions over AWGN channels," *IEEE Trans. Inf. Theory*, vol. 58, no. 8, pp. 5302–5322, August 2012.

[40] A. Wyner, "Bounds on communication with polyphase coding," *Bell Syst. Tech. J.*, pp. 523–559, April 1966.

[41] M. Loéve, *Probability Theory.* Paris, France: New York:Van Nostrand, 1960.

[42] J.G.Smith, *On the information capacity of peak and average power constrained Gaussian channels.* Ph.D. dissertation., Dep. Elec. Eng., Univ. of California, Berkeley, CA, Dec. 1969.

[43] D. G. Luenberger, *Optimization by Vector Space Methods.* New York: New York:Wiley, 1969.

[44] S. Lang, *Complex Analysis.* 4th ed. Springer, 1999.

[45] I. S. Gradshteyn and I. M. Ryzhik, *Table of integrals, series, and products.* MA, USA: Academic Press, 2007.

[46] Y. Luke, "Inequalities for generalized hypergeometric functions," *Journal of Approximation Theory*, vol. 5, no. 1, pp. 41–65, January 1972.

[47] R. Bartle, *Elements of Real Analysis.* New York:Wiley, 1964.

[48] E. Karatsuba, "On the asymptotic representation of the Euler gamma function by Ramanujan," *J. Computat. Appl. Math*, vol. 135, pp. 225–240, 2001.

[49] H. Alzer, "On Ramanujan's double-inequality for the gamma function," *Bull. Lond. Math. Soc.*, vol. 35, pp. 601–607, 2003.

[50] ——, "Sharp upper and lower bounds for the gamma function," *Royal Society of Edinburgh*, vol. 139A, pp. 709–718, 2009.